# BLAST AND SHOCK PHENOMENA

## ■ INTRODUCTION ■

■■ Most of the physical damage to material that is caused by nuclear explosions near the earth's surface results from the blast and shock phenomena or from the thermal radiation phenomena associated with such explosions. This chapter describes the blast and shock phenomena, while the thermal radiation phenomena are described in Chapter 3.

■■ Damage to structures or materiel from blast and shock depends upon the location of the explosion (air burst, surface burst, subsurface burst), and the location of the structure or materiel (in the air, on or under the surface of the earth, or on or under a water surface). Accordingly, this chapter is divided into four sections. Section I describes the air blast phenomena from air and surface bursts. Section II deals with cratering phenomena and the associated problems of ejecta. Section III describes ground shock phenomena from near surface and subsurface (ground) explosions. Section IV describes the phenomena associated with underwater explosions.

## SECTION I
## ■ AIR BLAST PHENOMENA ■

■■ The shock wave that propagates through air as a consequence of a nuclear explosion is commonly referred to as a blast wave. The destructive effects of a blast wave are produced by its overpressure and its dynamic pressure, both expressed in pounds per square inch (psi). Overpressure, $\Delta p$, is the amount by which the static pressure in the blast wave exceeds the ambient

pressure. Dynamic pressure, $q$, is associated with the mass motion of air in the blast wave. It is approximately equal to the pressure that this strong wind develops when it hits a stationary object. Dynamic pressure is defined more completely in paragraph 2-8.

■■ When an ideal blast wave passes a given point, the first disturbance that is felt coincides with the arrival of the shock front, a discontinuity at which both overpressure and dynamic pressure rise abruptly to their peak values, as illustrated at point B in Figure 2-1. The over-
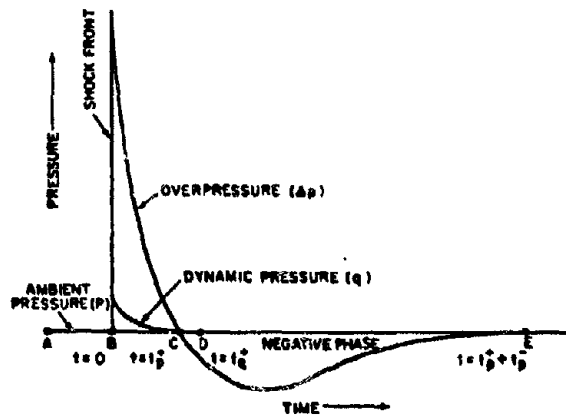


Figure 2-1. ■ Ideal Pressure-Time Relationships for a Blast Wave in the Low Pressure Region (below 5 psi) ■

pressure then follows an approximately exponential decline to a negative value, i.e., to a pressure below ambient, and gradually returns to zero. The phase that is above ambient pressure (between points B and C) is termed the positive phase; the phase that is below ambient pressure

must be assumed for possible military encounters.

## 2-1 Interpretation of Reliability Statements

The reliability statement that accompanies each set of blast-wave data in this chapter is, when possible, based on the width of the band that contains 90 percent of all data points. In the example given above (free air overpressure), there are many data points, and the width of this band may be established readily. In other cases, the reliability statements must be based on judgment. This is necessary when the data are too few to indicate the amount of scatter clearly, when large systematic errors are suspected, and when curves are obtained from theory and lack the support of experimental data.

## 2-2 Errors Due to Yield Scaling

Yield scaling is sufficiently accurate that the errors introduced are, in most air blast problems, masked by uncertainties in the experimental data. The exact amount of error attributable to yield scaling is unknown, but it is estimated to be a few percent. There are some exceptions to this rule.



Full scale nuclear tests have confirmed the scaling laws for yields to about 10 megatons (Mt), and scaling to 20 Mt is considered a reasonable extrapolation of available data. However, there is reason to question whether the scaling laws maintain their accuracy for still larger yields. Since the fireball of a 20 Mt burst is over a mile in diameter, nonuniformity of the atmosphere is a sufficiently large factor to modify develop-

ment of both the fireball and the blast wave, as will be described in subsequent paragraphs. This modification may cause significant deviations from the scaling laws. The scaling laws may be applied to yields less than 1 kt or more than 20 Mt, but the additional uncertainties involved should be recognized.

## 2-3 Errors Due to Altitude Scaling

Altitude scaling is less accurate than yield scaling, and the problem becomes significant at altitudes above about 40,000 feet. Below 40,000 feet, available data are not adequate to establish the magnitude of errors introduced by altitude scaling, but they indicate that these errors are probably small. Above 40,000 feet, where scaling errors become fairly large, the overpressure and dynamic pressure waveforms depart from the predicted values more than other conditions at the shock front.

## 2-4 Errors at Long Ranges

As mentioned previously, a nonuniform atmosphere can distort the blast wave. Variations of wind velocity or of temperature with altitude can produce focusing effects by channeling more energy in one direction at the expense of energy propagating in another direction. This effect is most pronounced at long ranges. It is the principal reason for assigning a wider tolerance to overpressure data below 1/2 psi (paragraph 2-24).

## 2-5 Effects of the Earth's Surface

Since the earth is not a perfect reflector, blast waves interacting with its surface cannot be predicted as dependably as blast waves in free space. The reliability of blast-wave data at the surface is discussed in paragraph 2-23.

## 2-6 Effect of Weapon Characteristics

Warheads with unusual radiating properties

develop a blast wave of

different intensity than the scaling laws predict (see paragraph 2-44).

## BLAST WAVE CALCULATIONS IN FREE AIR

The physical characteristics of the blast wave change as a function of time and distance as the blast wave moves out from the explosion. In a homogeneous atmosphere, where no boundaries or surfaces are present, these changes take place in a definite manner as a result of spherical divergence and irreversible energy losses to the air. The shock front peak overpressure and other shock wave parameters, such as velocity, that depend on the overpressure decrease with increasing distance, and the shock strength is attenuated with distance.

### 2-7 Peak Overpressure

The curve for free-air peak overpressure in a standard sea-level atmosphere is shown in Figure 2-2 as a function of distance from a 1 kt explosion. This curve can be used directly to predict incident overpressures from air bursts up to about 5,000 feet height of burst. The curve also may be used to predict incident overpressures for heights of burst up to 40,000 feet by using the altitude scaling procedure described in the following subsection. The curve may also be used to predict incident overpressures for heights of burst above 40,000 feet by using a reduced effective blast yield obtained from Figure 2-64.

Figure 2-3 shows a family of free air overpressure curves as a function of slant range for selected yields between 0.001 kt and 1,000 Mt. This figure eliminates the requirement for yield scaling, so it is more convenient to use for selected yields at heights of burst below 5,000 feet. For other yields and for higher burst heights, the curve in Figure 2-2 provides more accurate data for scaling.

### 2-8 Peak Dynamic Pressure

Dynamic pressures cause stationary targets to experience drag forces associated with the high-velocity winds that follow the shock front. In an ideal blast wave, dynamic pressure rises abruptly at the shock front to its peak value and then diminishes as overpressure decreases. Because of this decay behind the shock front, these strong gusts of wind cannot be compared directly with steady winds of the same velocity. During the negative overpressure phase, the transient winds reverse and blow at reduced velocities; the resulting values of dynamic pressure are small and act in the opposite direction. As a result of the momentum of air in motion, the positive dynamic pressure phase lasts slightly longer than the positive overpressure phase.

The dynamic pressure is proportional to the square of the wind velocity and to the density of the air behind the shock front as follows

$$q = \frac{1}{2}\rho_s u^2,$$

where $q$ is the dynamic pressure, $\rho_s$ is the density of the air behind the shock front, and $u$ is the particle (wind) velocity behind the shock front. These latter two quantities may be related to the overpressure under ideal conditions by equations that will be given in the succeeding subsection (paragraphs 2-15 and 2-17).

Peak dynamic pressure is shown as a function of distance from a 1 kt free air explosion in a standard sea level atmosphere in Figure 2-4.

Dynamic pressure and overpressure are considered separately not only because they have different origins, but also because they react differently with the target. For example, a telephone pole is not particularly sensitive to overpressure; but a dynamic pressure of the order of 1 psi is sufficient to break it.

2-4

## 2-9 Time of Arrival

At breakaway (i.e., the instant that the shock front moves beyond the fireball) the shock front from a sea-level burst has a velocity of approximately seven times the velocity of sound. Shock front velocity decreases as peak overpressure decreases; it approaches the velocity of sound as peak overpressure approaches zero. The time of arrival of the shock front is shown as a function of distance from a 1 kt free air explosion in a homogeneous sea level atmosphere in Figure 2-5.

## 2-10 Duration of the Positive Phases of Overpressure and Dynamic Pressure

As illustrated in Figure 2-1, both the overpressure and the dynamic pressure rise rapidly to peak values, decay to negative values, and finally return to zero. It is during the positive phase of the overpressure and/or the dynamic pressure that most of the physical damage is caused to structures, materiel, or personnel. The positive phase durations of the overpressure pulse $(t_p^+)$ and the dynamic pressure $(t_q^+)$ are shown in Figure 2-6 as a function of distance from a 1 kt free air explosion in a homogeneous sea level atmosphere.

## 2-11 Impulse

The ideal parameter for specifying the intensity of a blast wave would be one that has a simple definition and that relates directly to damage potential. Peak overpressure serves this function approximately for many applications. Impulse, which combines the effects of pressure and duration, is another of the parameters that approaches this ideal for some types of targets.

Impulse may be defined as the product of the average pressure and the time during which the pressure acts. Mathematically, the positive-phase overpressure impulse $I_p$ is defined as

$$I_p = \int_{t=0}^{t=t_p^+} \Delta p(t)dt.$$

Negative-phase impulse is similarly defined in terms of the underpressure; it is usually less significant than the positive-phase impulse. For this reason, the term overpressure impulse is conventionally interpreted to mean positive phase overpressure impulse.

Dynamic pressure impulse is similarly defined as the time integral

$$I_q = \int_{t=0}^{t=t_q^+} q(t)dt.$$

Figure 2-7 shows positive overpressure impulse as a function of range from a 1 kt free air burst in a standard sea level atmosphere. Comparison of Figures 2-2 and 2-7 shows that overpressure impulse falls off much less rapidly with distance than does peak overpressure. This is because the pressure pulse broadens (becomes more extended in time) as the peak overpressure declines.

Figure 2-7 also shows a curve representing dynamic pressure impulse. Near the burst, dynamic pressure impulse is limited by the relatively small volume of air enclosed by the shock front. This small amount of air can only sustain a strong wind for a short time interval; consequently, the dynamic pressure pulse is very narrow (short duration) at short ranges. At scaled distances between 200 and 400 feet, the duration of the dynamic pressure pulse decreases almost as rapidly as peak dynamic pressure increases with decreasing distance; as a result, dynamic pressure impulse remains nearly constant over this range of distances.

## Problem 2-1. Calculation of Free Air Peak Overpressure

█████ Figure 2-2 shows the peak overpressure as a function of slant range from a 1 kt explosion in a homogeneous sea level atmosphere at heights of burst up to about 5,000 feet. For higher burst heights, this figure may be used together with the altitude scaling procedures described in paragraph 2-14 and illustrated in problem 2-6. Figure 2-2 only applies to *free air* overpressure. Overpressures at the surface should be obtained from the subsection "BLAST WAVE PHENOMENA AT THE SURFACE."

████ *Scaling.* For yields other than 1 kt, the distance for any specified overpressure is

$$\frac{d}{d_1} = W^{1/3},$$

where $d_1$ is the distance from the explosion obtained from Figure 2-2 for 1 kt, and $d$ is the corresponding distance for a yield of $W$ kt.

████ *Example* █████

*Given:* A 5 kt explosion at 4,000 feet.

*Find:* The coaltitude distance to which 7 psi overpressure will extend.

*Solution:* From Figure 2-2, an overpressure ∪f 7 ⼞∽ ∾:ll extend to 1,000 feet for explosions below about 5,000 feet.

*Answer:* The corresponding distance for a 5 kt weapon is

$$d = d_1 \times W^{1/3} = 1,000 \times (5)^{1/3} = 1,710 \text{ feet.}$$

████ *Reliability* ██·

█ The curve showr. in Figure 2-2 is a theoretical curve that agrees well with experimental data. For scaled ranges up to 1,000 feet (overpressures greater than 7 psi at sea level) the values of peak overpressure obtained from the curve are estimated to be within ±15 percent of the overpressure that a given nuclear burst will produce. This portion of the overpressure-distance curve has been verified by analyses of data obtained by high-speed photography.

████ For scaled distances greater than 1,000 feet (overpressures below 7 psi) the values of peak overpressure obtained from the curve are estimated to be within ±30 percent the overpressures that a given burst will produce. This portion of the curve is based on theore ical calculations that agree closely with the empirical curve in the high overpressure region. The experimental data for this portion of the curve consist of both airborne pressure gages (either in parachuted canisters or aircraft in flight) and pressure gages mounted on towers above the ground. Since atmospheric effects (see paragraph 2-16) influence overpressures strongly, greater scatter is found in the data on both sides of the curve in this region.

████ *Related Material:* See paragraph 2-7. See also paragraph 2-14 through 2-15 and Problem 2-6 for scaling to altitudes up to 40,000 feet. See paragraphs 2-42 through 2-44 for scaling above 40,000 feet.
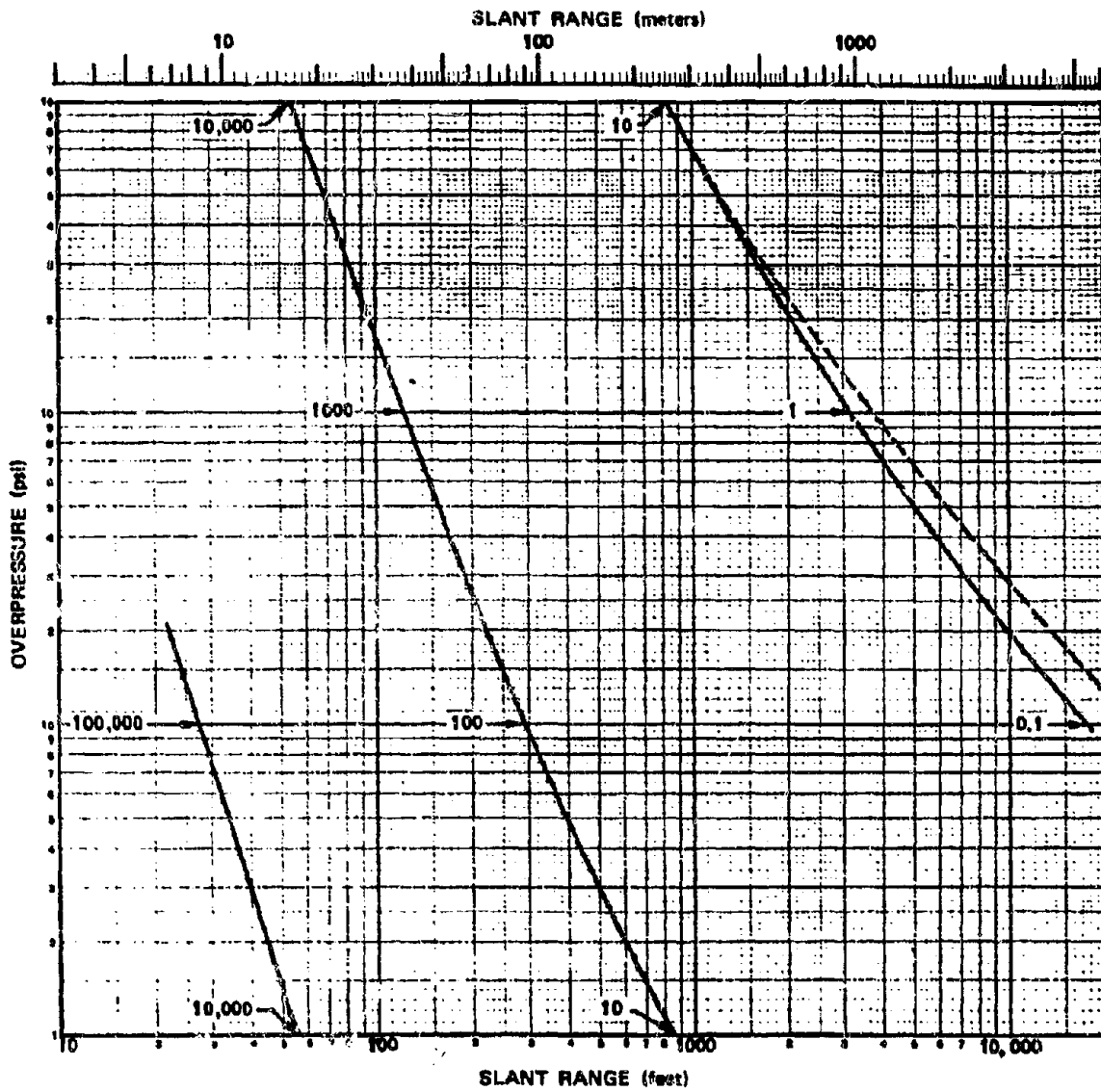
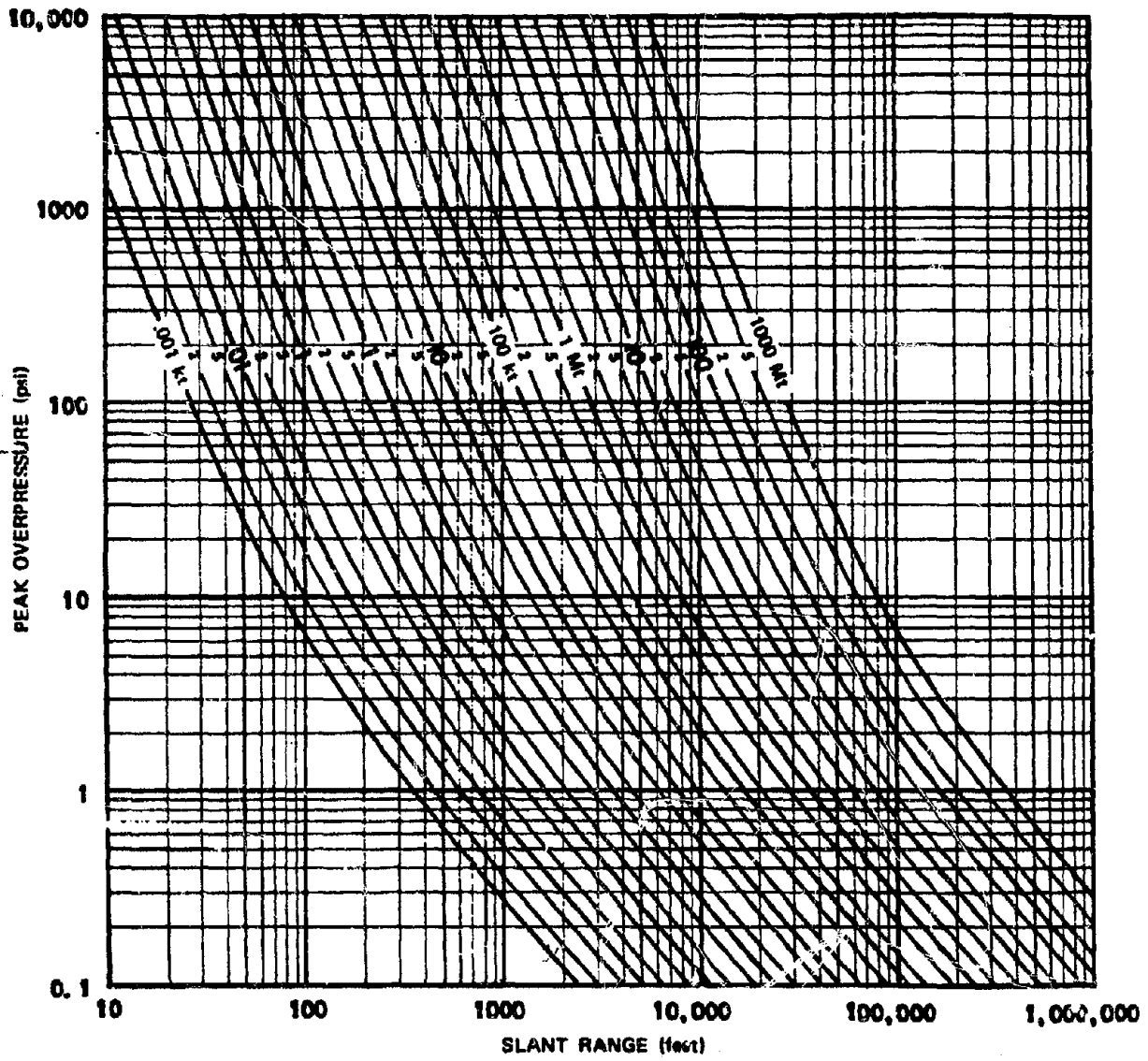Figure 2-2. ██ Peak Overpressure from a 1 kt Free Air Burst in a Standard Sea Level Atmosphere ██

Figure 2-3. ▓ Peak Overpressure in Free Air as a Function of Yield and Slant Range ▓

## Problem 2-2. Calculation of Free Air Peak Dynamic Pressure

Figure 2-4 shows the peak dynamic pressure as a function of slant range from a 1 kt explosion in a homogeneous sea level atmosphere at heights of burst up to about 5,000 feet. For higher burst heights, this figure may be used together with the altitude scaling procedures described in paragraph 2-14 and illustrated in problem 2-6. Figure 2-4 only applies to *free air* peak dynamic pressure. The horizontal component of the peak dynamic pressure at the surface should be obtained from the subsection "BLAST WAVE PHENOMENA AT THE SURFACE."

Figure 2-4 shows peak dynamic pressure with respect to a stationary target. If the target velocity is appreciable compared to the peak particle velocity (wind) at the shock front, the procedures suggested in paragraph 2-15 should be used.

Scaling. For yields other than 1 kt, the distance for any specific peak dynamic pressure is

$$\frac{d}{d_1} = W^{1/3},$$

where $d_1$ is the distance from the explosion obtained from Figure 2-4 for 1 kt, and $d$ is the corresponding distance for a yield of $W$ kt.

Example
Given: A target is located at an altitude of 3,000 feet and is 2,600 feet from a 100 kt explosion at the same altitude.

*Find:* The peak dynamic pressure to which the target is expected to be exposed.

*Solution:* The corresponding distance from a 1 kt free air explosion is

$$d_1 = \frac{d}{W^{1/3}} = \frac{2,600}{(100)^{1/3}} = 560 \text{ feet.}$$

*Answer:* From Figure 2-4, a peak dynamic pressure of 12 psi is expected to occur 560 feet from a 1 kt free air explosion. This same peak dynamic pressure would be expected 2,600 feet from a 100 kt explosion.

*Reliability:* Peak dynamic pressures obtained from this curve are estimated to be reliable to ±15 percent for pressures greater than 2 psi and to ±20 percent for smaller pressures. These estimates of reliability apply to yields between 1 kt and 20 Mt. Outside this range of yields, the curve may be used with somewhat less confidence.

*Related Material:* See paragraph 2-8. See also paragraphs 2-13 through 2-15 and Problem 2-6 for scaling to altitudes up to 40,000 feet. See paragraphs 2-42 through 2-44 for scaling above 40,000 feet. See paragraph 2-25 for a discussion of dynamic pressure along the surface of the earth.
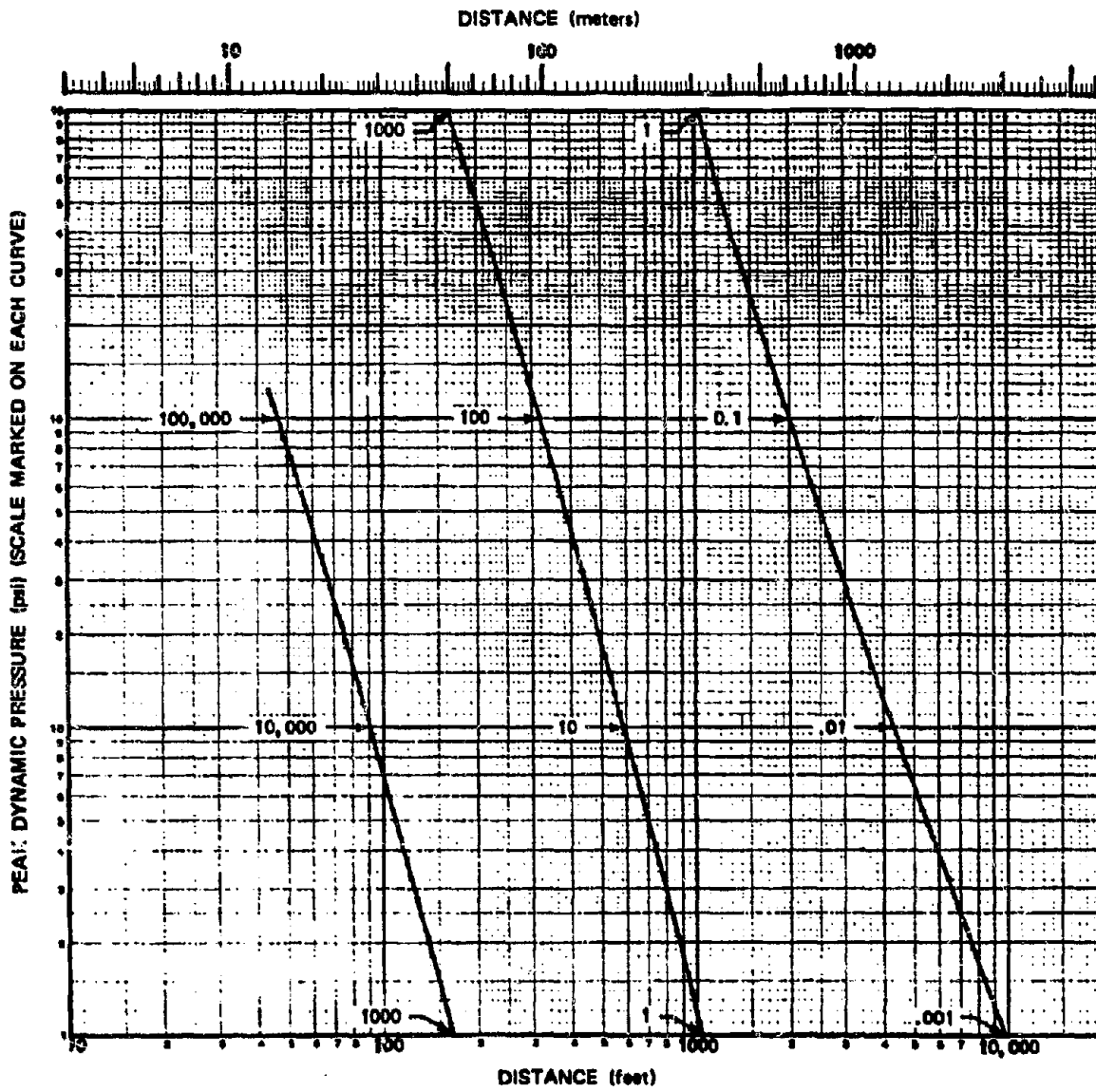
DISTANCE (meters)



Figure 2-4. Peak Dynamic Pressure from a 1 kt Free Air Burst in a Standard Sea Level Atmosphere

DISTANCE (feet)

## Problem 2-3. Calculation of Time of Arrival of the Shock Front from a Free Air Burst

■ Figure 2-5 shows the time of arrival of the shock front from a 1 kt free air burst in a standard sea level atmosphere as a function of distance from the burst. Figure 2-5 applies to bursts at altitudes up to 5,000 feet.

■ Scaling. For yields other than 1 kt, scale as follows:

$$\frac{t}{t_1} = W^{1/3} = \frac{d}{d_1}$$

where $t_1$ is the time of arrival of the shock front at a distance $d_1$ from a 1 kt explosion, and $t$ is the corresponding time at a distance $d$ from a yield of $W$ kt. At scaled distances greater than 1,500 feet ($d_1 > 1,500$ feet), the blast wave travels only slightly faster than the speed of sound, and the time of arrival may be approximated by

$$t = \frac{d - 600 \ W^{1/3}}{1,116} \ \text{sec},$$

where $d$ is the distance of interest, in feet, from an explosion of yield $W$ kt, and $t$ is the time of arrival of the shock front at that distance. The constant 1,116 is the speed of sound in air at a temperature of 59°F (15°C). The term 600 $W^{1/3}$ is a measure of the scaled distance from the burst beyond which the shock wave travels at approximately the speed of sound. The approximation may be extended by noting that the speed of sound increases by about 1 percent for each 10°F rise from the standard 59°F (1.8 percent for each 10°C rise from 15°C) and decreases by the same percentage for corresponding temperature decreases below standard.

■ Example ■
Given: A 100 kt explosion in free air in a sea level atmosphere.

Find: The time of arrival of the shock front at a point 40,000 feet from the explosion.

Solution: The corresponding distance from a 1 kt explosion is

$$d_1 = \frac{d}{W^{1/3}} = \frac{40,000}{(100)^{1/3}} = 8,600 \ \text{feet}.$$

From Figure 2-5, the time of arrival of the shock front at a point 8,600 feet from a 1 kt explosion is 7.2 seconds.

Answer: The corresponding time of arrival at a distance of 40,000 feet from a 100 kt explosion is

$$t = t_1 W^{1/3} = 7.2 \times (100)^{1/3} = 33.4 \ \text{sec}.$$

Since $d_1$ is greater than 1,500 feet, an alternate method for obtaining the time of arrival would be to use the equation presented above:

$$t = \frac{d - 600 \ W^{1/3}}{1,116} = \frac{40,000 - (600)(100)^{1/3}}{1,116}$$

$$= 33.3 \ \text{sec}.$$

■ Reliability: The times of arrival obtained from Figure 2-5 are estimated to be within ±15 percent of the true value for yields between 1 kt and 20 Mt. The curve may be used with less confidence outside this range of yields.

■ Related Material: See paragraph 2-9. See also paragraph 2-14 for scaling of times of arrival for burst altitudes above 5,000 feet. See paragraph 2-26 for time of arrival of the shock front at points on the surface.
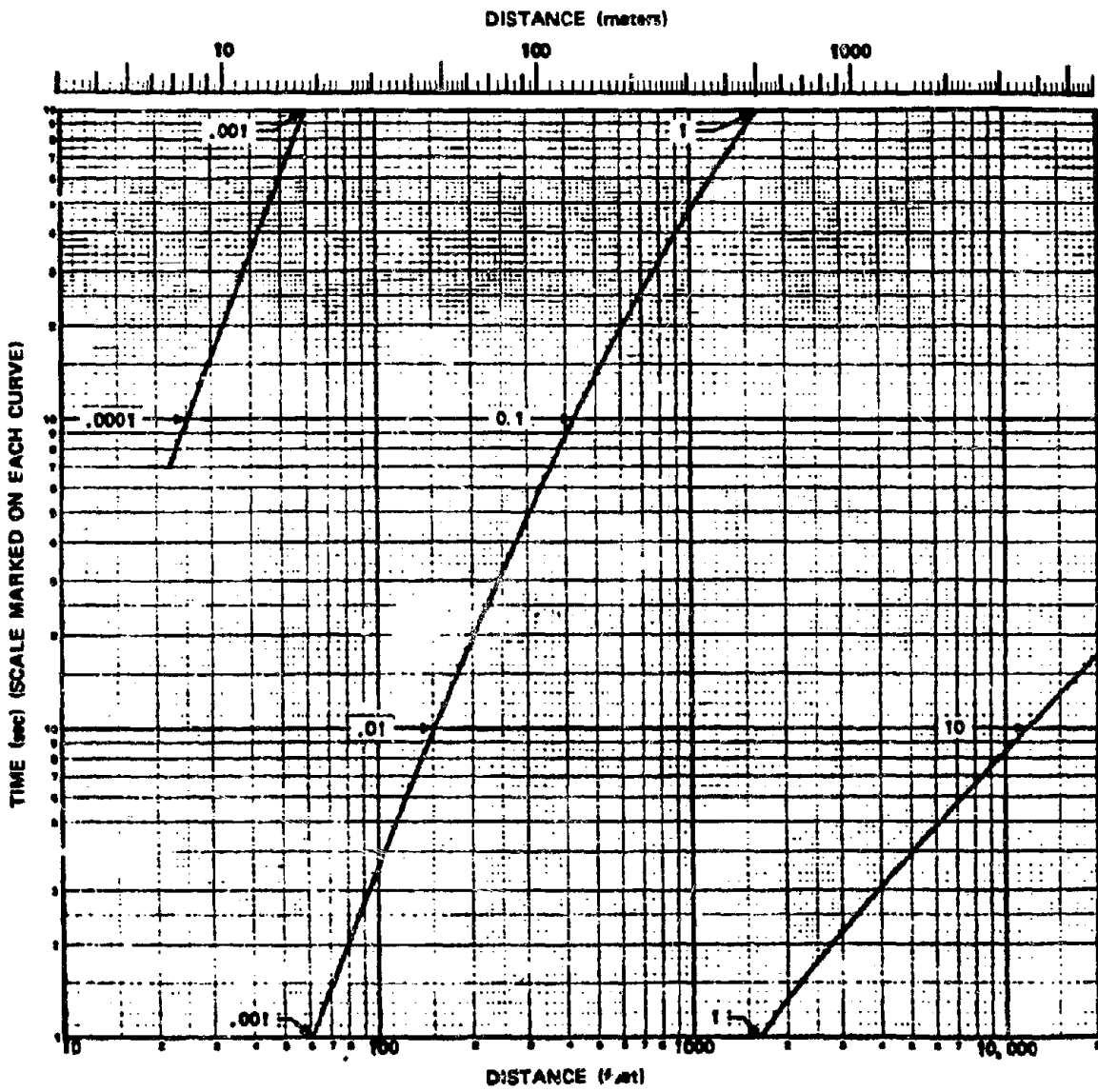
Figure 2-5. ███ Time of Arrival of the Shock Front from a 1 kt Free Air Burst in a Standard Sea Level Atmosphere ███

## Problem 2-4. Calculation of the Duration of the Positive Phase of the Overpressure and Dynamic Pressure

■ Figure 2-6 shows the durations of the positive phase of the overpressure and the dynamic pressure as a function of distance from a 1 kt free air explosion in a standard sea level atmosphere for heights of burst below 5,000 feet. For higher burst heights, this figure may be used together with the altitude scaling procedures described in paragraph 2-14. Figure 2-4 only applies to *free air* bursts. Positive phase durations at the surface should be obtained from the subsection "BLAST WAVE PHENOMENA AT THE SURFACE."

■ *Scaling.* For yields other than 1 kt, the positive phase durations scale as follows:

$$\frac{t_p^+}{t_{p1}^+} = \frac{t_q^+}{t_{q1}^+} = W^{1/3} = \frac{d}{d_1}$$

where $t_{p1}^+$ and $t_{q1}^+$ are the positive phase durations of the overpressure and the dynamic pressure, respectively, at a distance $d_1$ from a 1 kt explosion, and $t_p^+$ and $t_q^+$ are the corresponding positive phase durations at a distance $d$ from a yield of $W$ kt.

■ *Example* ■
*Given:* A 500 kt explosion in free air in a standard sea level atmosphere.

*Find:* The positive phase durations of the overpressure and the dynamic pressure at a point 8,000 feet from the explosion.

*Solution:* The corresponding distance from a 1 kt explosion is

$$d_1 = \frac{d}{W^{1/3}} = \frac{8,000}{(500)^{1/3}} = 1,000 \text{ feet.}$$

From Figure 2-6, the positive phase durations of the overpressure and the dynamic pressure at a distance of 1,000 feet from a 1 kt explosion are

$$t_{p1}^+ = 0.22 \text{ sec,}$$

$$t_{q1}^+ = 0.30 \text{ sec.}$$

*Answer:* The corresponding durations at a distance of 8,000 feet from a 500 kt explosion are

$$t_p^+ = t_{p1}^+ \times W^{1/3} = (0.22)(500)^{1/3} = 1.7 \text{ sec,}$$

$$t_q^+ = t_{q1}^+ \times W^{1/3} = (0.30)(500)^{1/3} = 2.4 \text{ sec.}$$

■ *Reliability* ■
■ Data for $t_p^+$ are derived from theoretical calculations that are supported by experimental data from bursts with yields between 1 and 50 kt. Over this range of yields, reliability is estimated to be ±15 percent. Since the accuracy of scaling to larger yields has not been confirmed experimentally, reliability is estimated to be ±30 percent for yields between 50 kt and 20 Mt. The curve may be used, with somewhat less confidence, for yields below 1 kt and above 20 Mt.

■ Data for $t_q^+$ are derived from theoretical calculations, and a few data points give limited experimental confirmation. The curve is estimated to be reliable within ±20 percent for yields between 1 and 50 kt and within ±40 percent for yields between 50 kt and 20 Mt. Outside these ranges of yields, the curve may be used with somewhat less confidence.

■ *Related Material:* See paragraph 2-10. See also paragraph 2-12 for a discussion of waveforms. See paragraph 2-27 for data concerning positive phase durations at the ground surface.
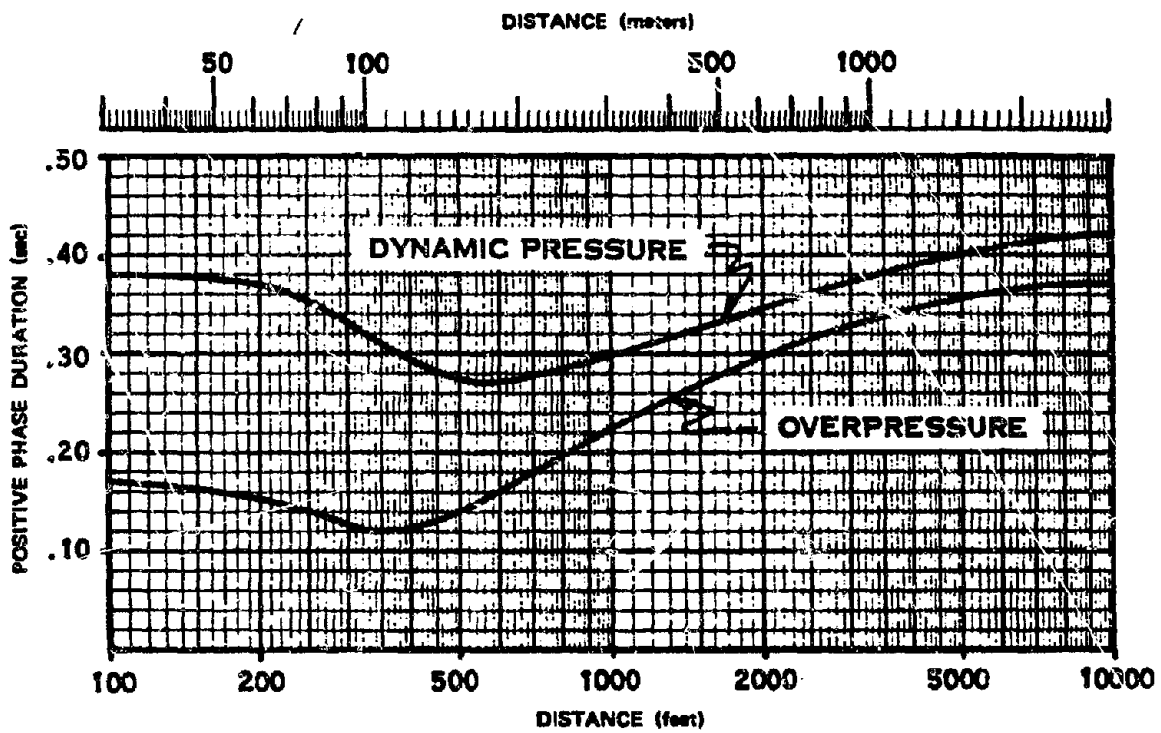
Figure 2-6. ▮ Duration of Positive Overpressure and Dynamic Pressure Phases for a 1 kt
Free Air Burst in a Standard Sea Level Atmosphere ▮

## Problem 2-5.  Calculation of Impulse

██ Figure 2-7 shows the overpressure and dynamic pressure impulse as a function of distance from a 1 kt free air explosion in a standard sea level atmosphere for heights of burst below about 5,000 feet. For higher burst heights, this figure may be used together with the altitude scaling procedures described in paragraph 2-14. Figure 2-5 applies only to *free air* bursts. Positive phase overpressure impulse should be obtained from the subsection "BLAST WAVE PHENOMENA AT THE SURFACE."

██ *Scaling.* For yields other than 1 kt, the overpressure impulse and dynamic pressure impulse scale as follows:

$$\frac{I}{I_1} = W^{1/3} = \frac{d}{d_1}$$

where $I_1$ is either the overpressure impulse or the dynamic pressure impulse at a distance $d_1$ from a 1 kt explosion, and $I$ and $d$ are the corresponding values of impulse and distance from a yield of $W$ kt. ██
██ *Example* ██
*Given:* A 400 kt explosion in free air in a standard sea level atmosphere.

*Find:* The positive phase overpressure and dynamic pressure impulses at a distance of 4,400 feet.

*Solution:* The corresponding distance from a 1 kt explosion is

$$d_1 = \frac{d}{W^{1/3}} = \frac{4,400}{(400)^{1/3}} = 600 \text{ feet.}$$

From Figure 2-7, the overpressure and dynamic pressures at a distance of 600 feet from a 1 kt explosion are

$$I_{p1} = 8.5 \text{ psi-sec,}$$

$$I_{q1} = 4.4 \text{ psi-sec.}$$

*Answer:* The corresponding impulses at a distance of 4,400 feet from a 400 kt explosion are

$$I_p = I_{p1} \times W^{1/3} = (8.5)(400)^{1/3} = 62 \text{ psi-sec,}$$

$$I_q = I_{q1} \times W^{1/3} = (4.4)(400)^{1/3} = 32 \text{ psi-sec.}$$

██ *Reliability:* Conventional practice and availability of data have favored the use of peak overpressure rather than overpressure impulse for blast wave calculations. Consequently, there have been few impulse measurements, and reliable experimental data have not been obtained. The impulse curves were obtained theoretically. The overpressure impulse data were obtained from computer code calculations (Problem M, DASA 1200, see bibliography). Values for dynamic pressure impulse were calculated from the relations of effective triangular duration described in paragraph 2-12. Overpressure impulse as shown in Figure 2-7 is estimated to be reliable within ±20 percent. No reliability estimate can be assigned to the dynamic pressure impulse curve. A portion of the latter curve is broken to indicate that measurement of waveform area is less accurate at short ranges.

██ *Related Material:* See paragraph 2-11. See also paragraphs 2-13 through 2-15 for scaling to altitudes up to 40,000 feet. See paragraph 2-28 for a discussion of positive phase overpressure impulse along the surface of the earth.
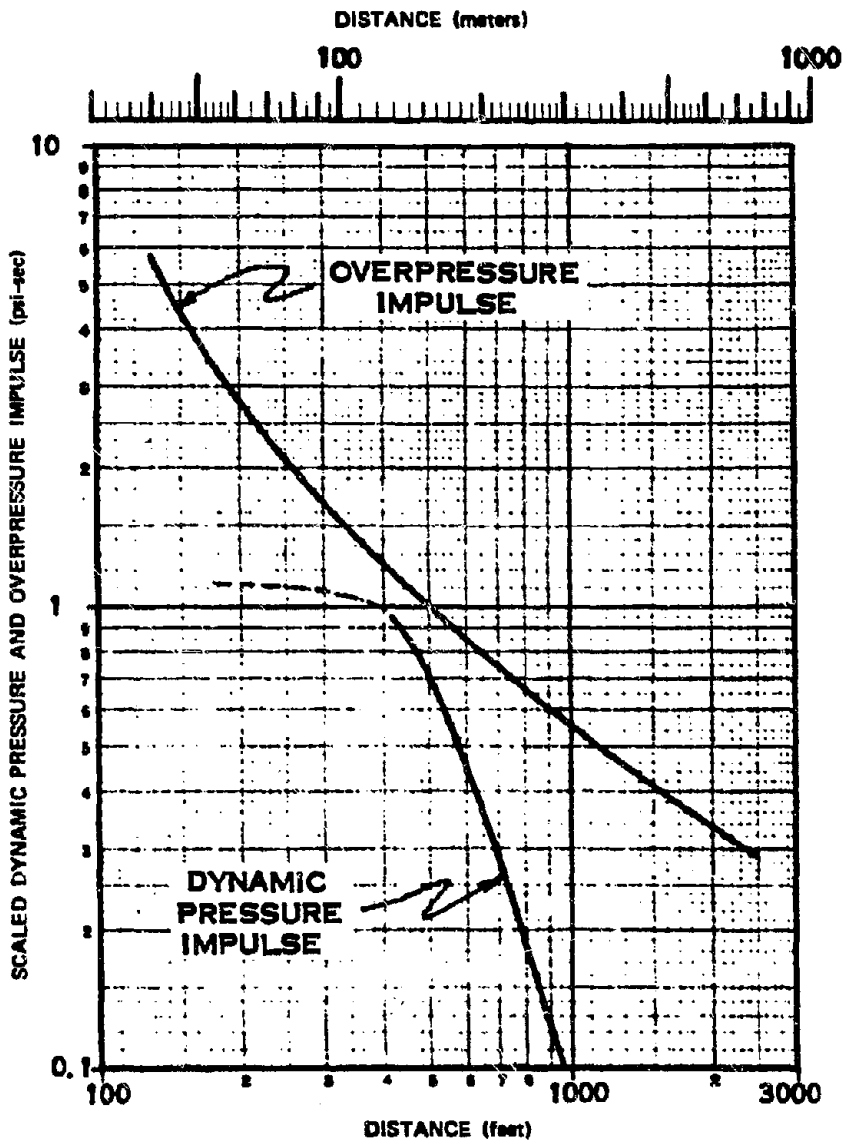
Figure 2-7. ▮ Overpressure and Dynamic Pressure Impulse from 1 kt Free Air Burst in a Standard Sea Level Atmosphere ▮

## 2-12 Waveforms

Damage inflicted to a target by a blast wave generally is a complex function of peak overpressure, peak dynamic pressure, pulse durations, and structural response characteristics of the target. Usually, all details of the method by which a target interacts with a blast wave are not identified. The strength of the blast wave that will damage the target generally is specified in terms of a pair of parameters. For example, weapon yield and peak overpressure, distance and peak overpressure, or peak overpressure and positive-phase duration are, for an ideal blast wave, adequate to specify uniquely all properties of the blast wave. If a blast wave, so defined, is found by experiment to damage a certain target, further analysis of the interaction usually is not necessary.

This discussion of waveforms and the preceding discussion of impulse are not included so much to provide a basis for calculations as to provide an understanding of blast wave phenomena.

At a given point in space, the rate of decay of overpressure after the shock front passes depends on the peak overpressure. Overpressure waveforms are shown in Figure 2-8 in terms of normalized coordinates. The overpressure at a given time is expressed as a fraction of peak overpressure, and time is expressed as a function of positive phase duration. These normalized variables are $\Delta p(t)/\Delta p$ and $t/t_p^+$, where $\Delta p(t)$ and $t$ are instantaneous values of overpressure and time, $\Delta p$ is peak overpressure, and $t_p^+$ is the positive phase duration of the overpressure. Similarly, dynamic pressure waveforms are shown in Figure 2-9 in terms of the normalized variables for dynamic pressure, $q(t)/q$, where $q(t)$ is the instantaneous value of dynamic pressure and $q$ is the peak value, and normalized time $t/t_q^+$. Note that, since dynamic pressure duration is longer than overpressure duration, Fig-

ures 2-8 and 2-9 do not have a common time base.

Both sets of waveforms show that close to the burst, where peak pressures are high, the pressure drops rapidly from its peak value. At greater distances and lower peak pressures, the drop in pressure is slower, and the waveform is much broader. This broadening of the pressure pulse with distance has more influence on effective pulse duration than changes in $t_p^+$ and $t_q^+$ have. At any specified distance, dynamic pressure decays more rapidly than overpressure for a given yield.

For low values of peak overpressure and peak dynamic pressure, the variation of pressure with time behind the shock front may be approximated by the equations

$$\Delta p(t) = \Delta p(1 - t/t_p^+)e^{-t/t_p^+}$$

$$q(t) = q(1 - t/t_q^+)^2 e^{-2t/t_q^+}.$$

These equations correspond most nearly to the 7.5 psi overpressure curve and the 7.5 psi dynamic pressure curve. They may be used with reasonable accuracy for peak pressures of 0 to 25 psi.

In damage estimates, it is frequently useful to approximate the actual shock waveform by the equivalent triangular waveform, which is defined as one that has the same peak amplitude and the same area as the actual waveform, but has a triangular shape and a shorter time duration than the actual waveform. Since the equivalent triangular waveform has the same area as the actual waveform, it represents the same impulse. The time duration of this equivalent waveform is obtained by multiplying actual time duration by the triangular duration correction factor $C_t$, which is shown in Figure 2-10 separately for overpressure and dynamic pressure.
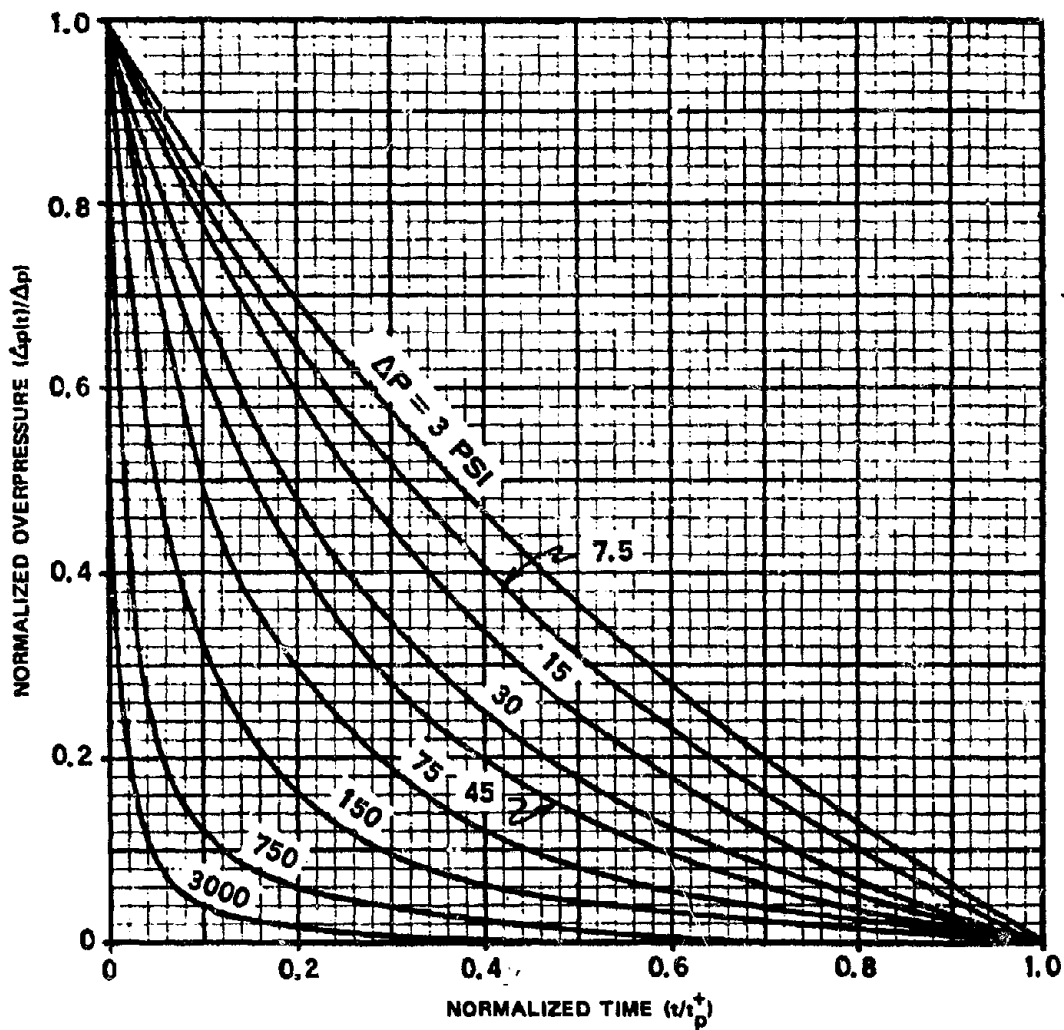
Figure 2-8.  ▇  Positive Overpressure Waveforms for an Ideal Shock Wave in a Standard Sea Level Atmosphere ▇
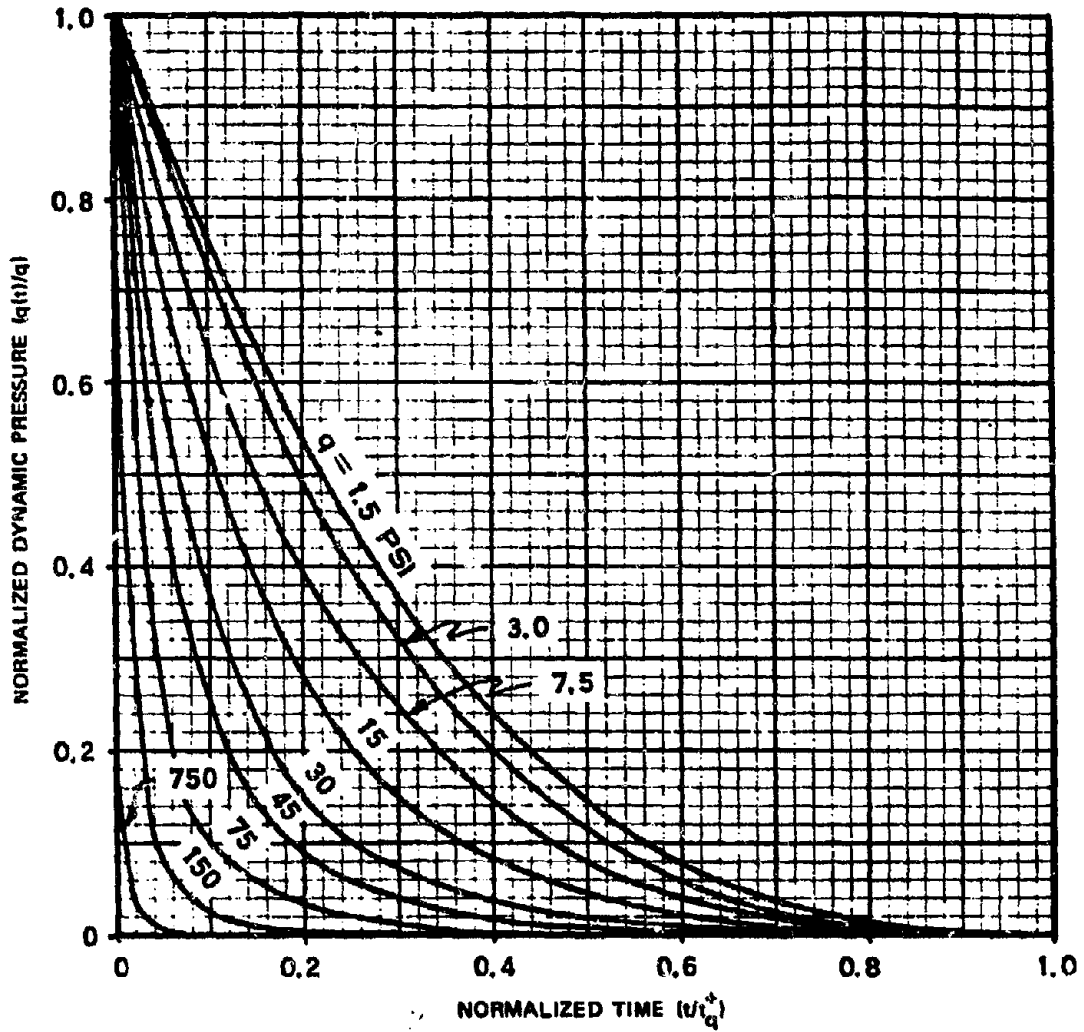
Figure 2-9. Positive Dynamic Pressure Waveforms for an Ideal Shock Wave in a Standard Sea Level Atmosphere
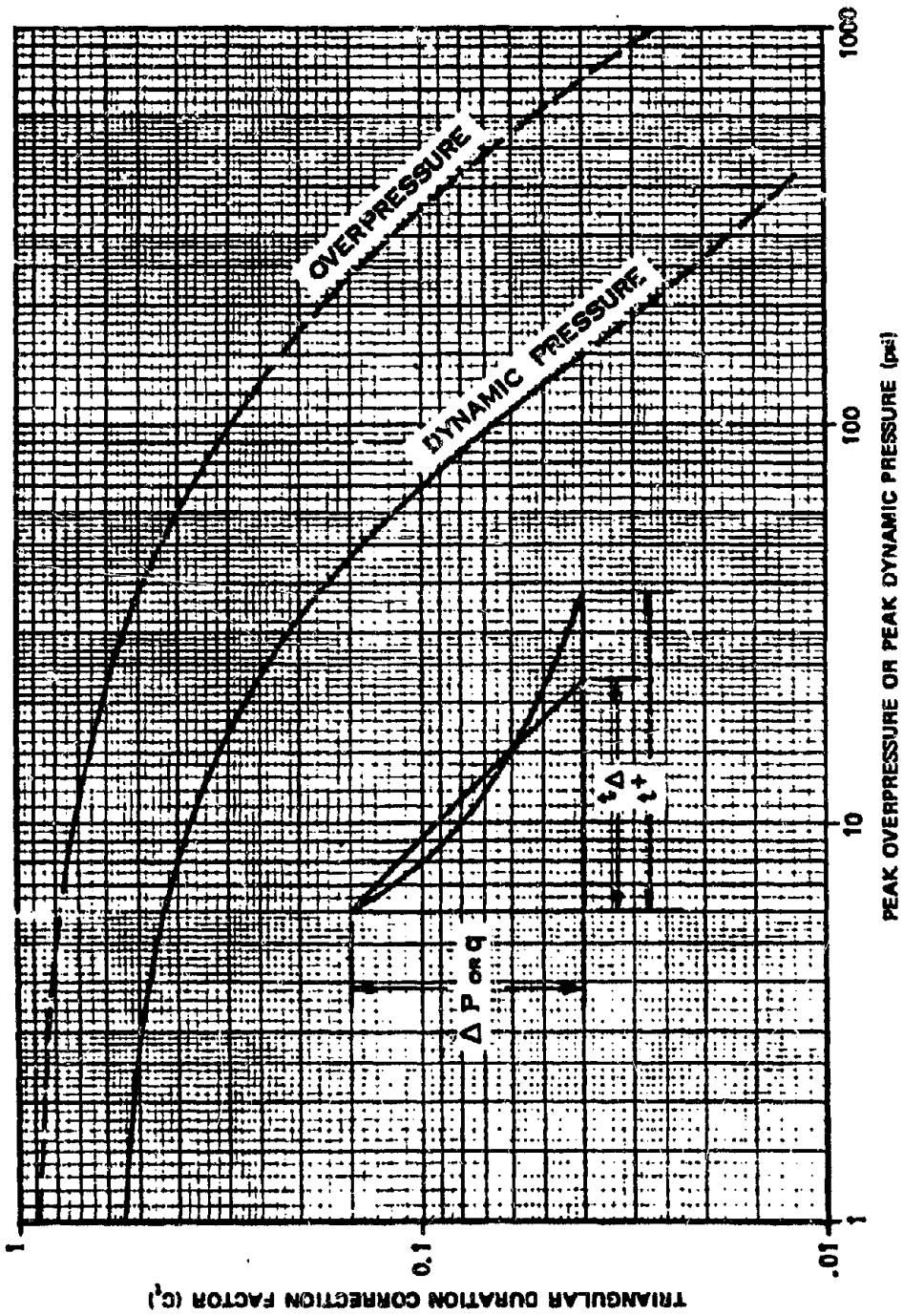
Figure 2-10. Effective Triangular Duration Correction Factors $(t\Delta = C_t t_p^+ \text{ or } t\Delta = C_t t_q^+)$

The time duration of the equivalent waveform is called the effective triangular duration of the pressure pulse, $t_\Delta$, where

$$t_\Delta = C_{tp} t_p^+ \quad \text{or} \quad t_\Delta = C_{tq} t_q^+$$

for overpressure and dynamic pressure, respectively.

The curves shown in Figures 2-8 and 2-9 are based on theory, and specific estimates of the amount by which actual blast waveforms can be expected to deviate from these curves cannot be made. The effective triangular waveform obtained by use of the triangular duration correction factors shown in Figure 2-10 are simplified representations of the actual waveforms. These triangular waveforms do not represent structural loading functions. The latter are described in Section II, Chapter 9, and specific loading functions used in some of the structural damage analyses for this manual are shown in Figure 11-1.

## RELATIONS BETWEEN SHOCK FRONT PARAMETERS

### 2-13 Generalized Scaling

The concept of scaling various blast wave parameters was introduced in the preceding subsection with reference to the corresponding parameter from a 1 kt explosion in a standard sea level atmosphere. The various curves were presented in terms of absolute values of distance, time, or impulse from a 1 kt explosion in free air in a standard sea level atmosphere. This convention of presenting the data in terms of a 1 kt explosion with scaling laws to relate the parameters to other yields will be adhered to in subsequent sections of this chapter as well as in succeeding chapters; however, the scaling laws are not necessarily limited to scaling from 1 kt. The "Sachs" scaling laws, which pertain to scaling of blast parameters, depend only on the rela-

tive yields of two weapons being considered. Thus, the distance scaling law given in Problems 2-1 and 2-2 could be written

$$\frac{d_2}{d_1} = \left(\frac{W_2}{W_1}\right)^{1/3},$$

where $d_2$ is the slant range (distance from the point of burst) from an explosion of $W_2$ kilotons and $d_1$ is the corresponding distance from an explosion of $W_1$ kilotons. Likewise, the time and impulse scaling laws given in Problems 2-3 through 2-5 could be written

$$\frac{t_2}{t_1} = \left(\frac{W_2}{W_1}\right)^{1/3}$$

$$\frac{t_{p2}^+}{t_{p1}^+} = \frac{t_{q2}^+}{t_{q1}^+} = \left(\frac{W_2}{W_1}\right)^{1/3},$$

and

$$\frac{I_2}{I_1} = \left(\frac{W_2}{W_1}\right)^{1/3},$$

where, in each case the subscript 2 refers to the value of the parameter for yield $W_2$ kt, and the subscript 1 refers to the value of the same parameter for a yield of $W_1$ kt. As mentioned above, $W_1$ will generally be taken to equal 1 kt as a matter of convenience in this manual.

The scaling laws are derived from the assumption that, at corresponding stages of development, the fireballs from two different nuclear explosions have the same energy per unit mass of air at points that are the same scaled distance from the point of burst. It is also assumed that, as the blast waves propagate outward from the fireballs, they maintain this property of equal energy densities at equal scaled

radii. The blast waves produced by two different nuclear explosions are thus assumed to be similar in all respects except for those relating to differences in size. Since, at a particular stage of development, the average energy densities throughout the two fireballs are equal, fireball volume is directly proportional to the amount of energy required to produce it; therefore, fireball radius is proportional to the cube root of the nuclear yield. Other pertinent distances, such as shock front radius, also follow this cube root scaling law.

## 2-14 Altitude Scaling ▇▇▇

▇ At higher altitudes, where air density is less than at sea level, the reasoning described above still applies. At equal scaled distances and —corresponding times, equal masses of air contain equal amounts of energy. Therefore, the volume of a sphere needed to contain a given amount of energy in this manner is larger at higher altitudes where the air is thinner. Specifically, this volume is inversely proportional to air density; and corresponding radii are inversely proportional to the cube root of air density. However, better results are obtained by scaling distance with the cube root of the ambient pressure (up to altitudes of 40,000 feet).* The altitude scaling for distance is

$$\frac{d_2}{d_1} = \left(\frac{W_2}{W_1}\right)^{1/3} \left(\frac{P_o}{P}\right)^{1/3},$$

where $P_o$ is the sea level ambient pressure, $P$ is the ambient pressure at the altitude of interest, and the other quantities are as previously defined.

▇ No pressure scaling factor is required for explosions in a standard sea level atmosphere since the effect of yield is taken into account by distance scaling, and, under similar ambient conditions, the pressures generated by explosions of different yields are equal at scaled distances.

When altitude must be considered, equal "shock strengths" occur at equal scaled distances. The term shock strength means the ratio of the absolute pressure behind the front to the ambient pressure, i.e., the shock strength, $\xi$ is,

$$\xi = \frac{\Delta p + P}{P} = \frac{\Delta p}{P} + 1,$$

which is a dimensionless quantity. At equal scaled distances,

$$\xi = \xi_o,$$

where $\xi$ is the shock strength at the altitude of interest and $\xi_o$ is the shock strength at the same scaled distance at sea level. This may be written

$$\frac{\Delta p}{P} + 1 = \frac{\Delta p_o}{P_o} + 1,$$

which leads to

$$\frac{\Delta p}{P} = \frac{\Delta p_o}{P_o},$$

---

*▇ The reasons for dismissing density in favor of pressure as a basis for calculating the altitude scaling factor for distance may be described as follows. In the early fireball region, where energy absorbed from the weapon completely overshadows any effect of initial air temperature, it would be expected that the only important question is the number of air atoms present. In this region, density scaling is appropriate. Examples of equations that are based on density scaling are given in paragraph 2-44; however, the situation is different over most of the range through which the blast wave propagates. Shock-front parameters correspond more directly to the pressure ratio across the shock front than to the density ratio. After the shock front reaches air not directly heated by the nuclear source, pressure ratio provides the better basis for scaling. The corresponding energy model for Sachs' scaling laws is that two free air blast waves are equivalent when the ratio:

$$\frac{\text{energy enclosed by the shock front}}{\text{ambient internal energy of the air enclosed by the front}}$$

is the same for both blast waves. This model may be derived by noting that the pressure of an ideal gas is proportional to internal energy per unit volume.

2-22

and the altitude scaling for pressure is

$$\frac{\Delta p}{\Delta p_0} = \frac{P}{P_0},$$

where $\Delta p$ is the overpressure at the altitude of interest, $\Delta p_0$ is the overpressure at the same scaled distance at sea level, and $P$ and $P_0$ are the corresponding ambient pressures. This same relation holds for other characteristic pressures, such as the total pressure behind the shock front and the dynamic pressure.

Two factors influence time of arrival: the speed of the blast wave and the distance that it must travel. Under standard sea level conditions, the speed of the blast wave depends on overpressure, which, in turn, depends only on scaled distance from the burst. When the scaling problem is not limited to the case of a sea level atmosphere, the assumed relation between shock speed and overpressure must be stated in more general terms: for a given shock strength (and hence for a given scaled distance), the Mach number of the shock front is always the same. As altitude is increased, the time required for the shock to reach a given scaled distance increases because (1) the actual distance is farther and (2) at the lower temperatures generally associated with higher altitudes, sound speed is slower (therefore, a given Mach number corresponds to a slower shock front speed). The altitude scaling for time is

$$\frac{t_2}{t_1} = \left(\frac{W_2}{W_1}\right)^{1/3} \left(\frac{P_0}{P}\right)^{1/3} \left(\frac{T_0}{T}\right)^{1/2},$$

where $T_0$ is the absolute temperature at sea level and $T$ is the absolute temperature at the altitude of interest. The factor $T_0^{1/2}/T^{1/2}$ appears in this expression because sound speed is proportional to the square root of absolute temperature. The factors involving yield and pressure are those in scaling distance. The same scaling rela-

tionships may be used for scaling the positive duration of the overpressure.

The altitude scaling for impulse may be obtained by multiplying the scaling equation for time by the scaling equation for pressure, i.e.,

$$\frac{I_2}{I_1} = \left(\frac{W_2}{W_1}\right)^{1/3} \left(\frac{P}{P_0}\right)^{2/3} \left(\frac{T_0}{T}\right)^{1/2}.$$

In the foregoing scaling relations, the subscript o was defined to represent ambient conditions (pressure or absolute temperature) at sea level. Strictly speaking this is not necessary, since the ratios of the values are the important quantities. However, since these equations are for use with the curves presented in the previous subsection, which are all shown for standard sea level conditions, it is convenient to scale from those conditions. In order to facilitate calculations based on the preceding equations, the following factors have been defined and are tabulated in Tables 2-1 and 2-2:

$$S_d = \left(\frac{P_0}{P}\right)^{1/3}$$

$$S_p = \frac{P}{P_0}$$

$$S_t = \left(\frac{P_0}{P}\right)^{1/3} \left(\frac{T_0}{T}\right)^{1/2},$$

so that if, as usual, $W_1$ is taken to be 1 kt, the equations may be shown in an abbreviated form as follows:

$$d = d_1 W^{1/3} S_d$$

$$\Delta p = \Delta p_0 S_p$$

$$q = q_0 S_p$$

$$t = t_1 W^{1/3} S_t$$

$$I = I_1 W^{1/3} S_p S_t.$$

Table 2-1. ███ Data Based on U.S. Standard Atmosphere, 1962 English Units ███

| Altitude feet | Temperature °F | Pressure psi | Altitude Scaling Factors | | | Density Ratio[*] $\rho/\rho_0$ | Temperature Ratio $T/T_0$ | Sound Speed ft/sec |
|---|---|---|---|---|---|---|---|---|
| | | | $S_d$ | $S_p$ | $S_t$ | | | |
| 0 | 59.0 | 14.696 | 1.000 | 1.0000 | 1.000 | 1.0000 | 1.000 | 1116 |
| 1 000 | 55.4 | 14.17 | 1.012 | .9644 | 1.016 | .9711 | .993 | 1113 |
| 2 000 | 51.9 | 13.66 | 1.025 | .9298 | 1.032 | .9428 | .986 | 1109 |
| 3 000 | 48.3 | 13.17 | 1.037 | .8963 | 1.048 | .9151 | .979 | 1105 |
| 4 000 | 44.7 | 12.69 | 1.050 | .8637 | 1.065 | .8881 | .973 | 1101 |
| 5 000 | 41.2 | 12.23 | 1.063 | .8321 | 1.082 | .8617 | .966 | 1097 |
| 10 000 | 23.4 | 10.11 | 1.133 | .6878 | 1.174 | .7386 | .931 | 1077 |
| 15 000 | 5.5 | 8.297 | 1.210 | .5646 | 1.278 | .6295 | .897 | 1057 |
| 20 000 | -12.3 | 6.759 | 1.295 | .4599 | 1.395 | .5332 | .863 | 1037 |
| 25 000 | -30.0 | 5.461 | 1.391 | .3716 | 1.528 | .4486 | .828 | 1016 |
| 30 000 | -47.8 | 4.373 | 1.498 | .2975 | 1.681 | .3747 | .794 | 995 |
| 35 000 | -65.6 | 3.468 | 1.618 | .2360 | 1.857 | .3106 | .760 | 973 |
| 40 000 | -69.7 | 2.730 | 1.753 | .1858 | 2.021 | .2471 | .752 | 968 |
| 45 000 | -69.7 | 2.149 | 1.898 | .1462 | 2.189 | .1945 | .752 | 968 |
| 50 000 | -69.7 | 1.692 | 2.056 | .1151 | 2.371 | .1531 | .752 | 968 |
| 55 000 | -69.7 | 1.332 | 2.226 | .09063 | 2.567 | .1206 | .752 | 968 |
| 60 000 | -69.7 | 1.049 | 2.411 | .07137 | 2.780 | .09492 | .752 | 968 |
| 65 000 | -69.7 | .826 | 2.611 | .05620 | 3.011 | .07475 | .752 | 968 |
| 70 000 | -67.4 | .651 | 2.826 | .04429 | 3.250 | .05857 | .756 | 971 |
| 75 000 | -64.7 | .514 | 3.058 | .03496 | 3.504 | .04591 | .762 | 974 |
| 80 000 | -62.0 | .406 | 3.307 | .02765 | 3.777 | .03606 | .767 | 978 |
| 85 000 | -59.3 | .322 | 3.574 | .02190 | 4.068 | .02837 | .772 | 981 |
| 90 000 | -56.5 | .255 | 3.861 | .01738 | 4.379 | .02236 | .777 | 984 |
| 95 000 | -53.8 | .203 | 4.168 | .01381 | 4.711 | .01765 | .782 | 988 |
| 100 000 | -51.1 | .162 | 4.497 | .01100 | 5.067 | .01396 | .788 | 991 |
| 110 000 | -41.3 | .103 | 5.225 | 7.011-3 | 5.817 | 8.692-3 | .807 | 1003 |
| 120 000 | -26.1 | .0667 | 6.040 | 4.537 | 6.607 | 5.428 | .836 | 1021 |
| 130 000 | -10.9 | .0438 | 6.948 | 2.982 | 7.470 | 3.446 | .865 | 1038 |
| 140 000 | 4.3 | .0292 | 7.953 | 1.988 | 8.410 | 2.222 | .894 | 1056 |
| 150 000 | 19.4 | .0197 | 9.064 | 1.343 | 9.431 | 1.454 | .924 | 1073 |
| 160 000 | 27.5 | .0135 | 10.29 | 9.176-4 | 10.62 | 9.770-4 | .939 | 1082 |
| 170 000 | 27.5 | 9.23-3 | 11.68 | 6.283 | 12.05 | 6.690 | .939 | 1082 |
| 180 000 | 18.9 | 6.31 | 13.26 | 4.292 | 13.80 | 4.652 | .923 | 1072 |
| 190 000 | 8.1 | 4.27 | 15.09 | 2.908 | 15.89 | 3.225 | .902 | 1060 |
| 200 000 | -2.7 | 2.87 | 17.23 | 1.954 | 18.36 | 2.217 | .881 | 1048 |

NOTE: 7.011-3 means $7.011 \times 10^{-3}$

[*] $\rho_0 = 2.38 \times 10^{-3}$ slugs/ft$^3$
    $= 7.65 \times 10^{-2}$ lbs/ft$^3$

**Table 2-2.** ██ Data Based on U.S. Standard Atmosphere, 1962 Metric Units ██

| Altitude km | Temperature °C | Pressure | | Altitude Scaling Factors | | | Density Ratio* $\rho/\rho_0$ | Temperature Ratio $T/T_0$ | Sound Speed m/sec |
|---|---|---|---|---|---|---|---|---|---|
| | | millibars | psi | $S_d$ | $S_p$ | $S_t$ | | | |
| 0 | 15.0 | 1013.25 | 14.696 | 1.000 | 1.0000 | 1.000 | 1.000 | 1.000 | 340.3 |
| .5 | 11.8 | 954.61 | 13.845 | 1.020 | .9421 | 1.026 | .953 | .989 | 338.4 |
| 1.0 | 8.5 | 898.76 | 13.035 | 1.041 | .8870 | 1.053 | .907 | .977 | 336.4 |
| 1.5 | 5.3 | 845.60 | 12.264 | 1.062 | .8345 | 1.081 | .864 | .966 | 334.5 |
| 2.0 | 2.0 | 795.01 | 11.531 | 1.084 | .7846 | 1.110 | .822 | .955 | 332.5 |
| 3.0 | -4.5 | 701.21 | 10.170 | 1.131 | .6920 | 1.171 | .742 | .932 | 328.6 |
| 4.0 | -11.0 | 616.60 | 8.943 | 1.180 | .6085 | 1.237 | .669 | .910 | 324.6 |
| 5.0 | -17.5 | 540.48 | 7.839 | 1.233 | .5334 | 1.309 | .601 | .887 | 320.5 |
| 6.0 | -24.0 | 472.18 | 6.848 | 1.290 | .4660 | 1.387 | .539 | .865 | 316.5 |
| 7.0 | -30.4 | 411.05 | 5.962 | 1.351 | .4057 | 1.472 | .482 | .842 | 312.3 |
| 8.0 | -36.9 | 356.52 | 5.171 | 1.416 | .3519 | 1.564 | -.429 | .820 | 308.1 |
| 9.0 | -43.4 | 308.01 | 4.467 | 1.487 | .3040 | 1.666 | .381 | .797 | 303.8 |
| 10 | -49.9 | 265.00 | 3.843 | 1.564 | .2615 | 1.777 | .338 | .775 | 299.5 |
| 12 | -56.5 | 193.99 | 2.814 | 1.735 | .1915 | 2.001 | .255 | .752 | 295.1 |
| 14 | -56.5 | 141.70 | 2.055 | 1.927 | .1399 | 2.222 | .186 | .752 | 295.1 |
| 16 | -56.5 | 103.53 | 1.502 | 2.139 | .1022 | 2.467 | .136 | .752 | 295.1 |
| 18 | -56.5 | 75.65 | 1.097 | 2.375 | .07466 | 2.739 | .0993 | .752 | 295.1 |
| 20 | -56.5 | 55.29 | .802 | 2.636 | .05457 | 3.040 | .0726 | .752 | 295.1 |
| 22 | -54.6 | 40.47 | .587 | 2.925 | .03995 | 3.359 | .0527 | .759 | 296.4 |
| 24 | -52.6 | 29.72 | .431 | 3.243 | .02933 | 3.706 | .0383 | .765 | 297.7 |
| 26 | -50.6 | 21.88 | .317 | 3.591 | .02160 | 4.086 | .0280 | .772 | 299.1 |
| 28 | -48.6 | 16.16 | .234 | 3.973 | .01595 | 4.500 | .0205 | .779 | 300.4 |
| 30 | -46.6 | 11.97 | .174 | 4.391 | .01181 | 4.952 | .0150 | .786 | 301.7 |
| 32 | -44.7 | 8.89 | .129 | 4.848 | 8.774-3 | 5.445 | .0111 | .793 | 303.0 |
| 34 | -39.4 | 6.63 | .0962 | 5.345 | 6.547 | 5.935 | 8.07-3 | .811 | 306.5 |
| 36 | -33.9 | 4.99 | .0723 | 5.880 | 4.920 | 6.452 | 5.92 | .830 | 310.1 |
| 38 | -28.3 | 3.77 | .0547 | 6.453 | 3.722 | 7.000 | 4.38 | .850 | 313.7 |
| 40 | -22.8 | 2.87 | .0416 | 7.067 | 2.834-3 | 7.581 | 3.26-3 | .869 | 317.2 |
| 42 | -17.3 | 2.20 | .0319 | 7.723 | 2.171 | 8.196 | 2.44 | .888 | 320.7 |
| 44 | -11.7 | 1.69 | .0246 | 8.424 | 1.673 | 8.844 | 1.84 | .907 | 324.1 |
| 46 | -6.2 | 1.31 | .0190 | 9.171 | 1.296 | 9.529 | 1.40 | .926 | 327.5 |
| 48 | -2.5 | 1.02 | .0148 | 9.968 | 1.010 | 10.29 | 1.07 | .939 | 329.8 |
| 50 | -2.5 | .798 | .0116 | 10.83 | 7.874-4 | 11.17 | 8.38-4 | .939 | 329.8 |
| 52 | -2.5 | .622 | .00903 | 11.76 | 6.141 | 12.14 | 6.54 | .939 | 329.8 |
| 54 | -5.6 | .485 | .00703 | 12.78 | 4.786 | 13.27 | 5.15 | .929 | 327.9 |
| 56 | -9.5 | .377 | .00546 | 13.91 | 3.716 | 14.54 | 4.06 | .915 | 325.5 |
| 58 | -13.5 | .291 | .00423 | 15.15 | 2.876 | 15.96 | 3.19 | .901 | 323.1 |
| 60 | -17.4 | .225 | .00326 | 16.52 | 2.217-4 | 17.54 | 2.50-4 | .888 | 320.6 |

NOTE: 8.774-3 means 8.774 x $10^{-3}$

*$\rho_0$ = 1.225 x $10^{-3}$ gm/cm$^3$ = 1.225 kg/m$^3$.

The use of other factors shown in Tables 2-1 and 2-2 will be explained in succeeding paragraphs. Figure 2-11 shows a curve for each of the scaling factors as a function of altitude, and thus presents the continuous variation of the scaling factors rather than the variation with incremental steps in altitude as provided in Tables 2-1 and 2-2.

Although $S_d$, $S_p$, and $S_t$ are called altitude scaling factors, their use is not limited to correcting for differences in altitude. Even if a burst occurs at sea level, $S_d$ and $S_p$ are affected by barometric pressure variations (typically these variations are ±5 percent), and $S_t$ is affected by temperature variations. When experimental data are analyzed, the actual pressure and temperature at the time of burst ordinarily are known and may be used in calculating the scaling factors. On the other hand, predictions of nuclear effects often must be made without any knowledge of what the weather will be when the burst occurs. In this case, $S_d$, $S_p$, and $S_t$ are usually based on handbook values of temperature and pressure, which are functions of altitude only as shown in Tables 2-1 and 2-2 and in Figure 2-11.

To this point, nothing has been said about differences between burst altitude and target altitude. The explanation has been presented as though the blast wave were propagating from burst to target through a uniform atmosphere. For many problems this assumption is essentially correct, but for long ranges the source and the target may be at entirely different altitudes and the scaling factors may vary appreciably over the path traveled by the blast wave. When this complication arises the altitude scaling factors are calculated on the basis of target altitude (i.e., for the altitude at the point in space where overpressure etc. are to be determined) rather than on the basis of burst altitude. Basic physical concepts fail to explain in a simple manner why this choice is made. This method, called "modified Sachs scaling," is used because it comes closer to giving answers that agree with experimental data.
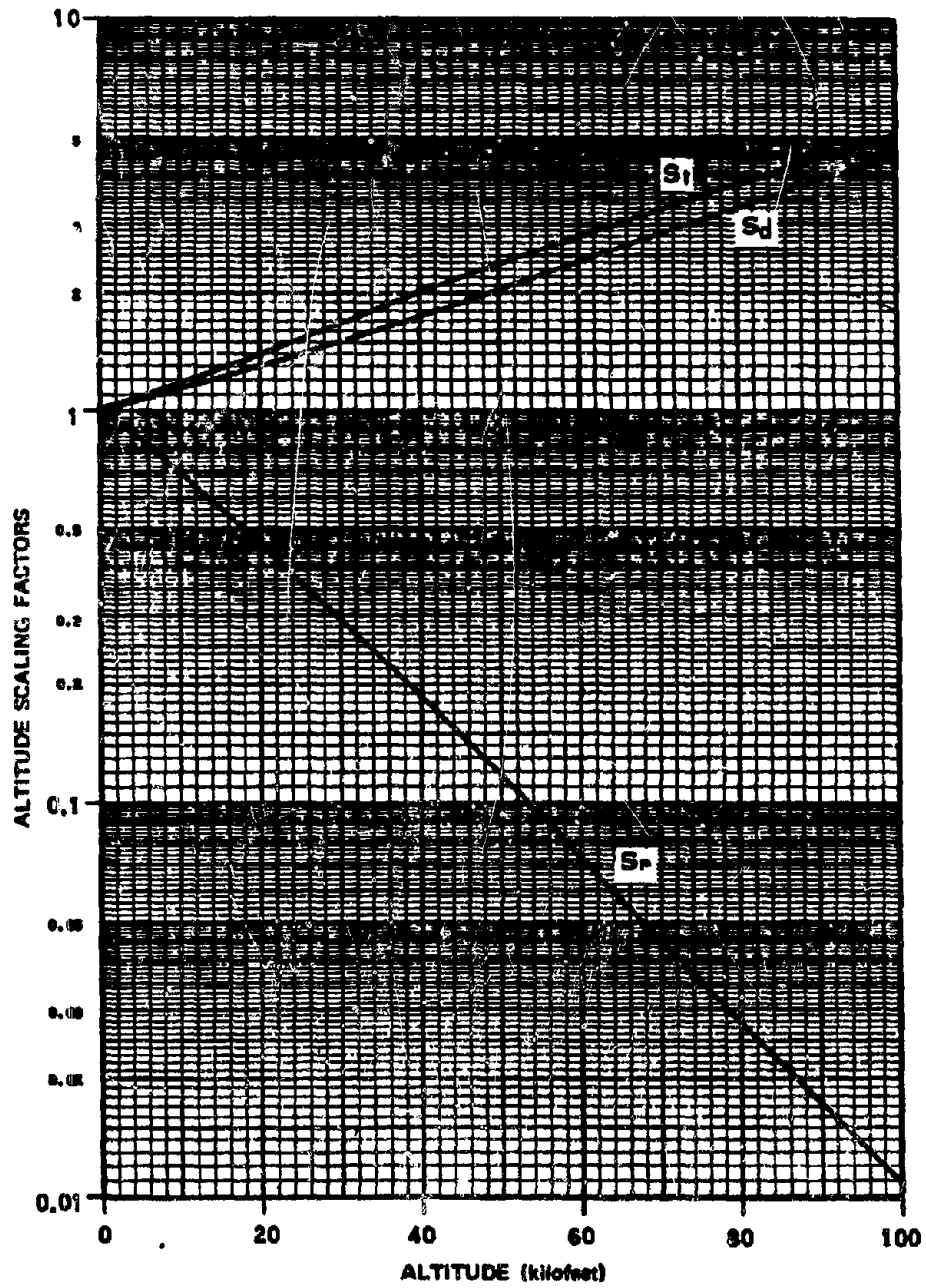
Figure 2-11. ██ Altitude Scaling Factors for
Blast Wave Calculations ██

## Problem 2-6. Calculation of Free Air Blast Parameters at Altitudes up to 40,000 Feet

█ The scaling factors presented in paragraph 2-14 may be used to scale the data from the curves for free air explosions in a sea level atmosphere presented in Figures 2-2 through 2-7 to higher altitudes. As mentioned in the last paragraph of 2-14, the scaling factors for the point of interest (target) are the factors to be used in making altitude corrections rather than the scaling factors for the burst altitude. These scaling factors apply to explosions or targets at altitudes up to 40,000 feet. The effective blast yield is reduced for explosions above about 40,000 feet, and, while the altitude scaling factors still may be applied, the reduced yield must be used in the scaling, as described in paragraph 2-42.

█ *Example* █

*Given:* A 100 kt explosion at an altitude of 20,000 feet.

*Find:* The maximum altitude of a target directly below the explosion such that the target will not experience a peak overpressure exceeding 7 psi, and the peak dynamic pressure that the target might be expected to receive.

*Solution:* Since the target altitude is unknown, and since the altitude scaling factors should be applied for the target altitude, an approximate solution is obtained first by using the low altitude distance scaling law. From Figure 2-2, an overpressure of 7 psi will extend to 1,000 feet for low altitude explosions. From the scaling provided in Problem 2-1, the corresponding distance from a 100 kt explosion is

$$d = d_1 W^{1/3} = (1,000)(100)^{1/3} = 4,640 \text{ feet.}$$

The approximate target altitude is

$$20,000 - 4,460 \approx 15,400 \text{ feet.}$$

This target altitude will be used to determine the altitude scaling factors. It may prove to be an adequate basis for determining altitude scaling factors; if not, successive approximations must be used. From Table 2-1,

$$S_d = 1.22$$

$$S_p = 0.56.$$

From the pressure scaling equation in paragraph 2-14,

$$\Delta p_0 = \frac{\Delta p}{S_p} = \frac{7}{0.56} = 12.5 \text{ psi.}$$

To account for the uncertainty of blast predictions (see Reliability, Problem 2-1), this overpressure is assigned of 12.5 ± 15 percent; i.e., it lies between 10.6 and 14.4 psi. Figure 2-2 shows that the corresponding scaled (1 kt) distance are between 840 and 725 feet. The corresponding distances from a 100 kt explosion are

$$d = d_1 W^{1/3} S_d = (840)(100)^{1/3}(1.22)$$
$$= 4,800 \text{ feet,}$$

and

$$d = d_1 W^{1/3} S_d = (725)(100)^{1/3}(1.22)$$
$$= 4,100 \text{ feet.}$$

The approximate target altitude is thus between

$$20,000 - 4,760 = 15,200 \text{ feet, and}$$

$$20,000 - 4,100 = 15,900 \text{ feet.}$$

Neither of these altitudes is sufficiently different from 15,400 feet to warrant repeating the calculation with new altitude scaling factors. In order

to insure that the peak overpressure will not exceed 7 psi, the lower altitude (greater distance from the explosion) is taken as the accepted altitude. For an actual distance of 4,800 feet, and a scaled distance of 725 feet (as determined above), the peak dynamic pressure obtained from Figure 2-4 is 4.6 psi. From the pressure scaling equation of paragraph 2-14,

$$q = q_o S_p = (4.6)(0.56) = 2.6 \text{ psi.}$$

The uncertainty in peak dynamic pressure is ±15 percent, therefore, the peak dynamic pressure is expected to fall between 2.2 and 3.0 psi.

*Answer:* The maximum altitude of a target directly below a 100 kt explosion at 20,000 feet such that the target will not experience an overpressure exceeding 7 psi is 15,200 feet. The peak dynamic pressure incident on the target will be between 2.2 and 3.0 psi, with an expected value of 2.6 psi.

*Note:* If the altitude at which the target would be assured of receiving at least 7 psi overpressure had been desired, an altitude of 15,900 feet would have been selected as the answer.

## 2-15 Velocity and Density █

█ For most blast-wave calculations, peak overpressure and peak dynamic pressure provide a satisfactory description of the shock front; but in a few situations a more detailed description is required. An example is the problem of dynamic pressure acting on a moving target. For this problem, the dynamic pressure data presented in paragraph 2-8 and Problem 2-2 cannot be used; instead, the dynamic pressure must be calculated from its defined value,

$$q = \frac{1}{2} \rho_s u^2 ,$$

where $u$ is peak wind velocity with respect to the target. To calculate this velocity, the peak wind velocity with respect to the ambient air must be evaluated first. This velocity may be calculated from the equation

$$u = \frac{c \Delta p}{\gamma P} \left( 1 + \frac{\gamma + 1}{2\gamma} \cdot \frac{\Delta p}{P} \right)^{-1/2} ,$$

where $c$ is the ambient speed of sound in air, $\gamma$ is the ratio of the specific heat of air at constant pressure to the specific heat of air at constant volume, and the other quantities have been defined. The value of $\gamma$ for air at moderate temperatures and pressures is 1.4. Using this value, the peak wind velocity becomes

$$u = \frac{5\Delta p}{7P} \cdot \frac{c}{\sqrt{1 + 6\Delta p/7P}} .$$

The value of the density, $\rho_s$, of the air behind the shock front is related to the ambient density, $\rho$, by

$$\frac{\rho_s}{\rho} = \frac{2\gamma P + (\gamma + 1) \Delta p}{2\gamma P + (\gamma - 1) \Delta p} ,$$

which becomes

$$\frac{\rho_s}{\rho} = \frac{7 + 6\Delta p/P}{7 + \Delta p/P}$$

for $\gamma = 1.4$. A third equation of interest is that for the shock velocity, $U$, which is

$$U = c \left( 1 + \frac{\gamma + 1}{2\gamma} \cdot \frac{\Delta p}{P} \right)^{1/2} ,$$

which becomes

$$U = c \left( 1 + \frac{6\Delta p}{7P} \right)^{1/2}$$

for $\gamma = 1.4$. These are three of the Rankine-Hugoniot equations, which are described in more detail in Appendix A.

█ A consistent set of units must be used in the equations presented above; however, since the pressures always appear as a ratio, if consistent units are used for the specific heats to obtain $\gamma$, as was done in obtaining a value of 1.4 for moderate temperatures and pressures, the only precaution necessary is to express $\Delta p$ and $P$ in the same units. Then $u$ and $U$ will be in the same units as $c$, and $\rho_s$ will be in the same units as $\rho$. Appendix B provides conversion factors for the various units. As mentioned previously, these equations and others are discussed in more detail in Appendix A. For convenience, a normalized set of values of these shock front parameters is shown in Figure 2-12. Since all quantities are normalized with respect to local (ambient) atmospheric conditions in Figure 2-12, neither yield nor altitude scaling is necessary. The constants to which the values of the various parameters are normalized may be obtained from Tables 2-1 or 2-2.

█ It is frequently convenient to relate the peak dynamic pressure and the reflected overpressure to the incident overpressure. Figure 2-13 shows such a relationship. The data in Figure 2-13 may be obtained from other figures and

scaling relations in this chapter; however, this figure presents one convenient relation between peak overpressure and both peak dynamic pressure and reflected overpressure. The reflected overpressure curve in Figure 2-13 is for a normally incident blast wave, i.e., the reflecting surface is facing the direction of propagation of the incident blast wave. The curve is convenient for obtaining estimates of the peak reflected over-pressures for systems subjected to a normally incident free air blast wave. Reflected pressures are discussed in more detail in paragraph 2-17. The reflected and dynamic pressures may be read directly from Figure 2-10 for any specific overpressure at sea level. For intermediate altitudes (up to 40,000 feet), the pressures must be scaled as described in paragraph 2-14 and illustrated in Problem 2-8.

## Problem 2-7. Calculation of the Peak Density Behind the Shock Front for an Intermediate Altitude Free Air Explosion

Figure 2-12 shows normalized values of the shock front velocity, peak particle (wind) velocity, and peak density for a shock wave in free air as a function of the shock strength. The shock and particle velocities are normalized to the local (ambient) speed of sound, which may be obtained directly from Tables 2-1 or 2-2 as a function of altitude. The peak density behind the shock front is normalized to the local air density, which also may be obtained from Tables 2-1 or 2-2 as a function of altitude by methods illustrated in the example below.

Scaling. Since all quantities in Figure 2-12 are normalized, no scaling is required; however, for intermediate altitude bursts, the shock strength at a specified distance must be determined by the blast scaling factor described in paragraph 2-14, as illustrated in the example.

Example

Given: A 10 kt explosion at 30,000 feet.

Find: The air density just behind the shock front 1,000 feet away and at the same altitude.

Solution: In order to find the shock strength, the peak overpressure must be determined. From Table 2-1, the altitude scaling factor for distance at 30,000 feet is

$$S_d = 1.5 .$$

The scaled (1 kt) distance at sea level corresponding to 1,000 feet from a 10 kt explosion at 30,000 feet is

$$d_1 = \frac{d}{S_d W^{1/3}} = \frac{1,000}{(1.5)(10)^{1/3}} = 310 \text{ feet.}$$

From Figure 2-2, the corresponding peak overpressure is

$$\Delta p = 84 \text{ psi.}$$

The reliability statement of Problem 2-1 suggests a ±15 percent tolerance for this overpressure. Therefore the shock strength is

$$\frac{\Delta p}{P} + 1 = \frac{84 + 14.7 \pm 12.6}{14.7} = 6.7 \pm 0.9 .$$

Since shock strengths are equal at equal scaled distance, this is the shock strength of interest. Figure 2-12 shows that the density ratios corresponding to shock strengths of 5.8 and 7.6 are

$$\rho_s/\rho = 3.1, \text{ and}$$

$$\rho_s/\rho = 3.5, \text{ respectively.}$$

From Table 2-1, the air density relative to sea level is

$$\rho/\rho_0 = 0.375.$$

Since $\rho_0 = 2.38 \times 10^{-3}$ slugs per cubic foot for the standard atmosphere (footnote, Table 2-1),

$$\rho = 0.375 \; \rho_0 = 8.92 \times 10^{-4} \text{ slugs/ft}^3 .$$

Answer: The air density just behind the shock front is expected to lie between

$$\rho_s = 3.1 \times 8.92 \times 10^{-4}$$

$$= 2.8 \times 10^{-3} \text{ slugs/ft}^3$$

and

$$\rho_s = 3.5 \times 8.92 \times 10^{-4}$$

$$= 3.1 \times 10^{-3} \text{ slugs/ft}^3 .$$

Reliability

The curves in Figure 2-12 were calculated from the equations and the equation-of-

state data in Appendix A. At sea level, these curves are believed to be accurate within a few percent. The high degree of accuracy of these data results from the use of pressure rather than range as the independent variable; uncertainty in the pressure-distance curve does not affect the accuracy of these curves directly.

Altitude scaling of shock front and particle velocities is, for the range of shock strengths shown in Figure 2-12, accurate within a few percent even at altitudes as high as 300,000 feet. Density scaling is accurate within 1 or 2 percent for shock strengths below about 60; at higher shock strengths, the accuracy depends on both shock strength and altitude. At 100,000 feet, the scaling error is about 2 percent of the calculated value for shock strengths below 100, below 10 percent for shock strengths below 500, and below 20 percent for shock strengths below 900. At 200,000 feet, the error is about 2 percent for shock strengths below 60, below 10 percent for shock strengths below 80, below 20 percent for shock strengths below 130, and rises to almost 50 percent for a shock strength of 900. Whenever these errors are large, they are in such a direction that actual density is higher than calculated density.

*Related Material:* See paragraphs 2-14 and 2-15. See also Problems 2-1 through 2-6, and Appendix A.
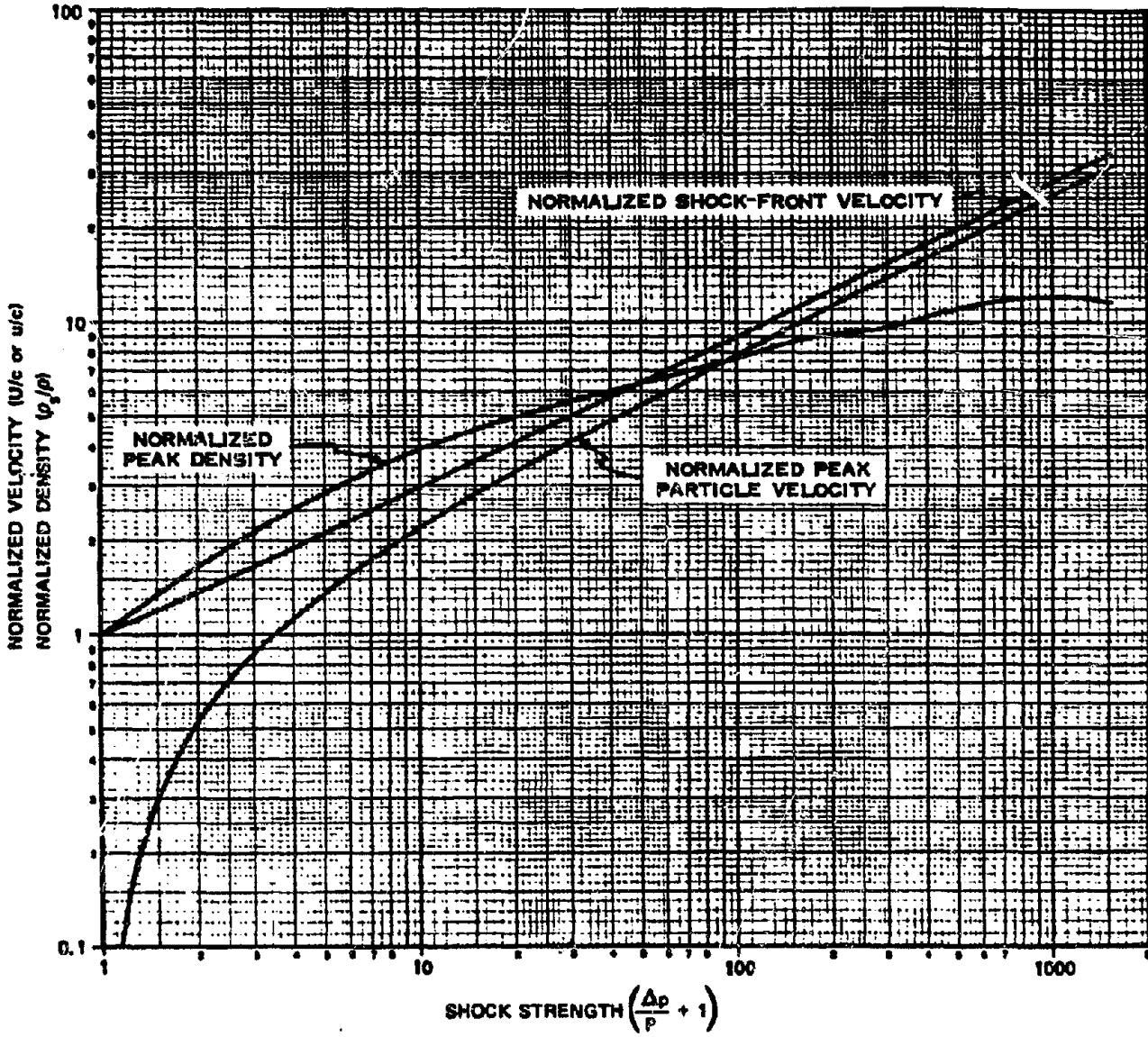
Figure 2-12. ▮ Shock Front Velocity, Peak Particle Velocity and Peak Density for a Shock Wave in Air ▮

## Problem 2-8. Calculation of Peak Dynamic Pressure for a Specified Overpressure
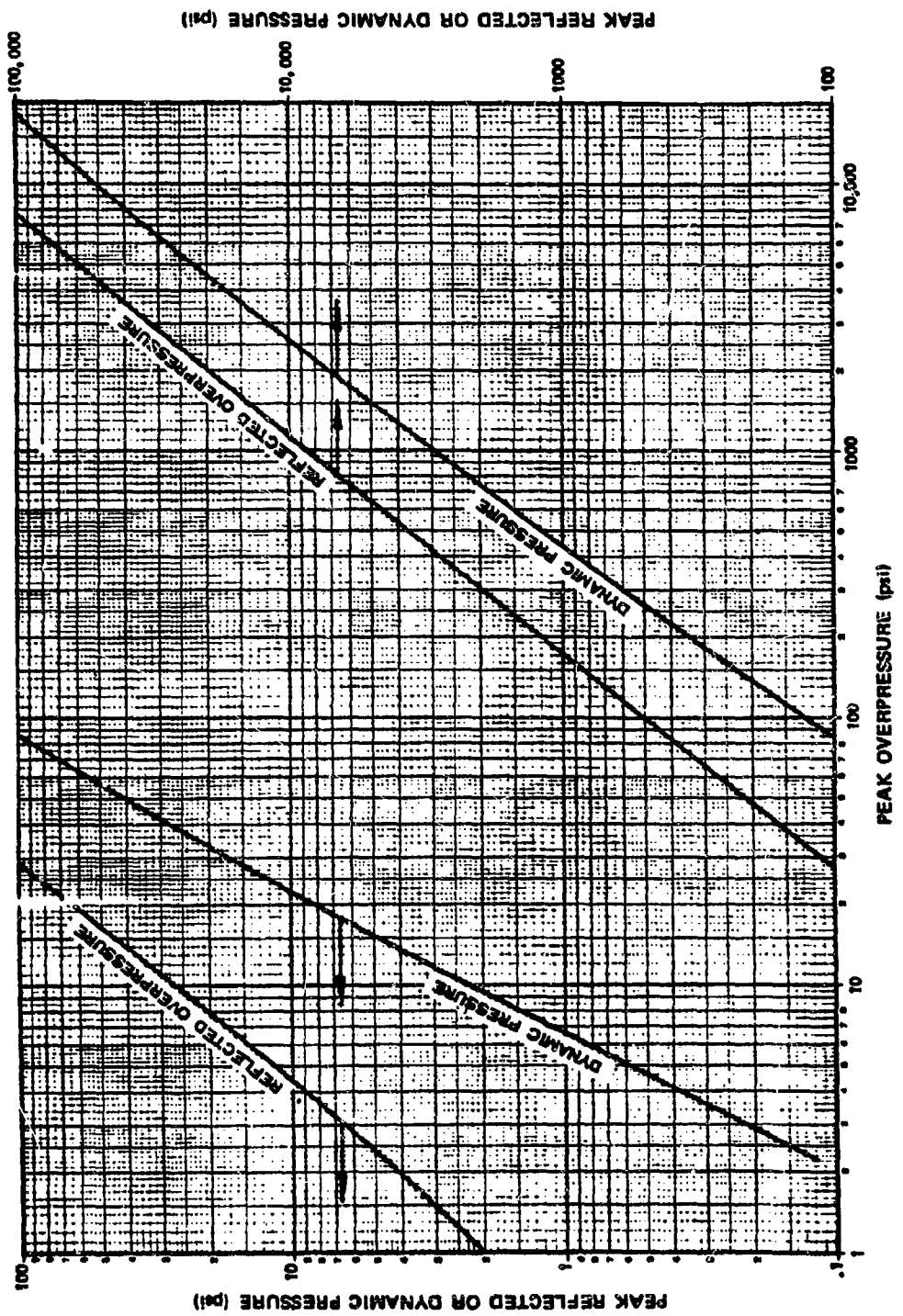
■ Figure 2-13 shows the peak reflected overpressure at normal incidence and the peak dynamic pressure as a function of peak overpressure for explosions in a standard sea level atmosphere.

■ Scaling. For intermediate altitude bursts (up to 40,000 feet), overpressure and dynamic pressure are scaled by the factors given in paragraph 2-14, i.e.

$$\Delta p = \Delta p_o S_p,$$

$$q = q_o S_p.$$

■ Example ■
Given: An explosion at 50,000 feet altitude.

Find: The peak dynamic pressure at a point coaltitude with the burst where the peak overpressure is 50 psi.

Solution: From Table 2-1, the pressure scaling factor is

$$S_p = 0.115.$$

The corresponding sea level overpressure is

$$\Delta p_o = \frac{\Delta p}{S_p} = \frac{50}{0.115} = 435 \text{ psi.}$$

From Figure 2-13, the peak dynamic pressure corresponding to a peak overpressure of 435 psi is 1,000 psi.

Answer: The corresponding peak dynamic pressure at 50,000 feet is

$$q = q_o S_p = (1,000)(0.115) = 115 \text{ psi.}$$

■ Reliability ■
The error in scaled values of dynamic pressure obtained from Figure 2-13 varies in almost exactly the same manner as the error in scaled density described in Problem 2-7.

■ The curve in Figure 2-13 for peak reflected overpressure may be scaled accurately over the approximate range of altitudes and over about half the range of shock strengths for which dynamic pressure scaling is accurate.

■ Related Material: See paragraphs 2-14 and 2-15. See also Problems 2-1 and 2-2 and Appendix A.

Figure 2-13. ▓ Peak Reflected Overpressure at Normal Incidence and Peak Dynamic Pressure as Functions of Peak Overpressure in a Standard Sea Level Atmosphere

## 2-16 Meteorological Phenomena

Nonuniformities in the atmosphere can produce mild focusing and dispersing effects that strengthen some portions of the blast wave and weaken others. Although these effects frequently occur near the surface, they are possible at any altitude and they may affect the blast wave in free air.

The manner in which these meteorological phenomena modify the blast wave may be illustrated by considering a layer of warm air, centered at burst altitude, as shown in Figure 2-14. Since the shock front velocity is greater in the warmer air, the shock front deviates from a perfect sphere. The modified shape causes the portion of the shock front that propagates through the warmer air to diverge and become weaker than the shock front as a whole.

At high shock strengths, the velocity of the shock front is much greater than sonic velocity, and it is a strong function of shock strength. This property tends to maintain a spherical shock front in spite of perturbations such as shown in Figure 2-14. Weakening the shock front reduces its speed, and the advance of the bulge becomes slower relative to the remainder of the shock front. This limits the distortion of the sphere and the divergence and weakening of the shock wave within the heated layer.
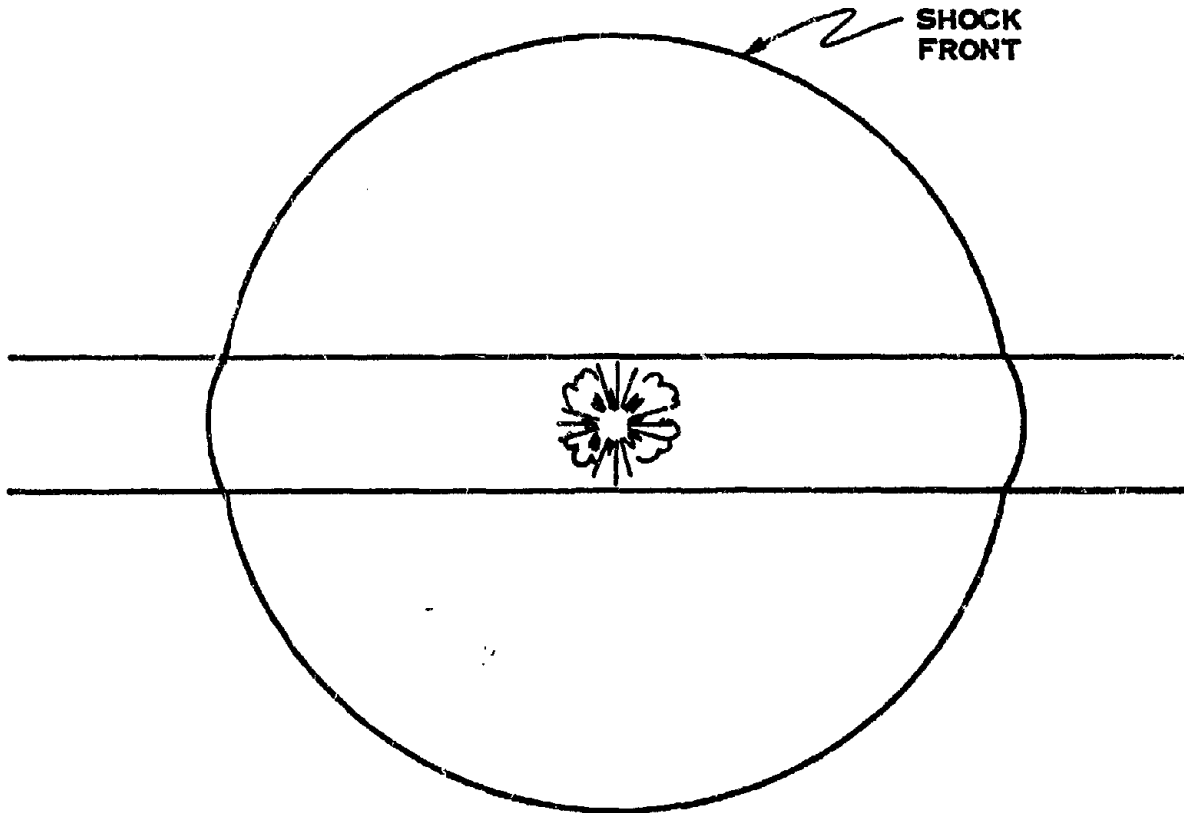


Figure 2-14. Distortion of Blast Wave by a Stratum of Warm Air

At low shock strengths, the reaction is different. The shock front velocity is only slightly greater than sound velocity and it is relatively insensitive to changes in shock strength. Development of a bulge and local weakening of the shock front can proceed much farther before changes in shock strength produce velocity changes that oppose further distortion.

For these reasons, a high overpressure blast wave is relatively insensitive to atmospheric disturbances, but a low pressure blast wave may be strongly affected. The factors that cause the disturbance can be any atmospheric nonuniformities that tend to distort the spherical shape of the shock front. Examples include shear winds and temperature gradients.

Shear winds are winds that change in velocity with changes in altitude. The velocity change may be in direction, in magnitude, or in both. Below 60,000 feet, the normal temperature gradient of the atmosphere produces lower temperatures at higher altitudes. This pattern tends to deflect blast energy upward. A temperature inversion is an increase in temperature with increasing altitude. This occurs normally at high altitudes. Above about 60,000 feet, temperature normally rises gradually with increasing altitude. The relatively sharp inversions that occur when a mass of warm air covers a mass of cold air are of more concern in blast calculations. Such an inversion can act as a mild reflecting surface, and downward deflection of the blast wave is intensified when the burst point is below the inversion.

These atmospheric effects normally produce only small deviations from predicted overpressure except for overpressures that are a small fraction of a psi. Larger deviations normally occur only when the blast wave is exposed to inhomogeneities in the atmosphere over an extended path. For example, when the burst and the target are at low altitudes and over 10 miles apart, observed overpressures have exceeded ten

times the predicted values. Such strong focusing effects are possible only when sound travels faster aloft than it does on the ground. Incidents of this type have often been associated with the high winds in the jet stream; in these instances, abnormally high overpressures are observed only in the general direction of the wind motion. Prediction of the magnitude of the deviations that inhomogeneities in the atmosphere introduce into the values of the blast wave parameters is complex, and presentation of numerical methods to estimate the magnitude of these effects is beyond the scope of this manual.

## BLAST-WAVE PHENOMENA AT THE SURFACE

When an air blast wave strikes a denser medium such as the earth's surface, it is reflected. If the surface is hard and flat, and if the incident blast wave has a very low peak overpressure, reflection follows simple laws, much like the reflection of light. If overpressures are moderate or high, or if the surface acts as a nonideal reflector, interactions between the blast wave and the surface can be complex. Study of the blast wave at the surface is largely concerned with these complex aspects of surface interactions.

### 2-17 Reflection at Normal Incidence

The peak reflected overpressure, $\Delta p_r$, produced by a normally incident* blast wave

---

*Although the various ways of describing the angle at which a blast wave strikes a surface are quite specific, they are not all consistent. A blast wave that strikes a surface head-on is said to be *normally incident*, because the direction of propagation makes an angle of 90° with the surface plane. However, the *angle of incidence* is defined as the angle between the shock front and the reflecting surface; its value is 0° for a head-on interaction. Reflection of a blast wave propagating along the surface as it strikes a rising slope is described in terms of slope angle, and slope angle is large for a steep slope. The head-on interaction that could occur at the face of a cliff occurs at a *slope angle* of 90°.

depends on the peak overpressure, $\Delta p$, and the peak dynamic pressure, $q$, of the incident blast wave. An approximate equation for peak reflected overpressure (valid for shock strengths up to 6 or 7, i.e., or overpressures of about 75 to 90 at sea level) is

$$\Delta p_r = 2\Delta p + (\gamma + 1)q,$$

where $\Delta p_r$ is the peak reflected overpressure, and the other quantities have been defined. If $\gamma$ is taken to be 1.4 (see paragraph 2-15),

$$\Delta p_r = 2\Delta p + 2.4\ q.$$

Using the defined value of $q$,

$$q = \frac{1}{2}\ \rho_s u^2,$$

and the Rankine-Hugoniot equations introduced in paragraph 2-15 leads to the relation

$$q = \frac{\Delta p^2}{2\gamma P + (\gamma + 1)\Delta p},$$

and, if $\gamma = 1.4$, this becomes

$$q = \frac{5}{2}\cdot\frac{\Delta p^2}{7P + \Delta p}.$$

Inserting this value of $q$ into the equation for the reflected overpressure gives

$$\Delta p_r = 2\Delta p\left(\frac{1 + 4\Delta p/P}{1 + \Delta p/P}\right)$$

This equation shows that, in the limiting case of low overpressures (at overpressures sufficiently low that dynamic pressure is negligible), the peak reflected overpressure is simply twice the peak overpressure of the reflected

wave. This relation is a general one that is valid for any angle of incidence. It is valid because at low overpressures the reflected shock wave has the same strength as the incident shock wave, and the peak reflected overpressure is the sum of the overpressures of the incident and reflected waves.

As $\Delta p$ becomes very large the equation given above indicates that the peak reflected overpressure rises to eight times the incident

No derivation of this expression for $q$ will be provided, but one numerical example will be shown below to establish its validity. The values for $\rho_s$ and $u$ shown in paragraph 2-15 for $\gamma = 1.4$ are

$$\rho_s = \rho\left(\frac{7P + 6\Delta p}{7P + \Delta p}\right)$$

$$u = \frac{5\Delta p}{7P}\cdot\frac{c}{\sqrt{\dfrac{7P + 6\Delta p}{7P}}}$$

$$u^2 = \frac{25\Delta p^2}{7P}\cdot\frac{c^2}{7P + 6\Delta p}$$

$$q = \frac{1}{2}\left[\rho\left(\frac{7P + 6\Delta p}{7P + \Delta p}\right)\right]\left[\frac{25\Delta p^2}{7P}\cdot\frac{c^2}{7P + 6\Delta p}\right]$$

Rearranging terms in this expression leads to

$$q = \left[\frac{5}{2}\cdot\frac{\Delta p^2}{7P + \Delta p}\right]\left[\frac{5}{7}\cdot\frac{\rho c^2}{P}\right].$$

It will be noted that the first term in brackets corresponds to the expression previously given for $q$. It should also be noted that the second term in brackets is dimensionless since both the numerator and denominator are in units of force per unit area. The sea level values of the parameters in the second term are

$$\rho = 2.38 \times 10^{-3}\ \text{slugs/ft}^3$$

$$c = 1,116\ \text{ft/sec}$$

$$P = 2,117\ \text{pounds/ft}^2$$

Inserting these values into the second term gives

$$\left(\frac{5}{7}\right)\frac{(2.38 \times 10^{-3})(1,116)^2}{2,117} = 1.$$

2-39

overpressure. However, this equation fails at these high overpressures. It is based on the assumption that $\gamma$ has a constant value, but $\gamma$ drops to values below 1.4 in strongly shocked air. More accurate calculations for the high shock strengths show higher reflected overpressures than this equation predicts.

Users of this manual will not use the equation for reflected overpressure very frequently; they will use it principally as an aid in understanding the reflection process. The numerical results that ordinarily are needed already have been calculated and have been incorporated in the various figures in this chapter.

## 2-18 Regular and Mach Reflection

The interaction between a blast wave and the surface of the earth is shown schematically in Figure 2-15. The reflected wave near the surface travels through a region that is heated and made denser than the ambient atmosphere by the incident shock front as it passes. Since shock front velocity is greater in heated air, a portion of the reflected shock can, under



Figure 2-15. Growth of the Mach Stem (Idealized)

appropriate conditions, overtake and merge with the incident shock. This forms a single shock front, called the Mach stem, which produces higher peak overpressures and peak dynamic pressures at or near the surface than would be produced at the same distance in free air. The characteristics of the blast wave at or near the surface depend on yield, height of burst, and properties of the reflecting surface. The region where the incident and reflected shocks have not merged to form a Mach stem is referred to as the region of regular reflection; the region where they have merged is referred to as the region of Mach reflection. As the Mach stem travels along the surface, the triple point (the point of intersection of the incident wave, the reflected wave, and the Mach stem) rises.

## 2-19 Blast Phenomena for Bursts in the Transition Zone

When the height of a burst is less than about $160W^{1/3}$ feet, additional phenomena affect the blast wave. If the burst is very close to the surface, within about $5W^{0.3}$ feet, fusion of the incident and reflected waves is complete, and the blast wave has a single, approximately hemispherical shock front. A burst this close to the surface is called a contact surface burst. The single shock front of a contact surface burst may be considered a special case of Mach stem formation in which the stem extends over the entire shock front.

If a warhead is detonated above $5W^{0.3}$ feet but below about $160W^{1/3}$ feet, the portion of the reflected shock front that passes through the central region of the fireball moves fast enough to overtake the incident wave and fuse with it. The blast wave thus forms a single shock front above the fireball, a double shock front between this area of fusion and the triple point (or the ground if the Mach stem is absent), and a single shock front below the triple point. The strength of the fused wave above the fireball
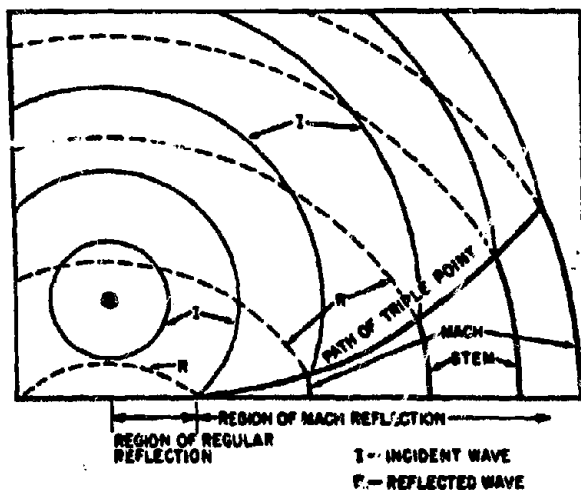
varies with burst height. Unless the burst is considerably closer to the surface than $160W^{1/3}$, the reflected wave only makes a weak contribution to this portion of the blast wave. One reason for this weak contribution is that the reflected shock front is strongly attenuated by spherical divergence (produced by the lens-like action of the fireball). Another factor may be the attenuation resulting from the dissipation of energy when the shock front passes through heated air. The region between about $5W^{0.3}$ feet and $160W^{1/3}$ feet is called the transition zone, and a burst within this region is a surface burst for purposes of air blast phenomena.

If a burst is above the transition zone, fusion of the incident and reflected shock fronts is confined to the Mach stem region, and the burst is called an air burst. An air burst that only produces weak reflection effects at the surface is called a free air burst. The properties of such explosions were discussed in paragraphs 2-7 through 2-12. A low air burst is sometimes called a near surface burst. As described in Chapter 1, the limits of the scaled heights of burst as well as the scaling laws for defining the various zones are different for the various phenomena. The definitions given above for the heights of a contact surface burst, a surface burst, the transition zone, and a free air burst only apply to air blast phenomena.

### 2-20 Near-Ideal and Nonideal Surface Conditions

An ideal surface is defined as a perfectly flat surface that reflects all of the energy, both thermal and blast, that strikes it. No part of the surface of the earth is ideal in this sense, but a few surfaces act essentially as ideal. These surfaces are classified as near-ideal. A near-ideal surface is one that provides blast wave phenomena that are essentially free of the mechanical and thermal effects that are described in succeeding paragraphs. Some of the surfaces considered

most nearly ideal are reasonably flat and consist of ice, hard-packed snow, frozen tundra, and water.

The phenomena that are characteristic of a mechanically nonideal surface are illustrated best by examples. When a blast wave that is traveling along a flat plain suddenly encounters a rising slope, a stronger overpressure impulse is produced than if the surface had remained flat. Buildings can decrease overpressure in certain areas by providing shielding from the blast; they also can increase overpressure in other areas by reflecting the blast wave. A very thick layer of snow will absorb a large amount of the blast energy that strikes it, which will produce a lower reflected overpressure than a near-ideal reflecting surface.

In most cases, blast wave calculations over mechanically nonideal surfaces are performed by first finding the desired blast parameters over a near-ideal surface. The results thus obtained then are corrected to account for the changes in blast wave properties produced by the mechanically nonideal features of the surface.

The phenomena produced by a thermally nonideal surface can distort overpressure and dynamic pressure waveforms of the blast wave at the surface. Whether or not the distortions are significant depends on height of burst and yield as well as the properties of the surface. Severe thermal effects are accompanied by the formation of a precursor, which alters several blast parameters severely. Precursors are described in the following paragraph.

Thermally nonideal surfaces may be defined loosely as those that absorb heat; thermally near-ideal surfaces reflect thermal energy incident upon them. Radiation from the fireball incident on thermally nonideal surfaces produces a layer of heated air that interacts with the blast wave, and which may form a precursor. This type of surface is sufficiently common that nearly all blast wave data at the surface are pre-

REFLECTED
BLAST
WAVE

INCIDENT
BLAST
WAVE

MACH STEM

REFLECTED
BLAST
WAVE

INCIDENT
BLAST
WAVE

PRECURSOR

PRECURSOR

DUST

PRESHOCK THERMAL LAYER

DUST

PRESHOCK THERMAL LAYER
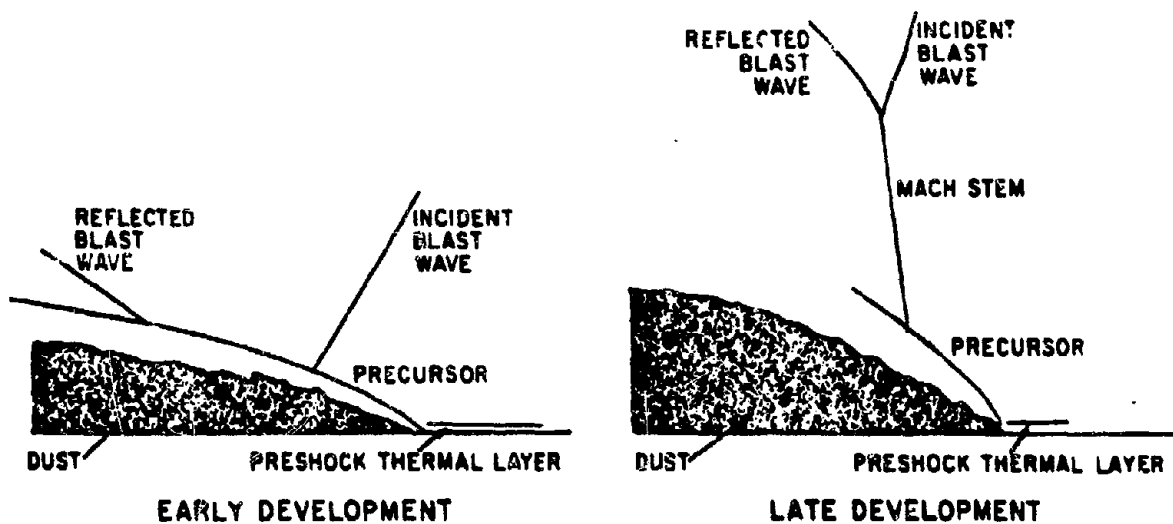
EARLY DEVELOPMENT

LATE DEVELOPMENT

Figure 2-16.    Precursor Characteristics

sented as two sets of charts: one set for near-ideal surfaces, and one set for thermally non-ideal surfaces. Methods of classifying surfaces with respect to thermal properties are discussed in paragraph 2-22.

## 2-21   Precursor Formation

Thermal radiation from the fireball of a surface or near-surface burst can cause the surface of the earth in the vicinity of ground zero to reach a temperature of several thousand degrees in a short time. "Popcorning" may then occur, wherein volatile substances vaporize explosively, throwing hot particles into the air. This (or similar heat transfer processes) produces a layer of heated air just above the surface almost instantly. When the height of burst is less than $650W^{1/3}$ feet, and when the earth is dusty and dark in color, the thermal layer usually is intense enough to disturb the blast wave near the ground surface seriously.

Under ideal conditions, none of the energy in a blast wave can propagate faster than

the shock front itself; thus, the shock front forms an envelope within which the blast energy is confined. The thermal layer, however, provides a way for this energy to penetrate the confining surface. The energy in a blast wave propagates faster through hotter air, and the thermal layer allows energy to move ahead of the main shock front, which produces shock wave patterns such as those shown in Figure 2-16. The auxiliary blast wave that moves ahead of the main shock wave is called a precursor.

Although the details of precursor formation are not well understood, its general patterns of pressure and flow have been observed and can be described. After the precursor forms, the main shock front no longer extends to the ground; if it does, the lower portion is so weakened and distorted that it is not easily recognized. Between the ground and the bottom edge of the main shock wave is a gap, probably not sharply defined, through which the energy that feeds the precursor may flow. Wind speed in this gap is higher than the wind speed behind the

main shock front.* Overpressure in the gap is lower than that behind the main shock front, and it is this overpressure difference which produces the higher than ideal wind velocities in the gap.

Ahead of the main shock front, the blast energy in the precursor is free not only to follow the rapidly moving shock front in the thermal layer, but also to propagate upward into the undisturbed air ahead of the main shock front. A near-equilibrium condition exists, because the energy continually fed into the precursor from the main blast wave tends to strengthen the precursor shock front, and the diverging flow pattern within the precursor itself tends to weaken it.

This description of what happens within a precursor explains some of the precursor characteristics shown in Figure 2-16. Only that portion of the precursor shock front remaining in the thermal layer travels faster than the main shock front; the energy diverging upward, out of this layer loses some of its forward speed, and the intersection of the precursor and main shock fronts indicates that the main shock is continually overtaking this upward-traveling energy. Dust, typically billowing to heights of more than 100 feet, shows the upward flow of air in the precursor. At later times, the lower edge of the main shock front is distorted by the action of the precursor.

Overpressure and dynamic pressure waveforms add information to that supplied by blast wave photographs. Typically, the waveform of a fully developed precursor shows a rounded leading edge and a slow rise to its peak amplitude. In severely disturbed waveforms, the pressure jump at the leading edge may be completely absent. These characteristics indicate that the precursor shock front is strongly attenuated and that, at least close to the ground, the precursor does not always have a true shock

front of significant amplitude. These results are consistent with the diverging flow pattern described above. Dynamic pressure waveforms often have high frequency oscillations that indicate severe turbulence. The long time durations seen in both overpressure and dynamic pressure waveforms indicate two effects: the early arrival of the initial pressure disturbance, and the sustaining effects of the strong winds developed within the precursor.

Peak amplitudes of the precursor waveforms show that overpressure has a lower peak value and dynamic pressure has a higher peak value than would appear over a surface that did not permit a precursor to form.† The drop in peak overpressure indicates the energy expended in producing the higher than ideal wind velocities. The higher dynamic pressure is partly due to the higher wind speeds, but dust loading, the increase in effective air density resulting from particulate matter carried by the wind, is believed to be a more important factor.

Additional information on precursors, particularly a description of typical precursor overpressure and dynamic pressure waveforms, is given in paragraphs 2-31 and 2-32.

* It is tempting to think of the wind in the gap as moving faster than the main shock front. However, two velocities characterize a shock wave: wind velocity and shock front velocity. The velocity of the main shock front is the velocity of propagation of the energy in the main shock. It should be compared not to the wind speed in the gap but to the velocity with which hydrodynamic energy propagates through the gap.

† In an ideal blast wave, this relative variation of peak values would be impossible. Peak overpressure and peak dynamic pressure have a fixed relation to one another, specified by the Rankine-Hugoniot equations (paragraph 2-17 and Appendix A). However, these equations only hold at the shock front. In an ideal blast wave, shock-front amplitudes are also peak amplitudes, but in a precursor the peak values do not occur at the shock front. Thus the relation between them is not limited by these equations.

## 2-22 Identification of Thermally Near-Ideal and Nonideal Surfaces

To predict blast-wave parameters accurately, the reaction of the surface to thermal radiation from the fireball should be known. Nuclear tests have shown that a few specific types of surface act essentially as thermally ideal surfaces and a few others tend to produce a significant thermal layer. Unfortunately, a theoretical model that quantitatively explains the phenomena of surface reaction and precursor formation has not yet been developed. Without such a model, the response of untested surfaces cannot be predicted with assurance.

Despite this uncertainty, predictions have been made. Surfaces are classified as either thermally near-ideal (unlikely to produce significant precursor effects) or thermally nonideal (expected to produce a precursor for suitable combinations of burst height and ground distance). No other categories are used, i.e., no attempt is made to subdivide surface classifications according to the strength of the precursor that can form.

Examples of surfaces that are considered thermally near-ideal and thermally nonideal are shown in Table 2-3. Items in the table that are confirmed by experiment are marked with an asterisk.

Dark surfaces tend to be thermally nonideal, because they absorb thermal radiation from the fireball. Light (reflecting) surfaces tend to be near-ideal. Asphalt is the strongest precursor-forming surface for which test results are known.

The effect of moisture has not been established definitely. Since any specified amount of absorbed energy can raise the temperature of a dry surface more than the same absorbed energy would raise the temperature of a wet surface, moisture is expected to inhibit the formation of a thermal layer. This should be particularly true when the moisture is in the form of ice. Nuclear tests show that the dry, sandy

Table 2-3. Examples of Thermally Near-Ideal and Thermally Nonideal Surfaces

| Thermally Near-Ideal (precursor unlikely) | Thermally Nonideal (precursor may occur for low air bursts) |
|---|---|
| *Water | *Desert sand |
| *Ground covered by white smoke layer | *Coral |
| Heat reflecting concrete | *Asphalt |
| Frozen tundra | *Surfaces with low, thick vegetation |
| Ice | *Surfaces covered by a dark smoke layer |
| Packed snow | Dark colored rock |
| Moist soil with sparse vegetation | Most agricultural areas; Residential areas in cities |
| Commercial and industrial areas | Dry soil with sparse vegetation |

soil of the Nevada Test Site is thermally non-ideal, and that water is a near-ideal surface (however, a blast wave over rough seas may fill the air with spray and produce a dynamic pressure effect similar to the dust loading encountered over desert surfaces). Untested surfaces classed as thermally near-ideal are listed in Table 2-3 in the order of increasing uncertainty.

■ Sparse vegetation probably should be ignored. Leaves or thick vegetation shield the ground, prevent popcorning, and minimize dust loading, but they also generate a heat-absorbing cloud of dark smoke when they absorb radiation from the fireball. The gases driven from the leaves have high sonic velocities. As a result, they create a thicker, and probably cooler, thermal layer than that formed over desert sand or asphalt. Taller vegetation is expected to produce a thicker thermal layer and a stronger precursor. The REDWING-Inca shot, over a surface covered by low grass and vines dominated by broadleafed shrubs about 10 feet high, produced a precursor, but the characteristic precursor waveforms were apparently suppressed to some extent because higher-than-ideal blast-wave velocities near the surface were eliminated by the vegetation.

■ Tests at the Nevada Test Site show weakened precursor action over areas covered by dark smoke (the surface was desert sand which forms a strong precursor). Presumably the smoke absorbs enough heat to form a thermal layer, but it shields the ground to prevent popcorning and dust loading of the air.

■ Variable conditions occur in cities. Commercial and crowded industrial areas are expected to act as thermally near-ideal surfaces. Although these areas contain many surfaces that are favorable to precursor formation (e.g., asphalt-coated roofs), a continuous thermal layer would not be expected. The tendency to form a precursor would be offset by its difficulty in propagating through a heavily built up

area. In typical residential areas, where the buildings are neither as close nor as tall as those in commercial areas, the surface is considered thermally nonideal.

■ The preceding descriptive information does not always provide clear guidelines for classifying surfaces. For example, the rules that might be applied to black, moist soil are conflicting. In such cases, blast-wave properties should be calculated for both near-ideal and thermally nonideal surface conditions in order to bracket the blast effects that can actually be expected.

## ■ BLAST-WAVE CALCULATIONS AT THE SURFACE ■

■ Height of burst (HOB) curves provide most of the data required to calculate blast-wave properties at the surface. The HOB charts in this subsection each show the distance from ground zero as a function of height of burst for several values of the various air blast parameters that would be expected to occur *along the surface* as a result of a 1 kt explosion.* For instance, any point on a curve for specified overpressure (see for instance Figure 2-17) shows a combination of burst height and ground distance at which a 1 kt explosion will produce that overpressure at the surface of the earth. Alternately, if a 1 kt burst occurs at a location corresponding to some point on a given overpressure curve, a target at the origin will receive that overpressure.

■ Separate families of curves are provided for near-ideal and thermally nonideal surface

_____

*As described in paragraph 2-13, the heights of burst and distances from ground zero could be expressed in terms of scaled distances, e.g., $kt/W^{1/3}$, with $W$ being the yield in $kt$. However, since other scaling laws apply to other phenomena, the convention of expressing absolute distances from a 1 kt explosion will be maintained throughout the remainder of this chapter and throughout the manual. When "scaled distances" are employed, e.g., Section I, Chapter 11, the exceptions will be indicated clearly.

conditions. Guidelines for classifying surfaces with respect to thermal properties are provided in paragraph 2-22. The effects of mechanically nonideal surfaces (paragraph 2-20) are discussed in paragraphs 2-37 through 2-41.

Many of the HOB curves show whether a given point on the surface is in the region of regular reflection or the Mach stem region (paragraph 2-18). This information is helpful if the target is some distance above the surface, because it indicates how closely blast-wave data at the surface correspond to blast-wave data at the target. The effect of target height on blast-wave parameters is discussed in paragraph 2-29.

The data for overpressure and dynamic pressure are peak values, regardless of where these peaks occur in the blast waveform. In an undisturbed blast waveform, these peak values occur at the shock front. If a precursor is present, they usually occur later in the waveform. Precursor overpressure and dynamic pressure waveforms are described in paragraphs 2-31 and 2-32.

Whenever ambient atmospheric conditions are different from standard sea level conditions (14.7 psi, 59°F), calculations of blast-wave parameters at the surface are more accurate if the altitude scaling factors described in paragraph 2-14 are applied. These factors may be used even if the departure from standard conditions is not caused by an altitude change.

## 2-23 Reliability

Blast-wave data at the surface are subject to the uncertainties described in paragraphs 2-1 through 2-6. As mentioned in paragraph 2-5, additional uncertainties arise because the earth is not a perfect reflector. Consequently, the blast wave at the surface is inherently less predictable than the blast wave in free air. Added to this problem is the difficulty of obtaining sufficient experimental data to cover all combinations of conditions. A blast parameter in free air may be

represented by a single curve; at the surface, the available data must be scattered to cover a family of curves. Moreover, variable surface conditions require that more than one family be plotted. Consequently, a limited number of nuclear tests cannot document blast-wave data at the surface as completely as in free air. The usual reliability statements are supplemented in this section by showing portions of the curves as dashed lines. The solid lines are based upon experimental data from full-scale nuclear tests; the dashed portions are based upon theory and high-explosive experiments. In some cases, data for the dashed portions of curves are based on the assumption that for certain combinations of ground range and burst height the data for thermally nonideal surfaces should agree with data taken over near-ideal surfaces. In general, the reliability statements apply to the dotted as well as the solid portion of the HOB curves; however, the reliability of the dotted portions is purely an estimate, while the reliability stated for the solid portions is based on experimental data.

Uncertainties in the data presented in the HOB charts usually are expressed in terms of ground distance rather than in terms of blast parameters. This is an important distinction. For example, a ±10 percent uncertainty in ground distance corresponds to an uncertainty in peak overpressure that may be as high as ±30 percent. The curves become nearly horizontal close to ground zero, and a variation in ground distance produces very little change in blast parameters. For these portions of the HOB charts, the uncertainty should be applied to burst height rather than to ground distance. When a precursor forms, the air blast waveforms are distorted severely, and prediction of blast parameters becomes highly uncertain. As mentioned in paragraph 2-2, the scaling of most blast-wave parameters is reasonably dependable in the yield range of 1 kt to 20 Mt; however, scaling becomes questionable for yields over 50 kt at thermally non-

ideal surfaces as a result of the difficulty in predicting the criteria for precursor formation.

■ The scaling of subkiloton explosions at scaled heights of burst between 150 and 1,000 feet have shown large errors that correspond to discrepancies as high as factors of 2 or 3 in effective yield.

■ Additional uncertainties appear in the measured data for contact surface bursts as a result of less dependable experimental determination of yield. This is caused in part by the difficulties added to radiochemical yield determination as a result of the large amount of crater material in the cloud and to the uncertainty introduced into yield determination by fireball size that result from uncertainties in the amount of energy absorbed by the earth.

## 2-24 Peak Overpressure ■

■ Figures 2-17 through 2-22 show the peak overpressure at the surface of the earth as a function of height of burst and distance from ground zero from a 1 kt explosion. Figure 2-23 shows peak overpressure as a function of distance from ground zero from a 1 kt contact surface burst. The same data could be obtained in less convenient form along the abscissas of Figures 2-17 through 2-20.

■ These figures show that the same ground range for a given peak overpressure is produced by a burst either at the surface or some short distance above the surface. At low overpressures, the greatest distance from ground zero occurs for an explosion at some higher distance above the surface. This effect is prominent at overpressures of 15 psi and less, and contours for these overpressures show a pronounced "knee" (the knee is defined as the extreme right projection of a contour line).

■ Figures 2-17 through 2-20 apply to near-ideal surface conditions; Figures 2-21 and 2-22

apply to thermally nonideal surfaces (suggestions for classifying various types of surfaces are given in paragraph 2-22). Figure 2-23 applies to near-ideal surfaces, but since the 1 kt reference burst detonated in contact with the surface is not expected to form a precursor, the curve also applies approximately to thermally nonideal surfaces.

■ The shaded areas in Figure 2-20 reflect the uncertainty in the prediction of very low overpressures. The shaded areas in Figures 2-21 and 2-22 correspond to the ground distances at which precursor cleanup occurs. In this phenomenon, the hydrodynamic energy of the blast wave collects behind a single, well-defined shock front, forming a nearly ideal blast wave. As this occurs, the peak overpressure usually rises instead of undergoing the normal amount of attenuation with increasing ground range. Uncertainty in the ground range at which cleanup occurs is reflected in the HOB curves as additional uncertainty in peak overpressure data at this range. This is indicated by shading of the 10 psi contour and a portion of the 15 psi contour.

## 2-25 Peak Dynamic Pressure ■

■ Figures 2-24 through 2-26 show peak dynamic pressure at the surface as a function of scaled height of burst and ground distance from a 1 kt explosion. These curves show conditions after the blast wave has been reflected from the surface; therefore, these charts do not represent the dynamic pressure of the incident wave. At ground zero the wind in the incident blast wave is completely stopped by the ground surface, and all of the incident dynamic pressure is transformed to static overpressure. Therefore, the height of burst curves show that the peak dynamic pressure is zero at ground zero. At other locations, reflection of the incident blast wave produces winds that, at the surface, must

blow parallel to the surface.* The dynamic pressures associated with these winds tend to produce horizontal forces; however, the direction of wind forces on a target surface depend not only on wind direction but also on surface orientation.

The thermal properties of the surface are less significant for prediction of dynamic pressure than for most blast parameters. Dynamic pressure only appears to be strongly enhanced by dust loading (or, in the case of a water surface, spray loading) of the air, whether or not a precursor is formed. The dynamic pressure height of burst curves are therefore classed as ideal, "light dust," and "heavy dust" surface conditions. Light dust conditions usually may be taken to be equivalent to near-ideal surfaces, and heavy dust equivalent to thermally nonideal, but there are exceptions. For example, a surface covered by thick vegetation is expected to produce a precursor but little dust. Conversely, the interaction of a blast wave with very rough seas is expected to produce heavy spray loading but no precursor.

Figure 2-24 shows peak dynamic pressure at an ideal surface in the very high pressure region. It is based almost entirely on theory, and does not include dust loading effects (it should be noted that the 200 psi contour of Figure 2-23 does not agree with that in either Figure 2-25 or 2-26). Figure 2-25 shows peak dynamic pressure for light dust conditions, and Figure 2-26 shows peak dynamic pressure for heavy dust conditions. Since the latter is based on limited data, height of burst curves can be drawn only for scaled burst heights up to 300 feet. As a guide to the way in which the heavy dust curves might be extrapolated, portions of the light dust curves are shown for 1 kt burst heights between 330 feet and 600 feet. These latter curves do not represent heavy dust conditions. They should be used only as a guide to obtain rough estimates.

Figure 2-27 is presented to aid in the explanation of the effects of dust on peak dynamic pressure. The curves are drawn from data from Figures 2-25 and 2-26, and theoretical data for an ideal reflector. At a scaled distance of about 400 feet, the contribution of light dust to dynamic pressure is about twice that of heavy dust. This suggests that the inertia of heavy dust limits its velocity initially and probably also limits the velocity of the air in the blast wave by the drag force it exerts. After these inertial forces are overcome, heavy dust contributes strongly to dynamic pressure. At a scaled range of 900 feet, heavy dust exhibits its maximum effect, but the effect of light dust has diminished considerably. This also suggests an inertial effect acting to sustain the momentum of the air in the blast wave.

The explanation that has been given is only one of several possible explanations of Figure 2-27 and represents an oversimplification. For example, the explanation does not include the varying amount of dust that a given surface adds to the blast wave as a function of range. More detail may be found in DASA 1200 (see bibliography).

A large scatter exists in dynamic pressure data under heavy dust conditions. This is due to the nature and the varying amounts of particulate matter in the air. Fine grains of sand are readily carried by the air stream, flow with it as a part of a continuous fluid, and present a relatively small measurement problem. Larger

---

*This statement ignores the turbulence that is often associated with dynamic pressure. It is uncertain whether or not vertical components of air velocity contribute to dynamic pressure significantly. Gages used to measure dynamic pressure are usually mounted so as to be sensitive only to the horizontal force produced by dynamic pressure. For this reason curves such as those in Figures 2-24 through 2-26 are often labeled "horizontal component of dynamic pressure." It is desirable to avoid this phrase, because it tends to imply, incorrectly, that the forces produced by dynamic pressure may be resolved into components that can be treated by the ordinary rules of vector algebra.

particles tend to plug gage openings, and their effect is difficult to measure. Large objects picked up by the blast wave and thrown through the air can be very destructive, but they cannot be measured as part of a continuous pressure record. Arbitrarily, dynamic pressure has been defined as representing the effects of only those particles that are small enough to behave essentially as air particles. Dynamic pressure as thus idealized cannot fully account for the destructive effects of blast momentum.

## 2-26 Time of Arrival ▮

▮ Figures 2-28 through 2-32 show the time of arrival of the blast wave from a 1 kt explosion in a standard, homogeneous, sea level atmosphere as a function of height of burst and distance from ground zero.

## 2-27 Duration of the Positive Phase of Overpressure and Dynamic Pressure ▮

▮ Figures 2-33 and 2-34 present families of curves that show values of the positive phase overpressure duration $(t_p^+)$ at points along the surface as a function of height of burst and ground distance from a 1 kt explosion in a sea level atmosphere.

▮ Because of limited data, similar curves cannot be drawn for dynamic pressure; however, the data suggest that, as in the case of free air (paragraph 2-10 and Problem 2-4), the ratio of these two durations is a function of pressure level. Duration of dynamic pressure $t_q^+$ may be estimated by using the curves for positive overpressure duration and the relations shown in Table 2-4. If surface conditions are such that heavy dust (or spray) loading is predicted, the longer times found in Figure 2-34 probably provide a better basis for determining $t_q^+$ even if the surface is considered thermally near-ideal and Figure 2-33 is used to determine $t_p^+$.

Table 2-4. ▮ Relations Between the Positive Duration of the Overpressure Blast Wave $(t_p^+)$ and the Positive Duration of the Dynamic Pressure $(t_q^+)$ for a 1 kt Explosion ▮

| $t_p^+$ (sec) | $t_q^+$ (sec) |
|---|---|
| 0.1 | 0.25 |
| .15 | .33 |
| .2 | .34 |
| .25 | .35 |
| .3 | .39 |
| .35 | .43 |
| .4 | .49 |

## 2-28 Overpressure Impulse ▮

▮ Figures 2-35 and 2-36 show the positive overpressure impulse (paragraph 2-11) at the surface as a function of height of burst and ground distance from a 1 kt explosion in a sea level atmosphere.

▮ Formation of a Mach stem changes the shape of the overpressure waveform by increasing the amplitude of the shock front without changing the area under the waveform appreciably. Consequently, the HOB curves for overpressure impulse differ from the HOB curves for peak overpressure in that the impulse curves do not show a characteristic change where they cross the boundary separating the region of regular reflection from the region of Mach reflection. Overpressure impulse at the surface appears to be primarily a function of slant range; it only fluctuates strongly as a function of reflecting angle for low heights of burst.

▮ Dynamic pressure impulse is another important blast-wave parameter, particularly under thermally nonideal conditions. Unfortun-

ately, it is a difficult parameter to measure, and there are not enough dependable data to allow HOB curves to be constructed.

## 2-29 Mach Stem Heights █▓

█▓ The changes that occur in a blast wave as the incident and reflected waves fuse to form a Mach stem are among the changes associated with reflection from a surface. A target above the triple point, the top of the Mach stem (see paragraph 2-18), receives two shocks that correspond to the arrival of the incident and the reflected waves. A target at or below the triple point receives a single shock. As mentioned in paragraph 2-25, the reflection process transforms part of the incident dynamic pressure into overpressure. Thus, a target below the triple point is subjected to a higher overpressure impulse and a lower dynamic pressure impulse than a target above the triple point. Since a typical airborne target is more sensitive to dynamic pressure than to overpressure, such a target is usually safer below the triple point.

█▓ The height of the Mach stem height affects tall structures on the ground. The nature of the response depends on whether the structure is more sensitive to overpressure or to dynamic pressure. The relative effects of a two shock front waveform and a single, nearly vertical shock wave also depend on the mechanical response properties of the target.

█▓ Above the triple point, the strength of the first (or incident) shock wave may be found from free air data, and the time interval between the two shocks depends on the height of the target above the triple point. Below the triple point, shock parameters may be approximated best by data from the HOB charts, i.e., from data which, strictly speaking, apply only to targets at the surface. When the scaled height (that corresponding to a 1 kt burst) of the Mach stem is 50 feet or less, blast-wave properties anywhere on the stem are essentially the same as those at the surface. For taller Mach stems, the shock-front becomes curved. This modifies blast-wave properties along the stem. Pressure values decrease and arrival times increase with height above the surface. These variations have not been studied as thoroughly as blast-wave conditions at the surface have been, and data to describe them quantitatively are not presented here.

█▓ The guidelines presented above must be applied with caution if a precursor is present. The two disturbing influences, dust and the thermal layer, are confined to a layer that is close to the ground. Above the region that is affected by the precursor, the near-ideal HOB curves are a better representation of the blast wave. The height above which the near-ideal curves apply is not known, but it is estimated to be between 50 and 300 feet (physical, not scaled height) under typical conditions.

█▓ Although there are indications that the height of the Mach stem is affected by thermal effects and by surface hardness, these effects are not large, and the curves may be applied to both near-ideal and thermally nonideal surfaces. Both thermal effects and surface roughness will, however, make the position of the triple point less predictable.

█▓ Figures 2-37 and 2-38 show the height of the Mach stem as a function of height of burst and ground distance from a 1 kt explosion in a sea level atmosphere.

## Problem 2-9.  Calculation of Peak Overpressure at the Surface

Figures 2-17 through 2-22 show the peak overpressure as a function of height of burst and horizontal distance from ground zero for a 1 kt explosion in a sea level atmosphere. Figures 2-17 through 2-19 provide data for thermally near-ideal surfaces, while Figures 2-20 through 2-22 provide the same data for thermally nonideal surfaces. Figure 2-23 shows the peak overpressure as a function of horizontal distance from a contact surface burst. The data contained in the curves of Figure 2-23 could be obtained from points along the abscissas of Figures 2-17 through 2-19; however, for some applications, Figure 2-23 may be more convenient to use.

*Scaling.* For yields other than 1 kt, the ground distance and height of burst for any specific overpressure scale as follows:

$$\frac{d}{d_1} = \frac{h}{h_1} = W^{1/3},$$

where $d_1$ and $h_1$ are the distance from ground zero and height of burst, respectively, for 1 kt, and $d$ and $h$ are the corresponding distance and height of burst for a yield of $W$ kt.

*Example 1*

*Given:* An 80 kt explosion 2,580 feet above a thermally nonideal surface.

*Find:* The horizontal distance from ground zero beyond which the peak overpressure will not exceed 3 psi.

*Solution:* The corresponding height of burst for 1 kt is

$$h_1 = \frac{h}{W^{1/3}} = \frac{2,580}{(80)^{1/3}} = 600 \text{ feet.}$$

From Figure 2-22, a peak overpressure of 3 psi extends to a distance of 2,900 feet from a 1 kt explosion at a height of burst of 600 feet.

*Answer:* The corresponding distance for an 80 kt weapon at 2,500 feet height of burst is

$$d = d_1 W^{1/3} = (2,900)(80)^{1/3} = 12,500 \text{ feet.}$$

As a result of the ±15 percent uncertainty in this distance (see "Reliability" below), the range beyond which the peak overpressure will not exceed 3 psi is

$$12,500 + (0.15)(12,500) = 14,400 \text{ feet.}$$

*Example 2*

*Given:* A 100 kt explosion at a height of 2,320 feet above a near-ideal surface.

*Find:* The peak overpressure at a distance of 1,860 feet from ground zero.

*Solution:* The corresponding distance and ground zero and height of burst for a 1 kt weapon are

$$d_1 = \frac{d}{W^{1/3}} = \frac{1,860}{(100)^{1/3}} = 400 \text{ feet,}$$

$$h_1 = \frac{h}{W^{1/3}} = \frac{2,320}{(100)^{1/3}} = 500 \text{ feet.}$$

*Answer:* From Figure 2-18, the peak overpressure at a ground distance of 400 feet and a height of burst of 500 feet is 50 psi.

*Reliability*

Ground distances obtained from Figures 2-18, 2-19, and 2-22 are estimated to be reliable within ±15 percent of the indicated ground range (or HOB for points close to ground

zero — see paragraph 2-23). Figure 2-17 is based on theory, confirmed by only a few data points; it is estimated to be reliable within ±20 percent. Figure 2-20 is reliable within ±15 percent of the indicated ground range, but the 1/2 - 1/4 psi curves are subject to the additional uncertainty indicated by the shaded areas. Figure 2-21 is based on data subject to considerable scatter from thermal effects; it is estimated to be reliable within ±20 percent.

For near-ideal surface conditions, these reliability estimates apply to yields between 1 kt and 20 Mt; for thermally nonideal surface conditions, the estimates apply to yields between 1 kt and 50 kt. Outside this range of yields, these curves may be used with somewhat less confidence.

*Related Material:* See paragraphs 2-13, 2-14, 2-17 through 2-20, and 2-22 through 2-24. See also Tables 2-1 and 2-2 for surface conditions that differ from standard sea level atmospheric conditions.
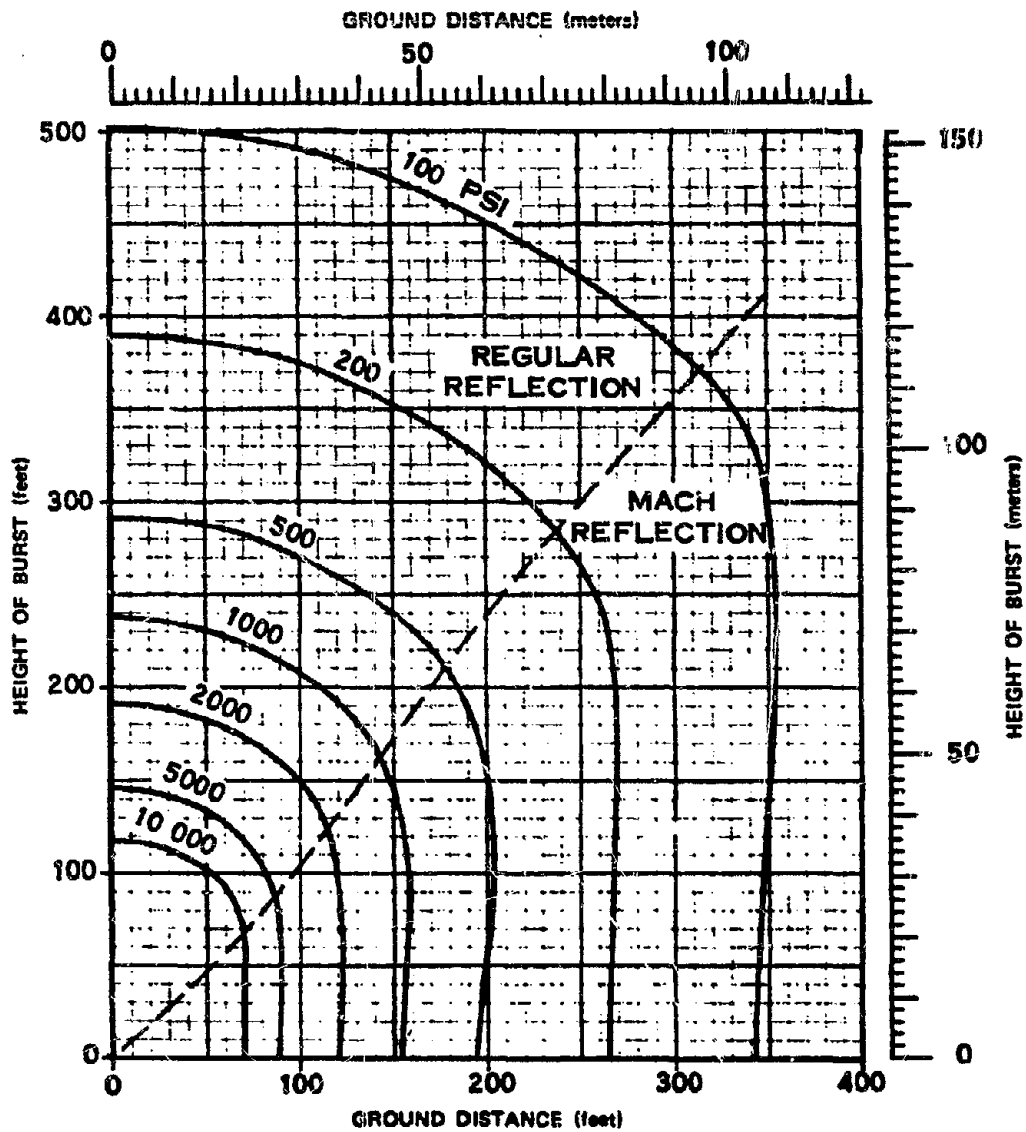
Figure 2-17. ▨ Peak Overpressures at the Surface for a 1 kt Burst Over a Near-Ideal Surface, Very High Overpressure Region ▨
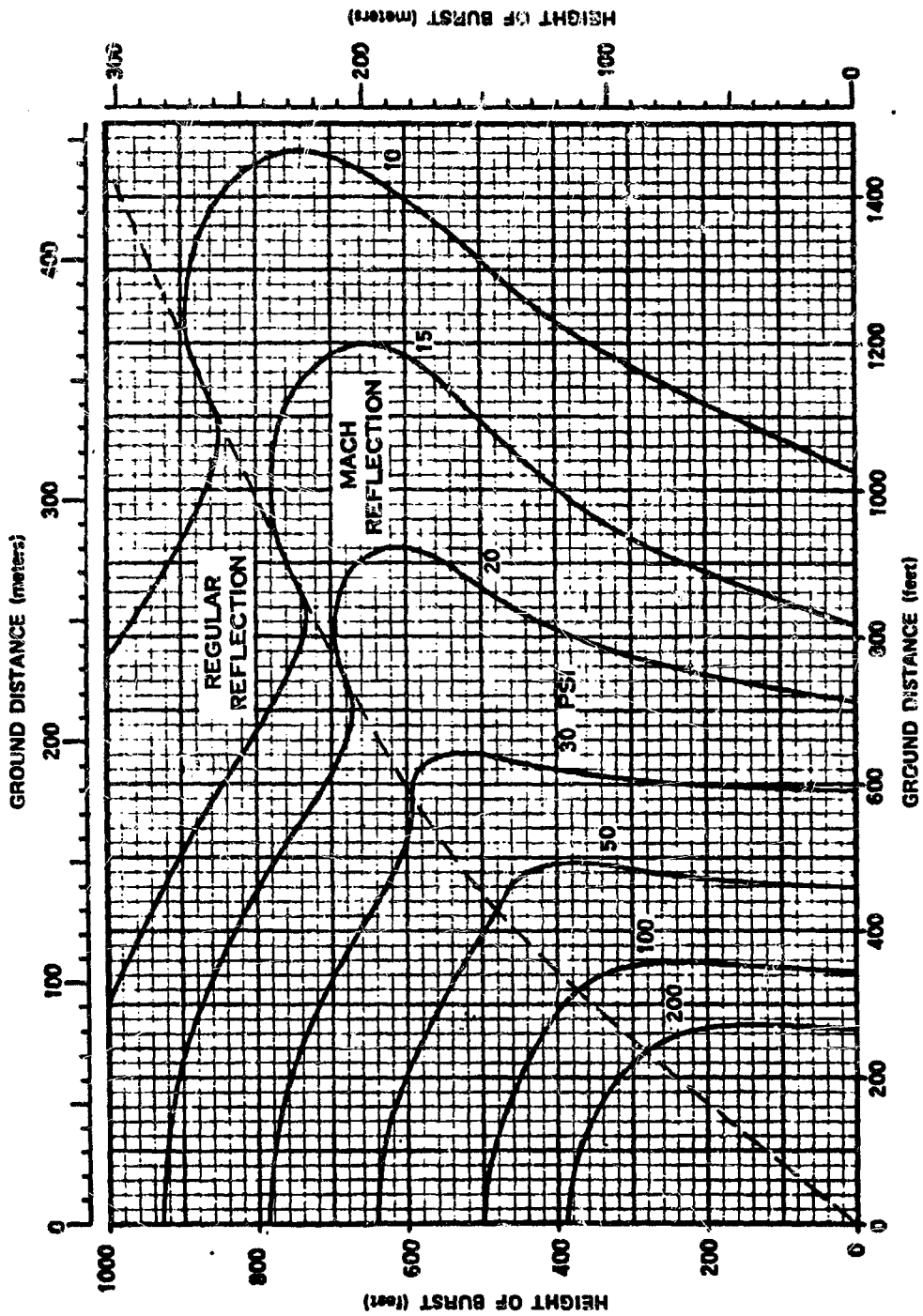
**Figure 2-18.** ▮ Peak Overpressures at the Surface for a 1 kt Burst Over a Near-Ideal Surface, High Overpressure Region
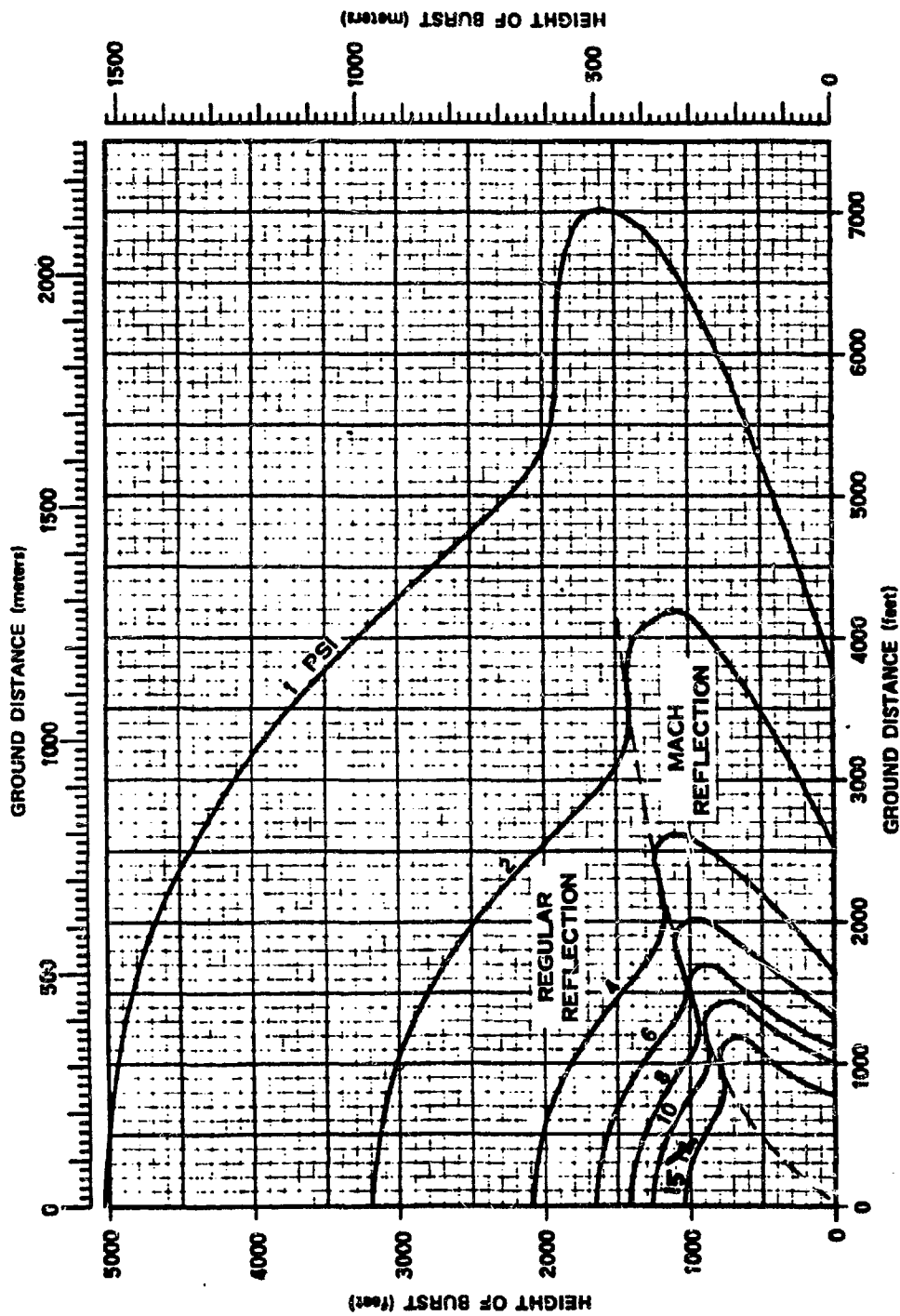
Figure 2-19.  Peak Overpressures at the Surface for a 1 kt Burst Over a Near-Ideal Surface, Low Overpressure Region
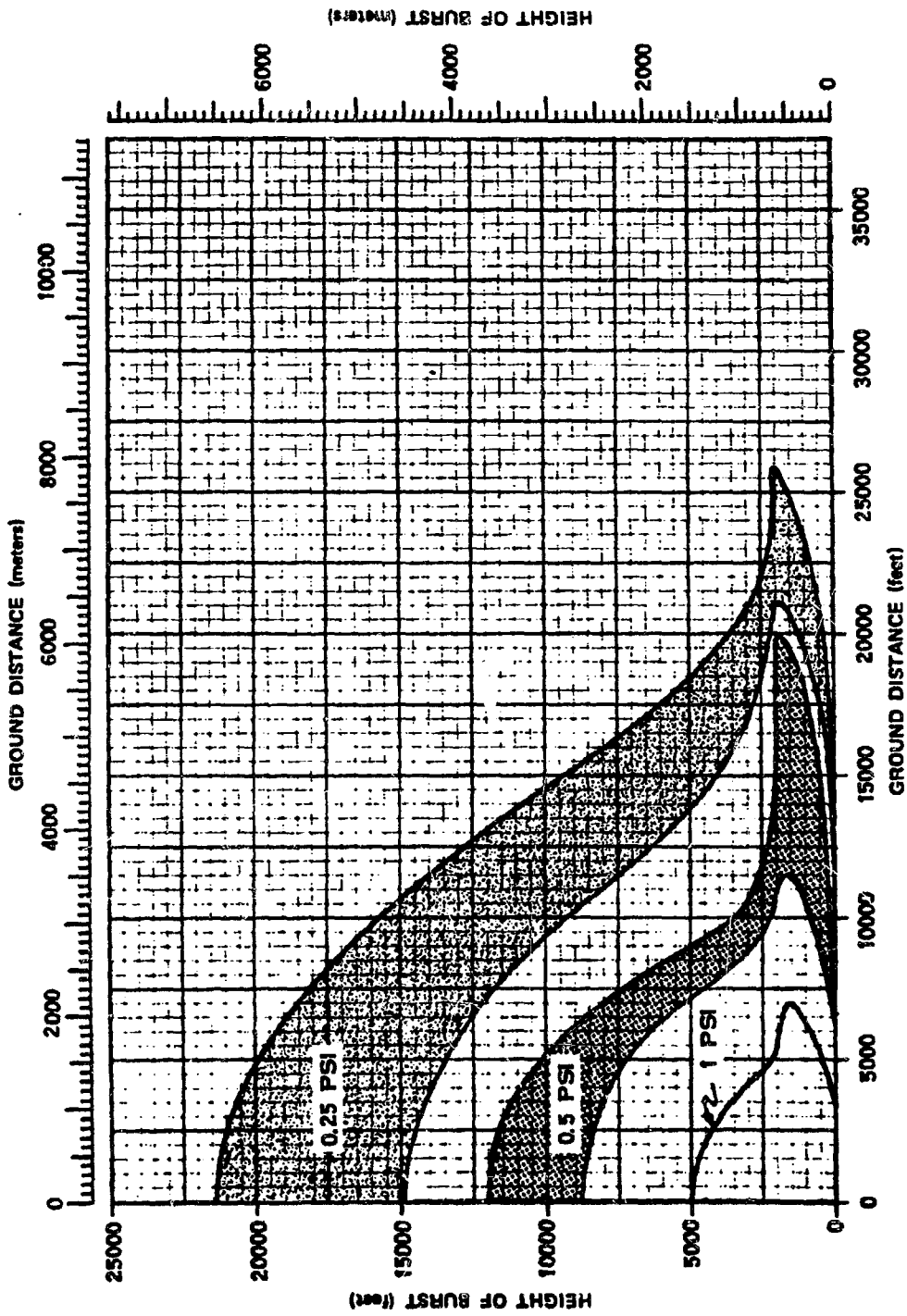
Figure 2-20. ■ Peak Overpressures at the Surface for a 1 kt Burst Over a Near-Ideal or Thermally Nonideal Surface, Very Low Overpressure Region
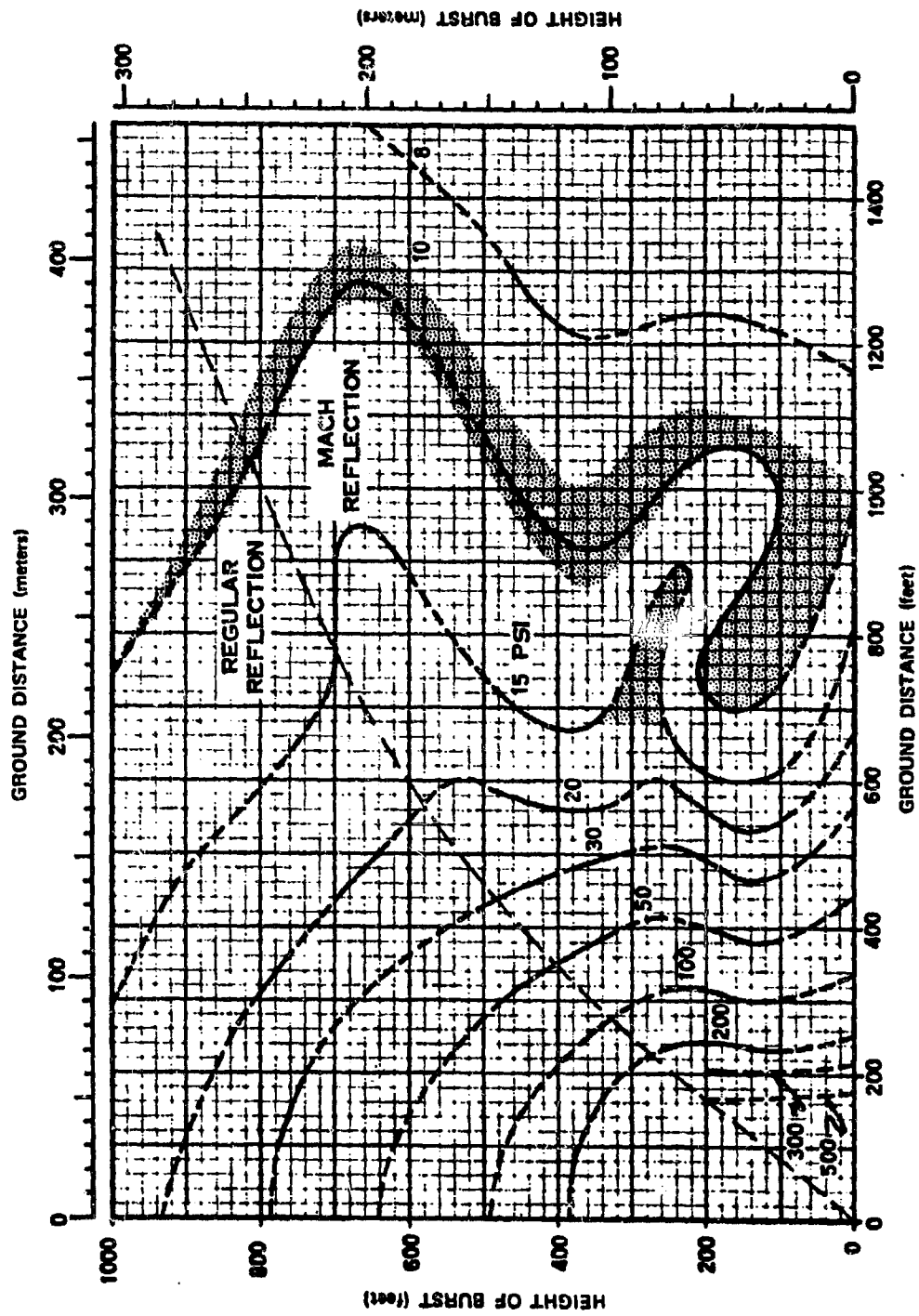
Figure 2-21. Peak Overpressures at the Surface for a 1 kt Burst Over a Thermally Nonideal Surface, High Overpressure Region
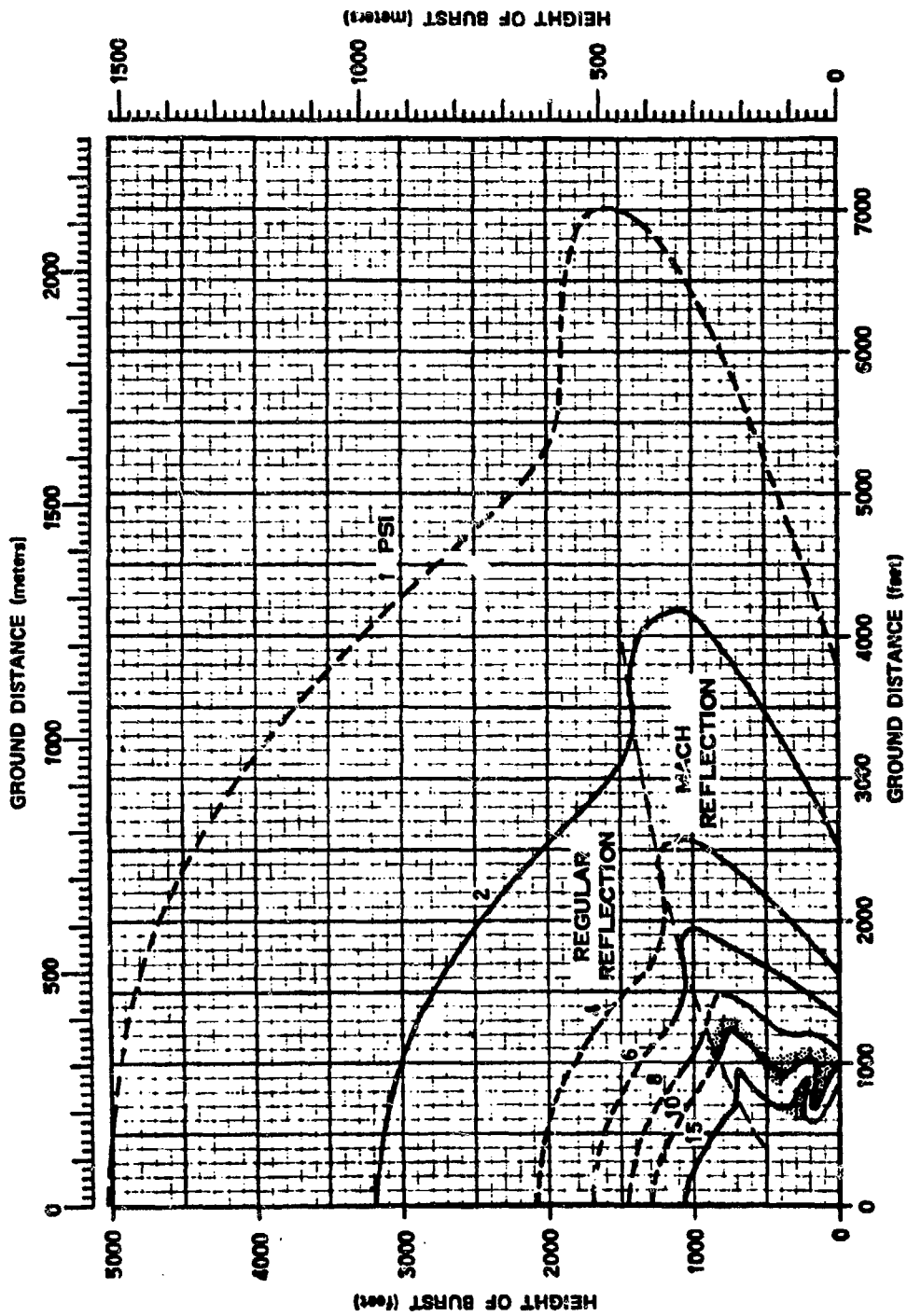
Figure 2-22. Peak Overpressures at the Surface for a 1 kt Burst Over a Thermally Nonideal Surface, Low Overpressure Region
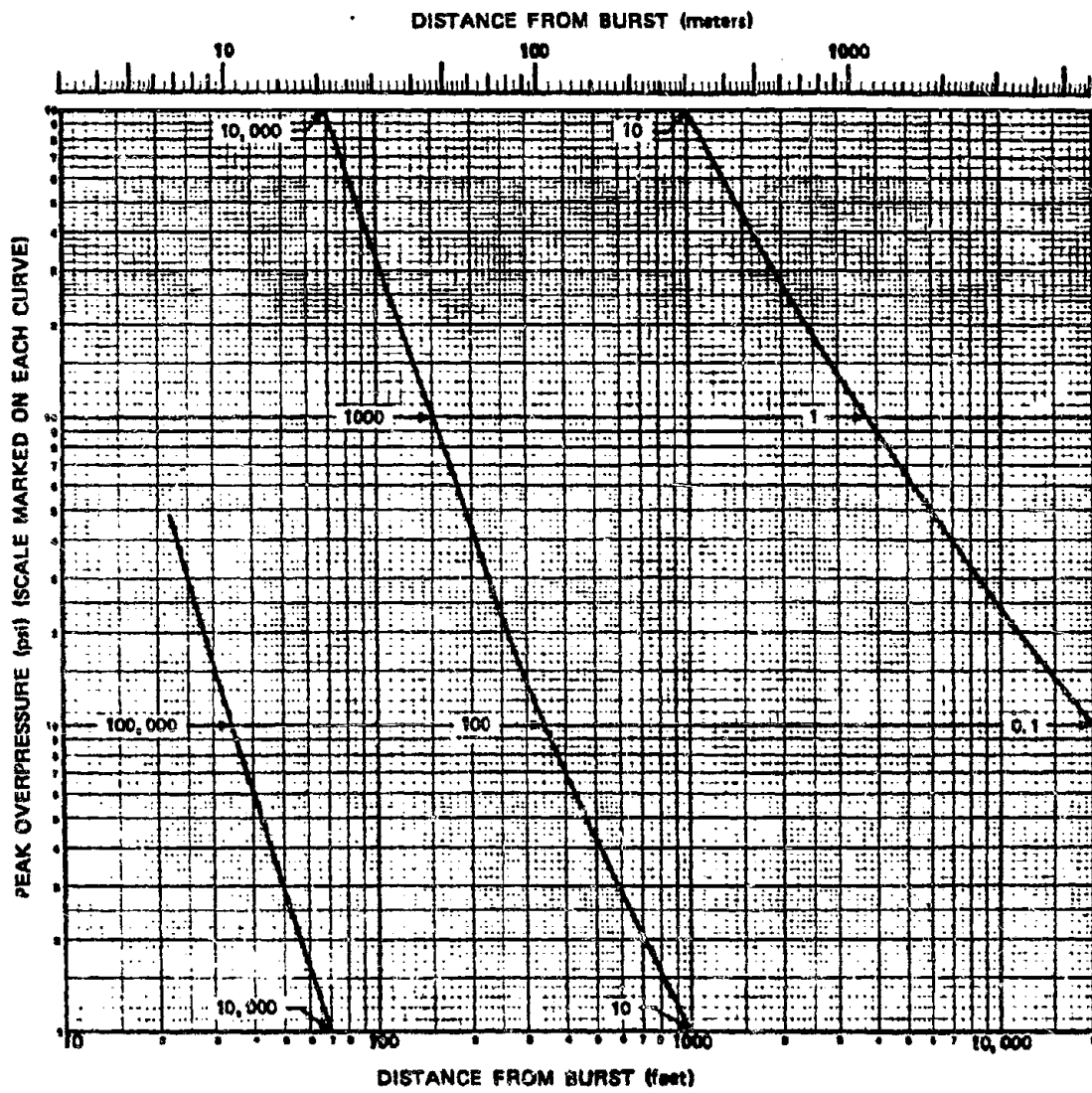
Figure 2-23. ■ Peak Overpressure from a Contact Surface Burst ■

Figures 2-24 through 2-26 show peak dynamic pressure at the surface as a function of height of burst and horizontal distance from ground zero for a 1 kt explosion in a sea level atmosphere. Figure 2-24 is based almost entirely on theorv and applies to peak dynamic pressure in the very high overpressure region at an ideal surface. Dust loading effects are not included in the curves of Figure 2-24. Figure 2-25 shows the peak dynamic pressure at the surface under light dust conditions, while Figure 2-26 shows similar data under heavy dust conditions. Figure 2-27 shows a comparison of the data from Figures 2-24 through 2-26 for a 1 kt explosion at a height of burst of 200 feet. A discussion of the comparisons is given in paragraph 2-25.

*Scaling.* For yields other than 1 kt, the ground distance and height of burst for any specific peak dynamic pressure scale as follows:

$$\frac{d}{d_1} = \frac{h}{h_1} = W^{1/3} ,$$

where $d_1$ and $h_1$ are the distance from ground zero and height of burst, respectively, for 1 kt, and $d$ and $h$ are the corresponding distance and height ot burst for a yield of $W$ kt. If the surface is above 5,000 feet, or if the surface atmospheric conditions differ from standard, the altitude scaling procedures given in paragraph 2-14 should be used.

*Example*
*Given:* A 160 kt explosion 3,000 feet above a light dust surface.

*Find:* The peak dynamic pressure at a distance of 6,000 feet from ground zero.

*Solution:* The corresponding height of burst and ground distance from a 1 kt explosion are

$$h_1 = \frac{h}{W^{1/3}} = \frac{3,000}{(160)^{1/3}} = 550 \text{ feet},$$

$$d_1 = \frac{d}{W^{1/3}} = \frac{6,000}{(160)^{1/3}} = 1,100 \text{ feet}.$$

*Answer:* From Figure 2-25, the peak dynamic pressure corresponding to a height of burst of 550 feet and a distance of 1,100 feet is about 3 psi. Since this value of peak dynamic pressure is below 6 psi, the actual value (see "Reliability" below) may be between that shown for ground distances of 1,100 ±25 percent (1,375 and 825 feet) or between about 1.5 and 7 psi; however, since the reliability estimates do not extend to yields above 50 kt, the precise limits cannot be stated.

*Reliability:* Distances for peak dynamic pressures below 6 psi are estimated to be reliable within ±25 percent. For dynamic pressures above 6 psi, the distances in Figure 2-25 (light dust) are estimated to be correct within ±50 percent; and distances in Figure 2-26 (heavy dust), to within +100 percent, or -50 percent. The reliability of Figure 2-24 has not been estimated. These reliability figures apply to yields between 1 and 50 kt. Outside this range of yields, scaling may introduce additional error.

*Related Material:* See paragraphs 2-13 through 2-15, 2-17 through 2-23 and 2-25. See also Tables 2-1 and 2-2 when atmospheric conditions at the surface differ from standard sea level conditions.

REGULAR
REFLECTION

100 PSI

200

500

1000

2000

5000

MACH
REFLECTION

10,000

HEIGHT OF BURST (feet)

HEIGHT OF BURST (meters)

GROUND DISTANCE (feet)
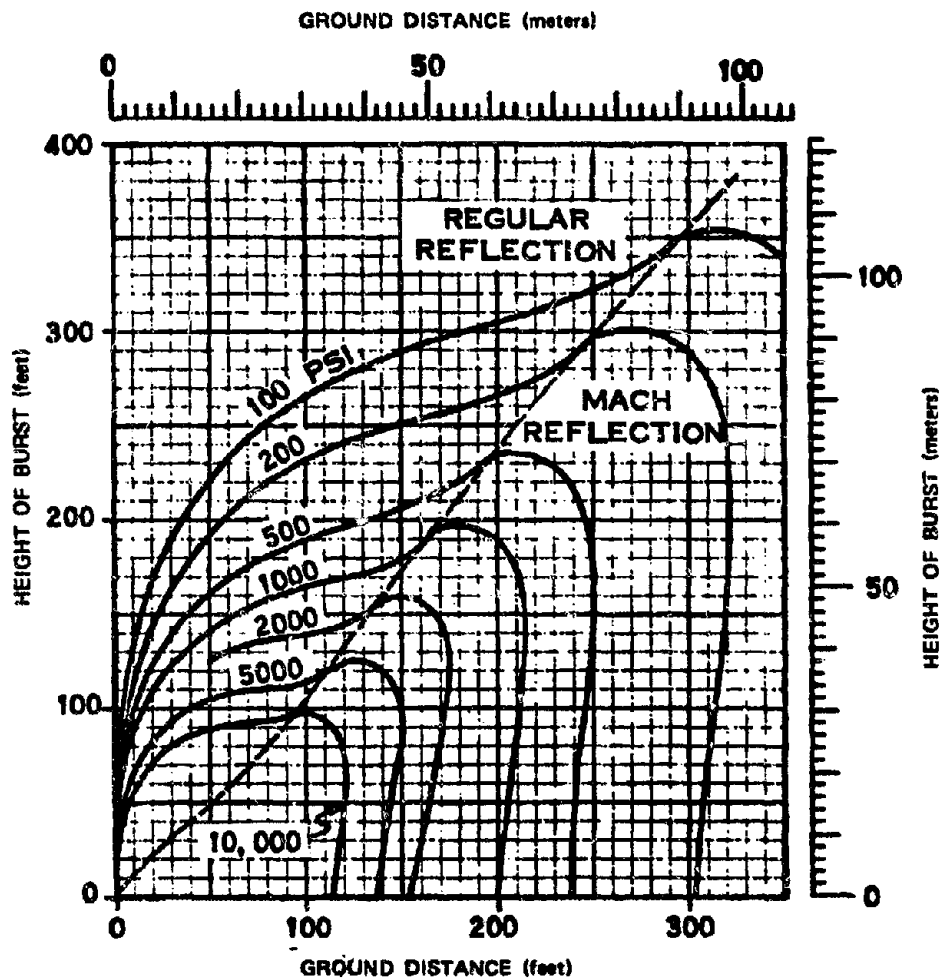
Figure 2-24. Peak Dynamic Pressure at the Surface from a 1 kt Explosion Over an Ideal Surface
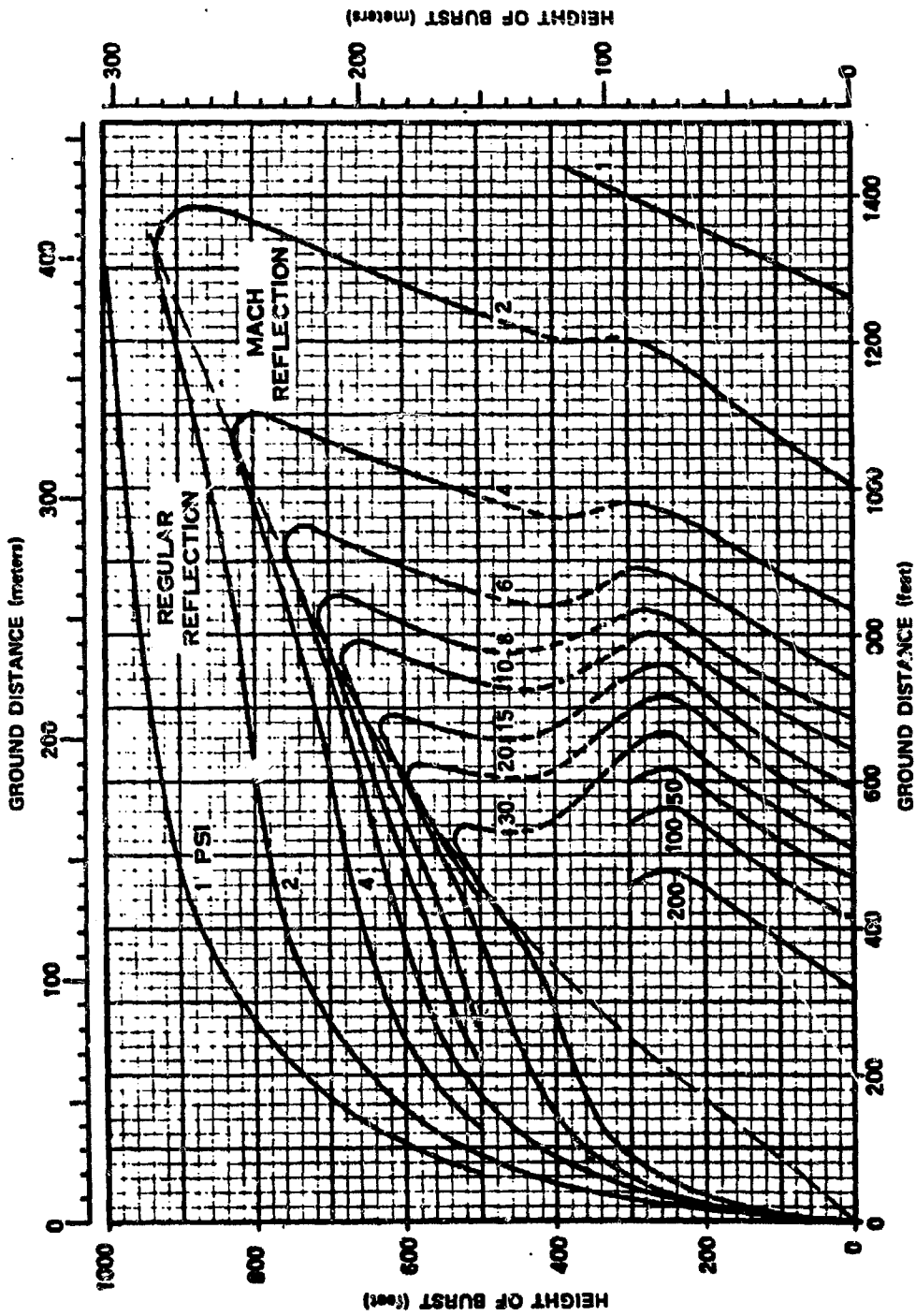
Figure 2-25. ▉ Peak Dynamic Pressure at the Surface from a 1 kt Explosion ▉ver a Surface with Light Dust Conditions
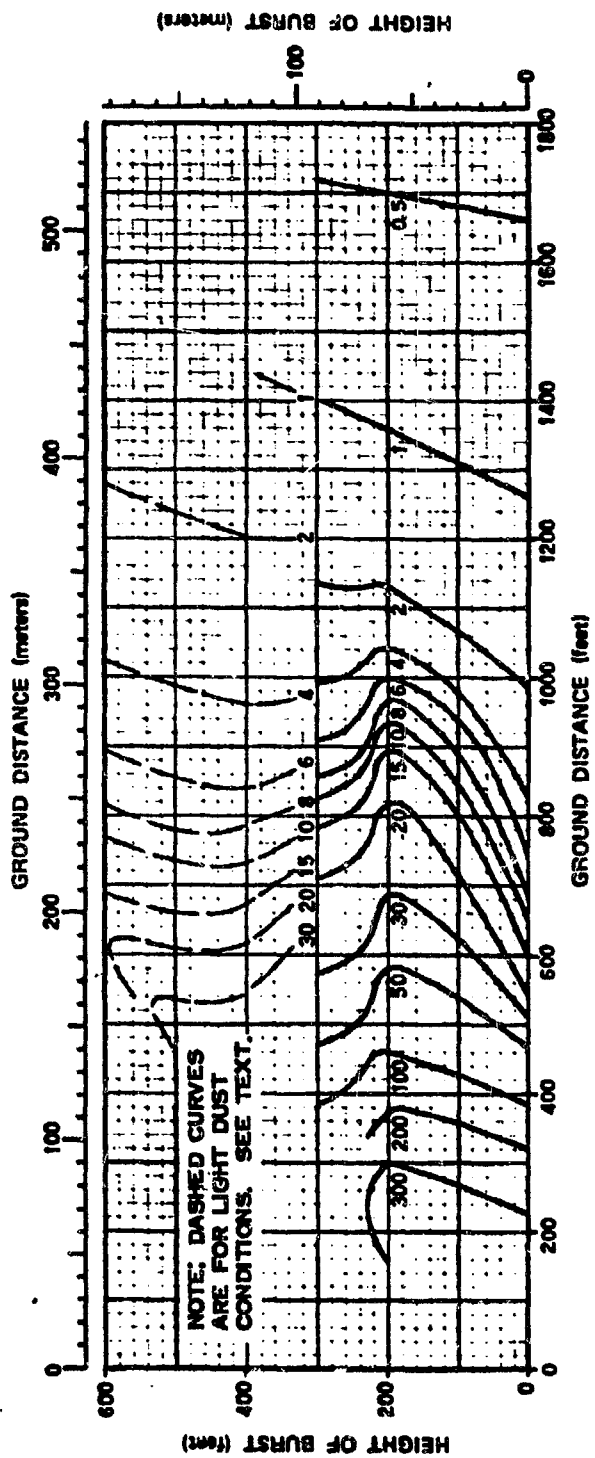
Figure 2-28. Peak Dynamic Pressure at the Surface from a 1 kt Explosion Over a Surface with Heavy Dust Conditions
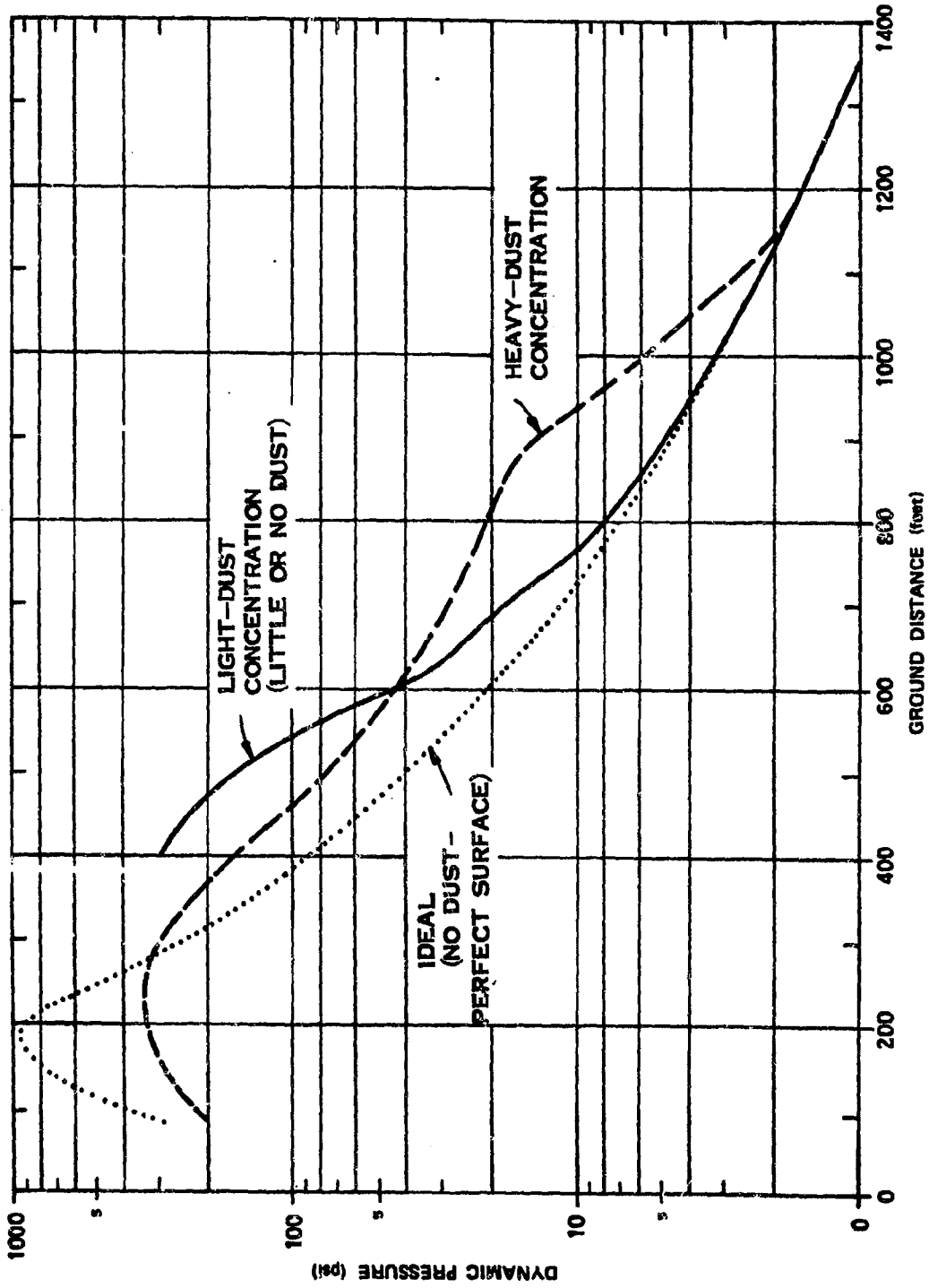
Figure 2-27. Comparison of Predicted Ideal, Light-Dust, and Heavy-Dust Dynamic Pressures for a 1 kt Explosion at a Height of Burst of 200 feet in a Sea Level Atmosphere

## Problem 2-11. Calculation of the Time of Arrival of a Blast Wave at the Surface

Figures 2-28 through 2-32 show the time of arrival of a blast wave as a function of height of burst and horizontal distance from a 1 kt explosion in a sea level atmosphere. Figures 2-28 and 2-29 apply to bursts over thermally near-ideal surfaces while Figures 2-30 through 2-32 apply to bursts over thermally nonideal surfaces.

*Scaling.* For yields other than 1 kt, the time of arrival, ground distance, and height of burst scale as follows:

$$\frac{t}{t_1} = \frac{d}{d_1} = \frac{h}{h_1} = W^{1/3},$$

where $t_1$, $d_1$, and $h_1$ are the time of arrival, ground distance and height of burst, respectively for 1 kt and $t$, $d$, and $h$ are the corresponding time and distances for a yield of $W$ kt. If the surface is above 5,000 feet, or if the surface atmospheric conditions differ from standard, the altitude scaling procedures given in paragraph 2-14 should be used.

*Example*
*Given:* An 8 kt explosion 400 feet above a thermally nonideal surface.

*Find:* The time of arrival of the blast wave at a horizontal distance of 1,200 feet from ground zero.

*Solution:* The corresponding height of burst and ground distance for a 1 kt explosion are

$$h_1 = \frac{h}{W^{1/3}} = \frac{400}{(8)^{1/3}} = 200 \text{ feet.}$$

$$d_1 = \frac{d}{W^{1/3}} = \frac{1,200}{(8)^{1/3}} = 600 \text{ feet.}$$

From Figure 2-31, the time of arrival of a blast wave at a ground distance of 600 feet from a 1 kt explosion 200 feet above a thermally non-ideal surface is 0.15 seconds.

*Answer:* The corresponding time of arrival for an 8 kt explosion is

$$t = t_1 W^{1/3} = (0.15)(8)^{1/3} = 0.30 \text{ sec.}$$

Under the specified conditions the ground range is reliable to within ±15 percent (see "Reliability" below), or the 1 kt ground distance could vary between 510 and 690 feet, providing arrival times from a 1 kt explosion of 0.12 and 0.19 seconds. The time of arrival from the 8 kt explosion may therefore be expected to fall between

$$t = t_1 W^{1/3} = (0.12)(8)^{1/3} = 0.24 \text{ sec, and}$$

$$t = t_1 W^{1/3} = (0.19)(8)^{1/3} = 0.38 \text{ sec,}$$

with an expected value of 0.30 seconds as previously calculated.

*Reliability:* Over near-ideal surfaces, the ground distance for a given arrival time is estimated to be reliable within ±10 percent. Over nonideal surfaces, two reliability estimates have been made: in the region of Mach reflection and for times less than about 0.8 sec per kt, the ground distances are estimated to be reliable within ±15 percent; at later times or in the region of regular reflection, the values are about ±10 percent. These reliability estimates apply to yields between 1 kt and 1 Mt. Outside this range of yields, the curves may be used with somewhat less confidence.

*Related Material:* See paragraphs 2-13 through 2-15 and paragraph 2-26. See also Tables 2-1 and 2-2.
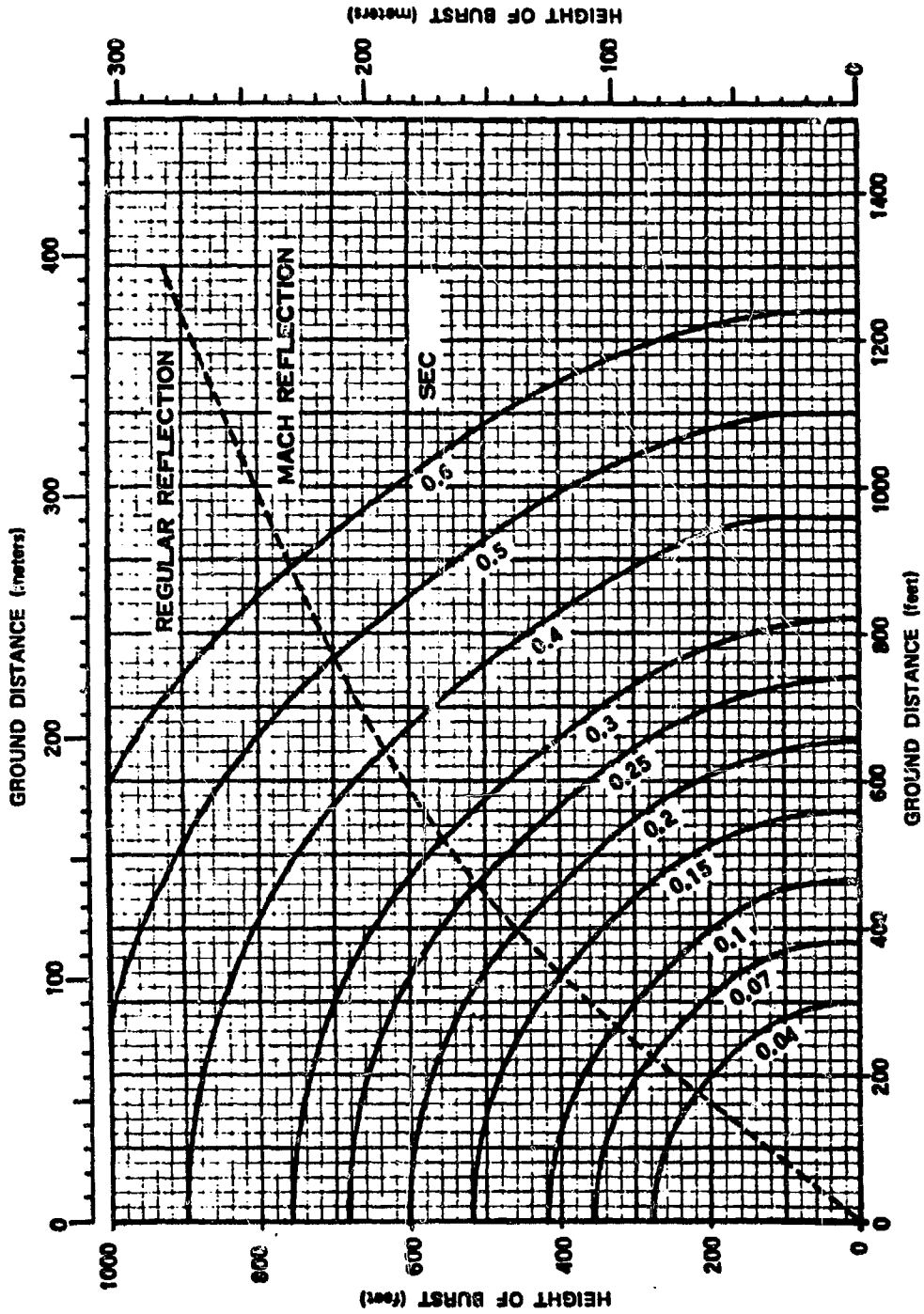
Figure 2-28. ▮ Time of Arrival of the Blast Wave Along the Surface from a 1 kt Explosion Over a Near-Ideal Surface, High Overpressure Region ▮
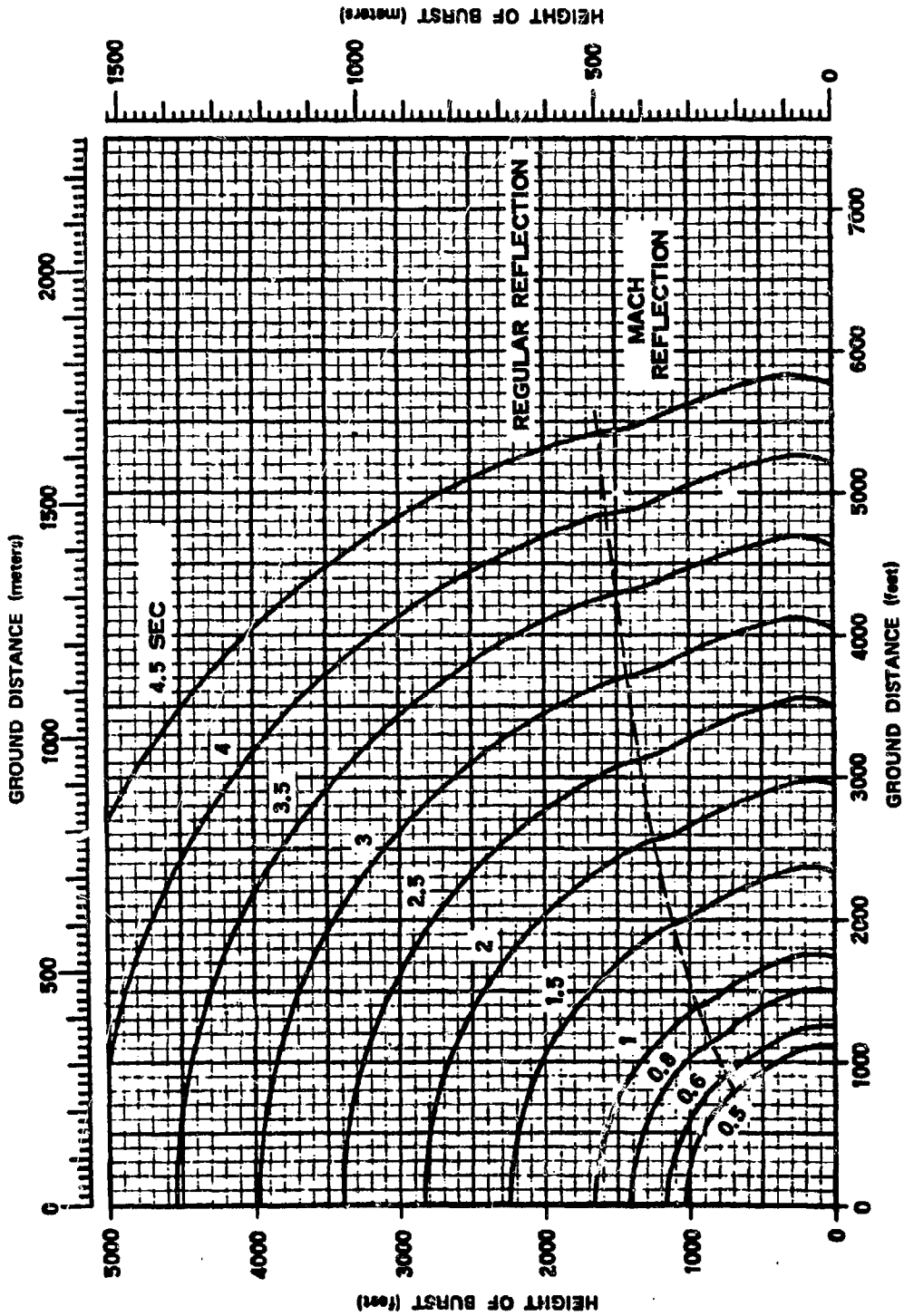
Figure 2-29. Time of Arrival of the Blast Wave Along the Surface from a 1 kt Explosion Over a Near-Ideal Surface, Low Overpressure Region

2-67

GROUND DISTANCE (meters)
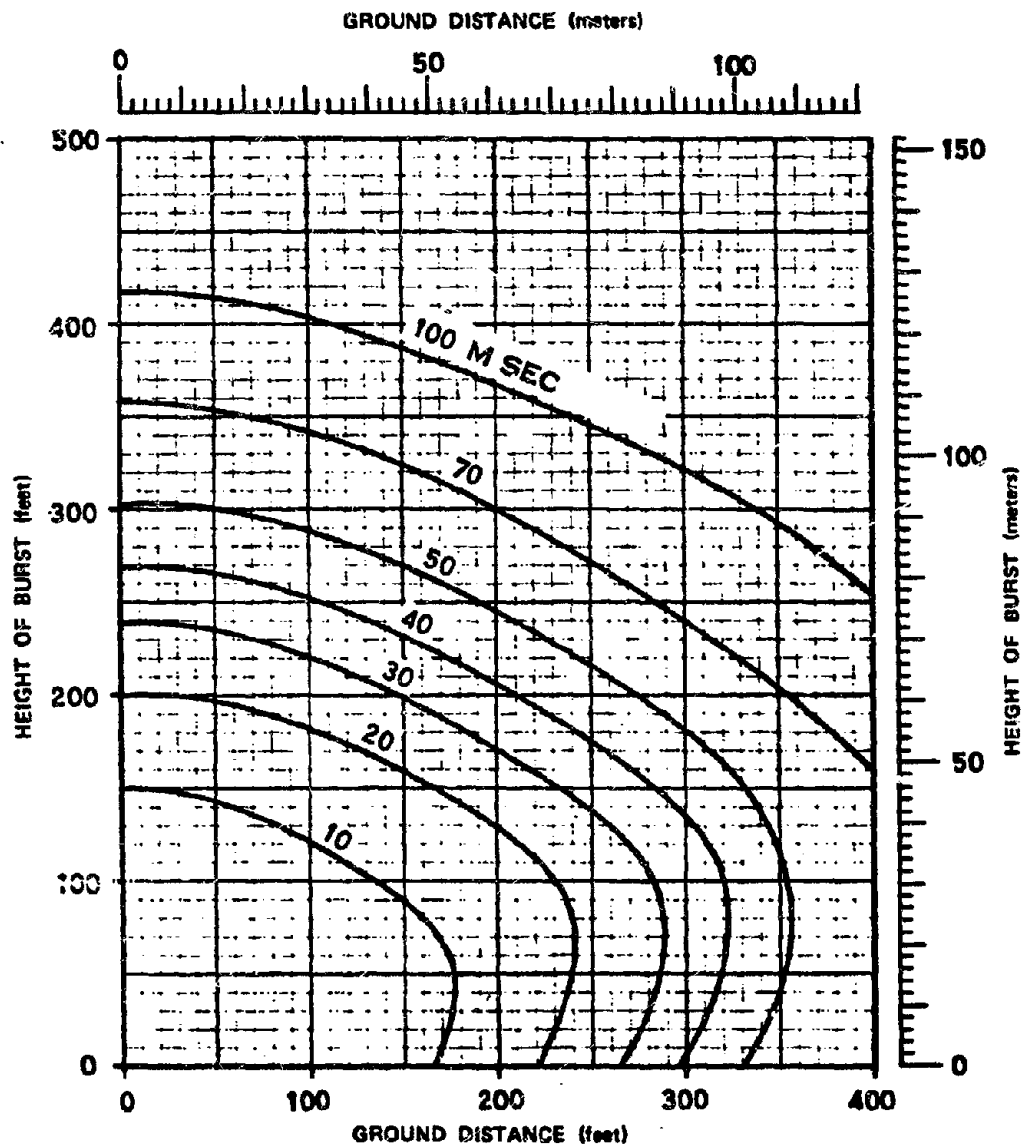


Figure 2-30. ■ Time of Arrival of the Blast Wave Along the Surface from a 1 kt
Explosion Over a Thermally Nonideal Surface, Very High Overpressure Region ■
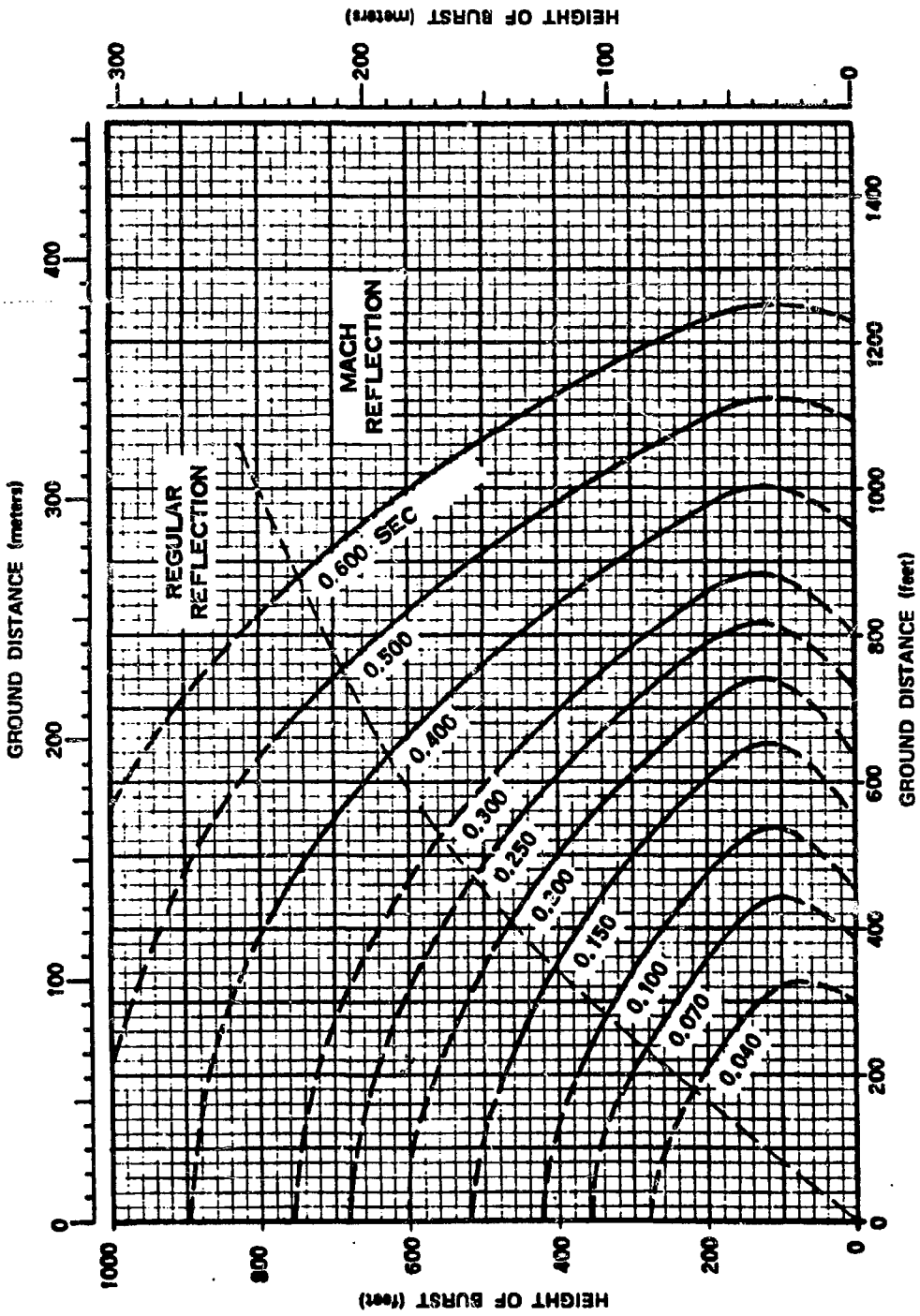
Figure 2-31. Time of Arrival of the Blast Wave Along the Surface from a 1 kt Explosion Over a Thermally Nonideal Surface, High Overpressure Region
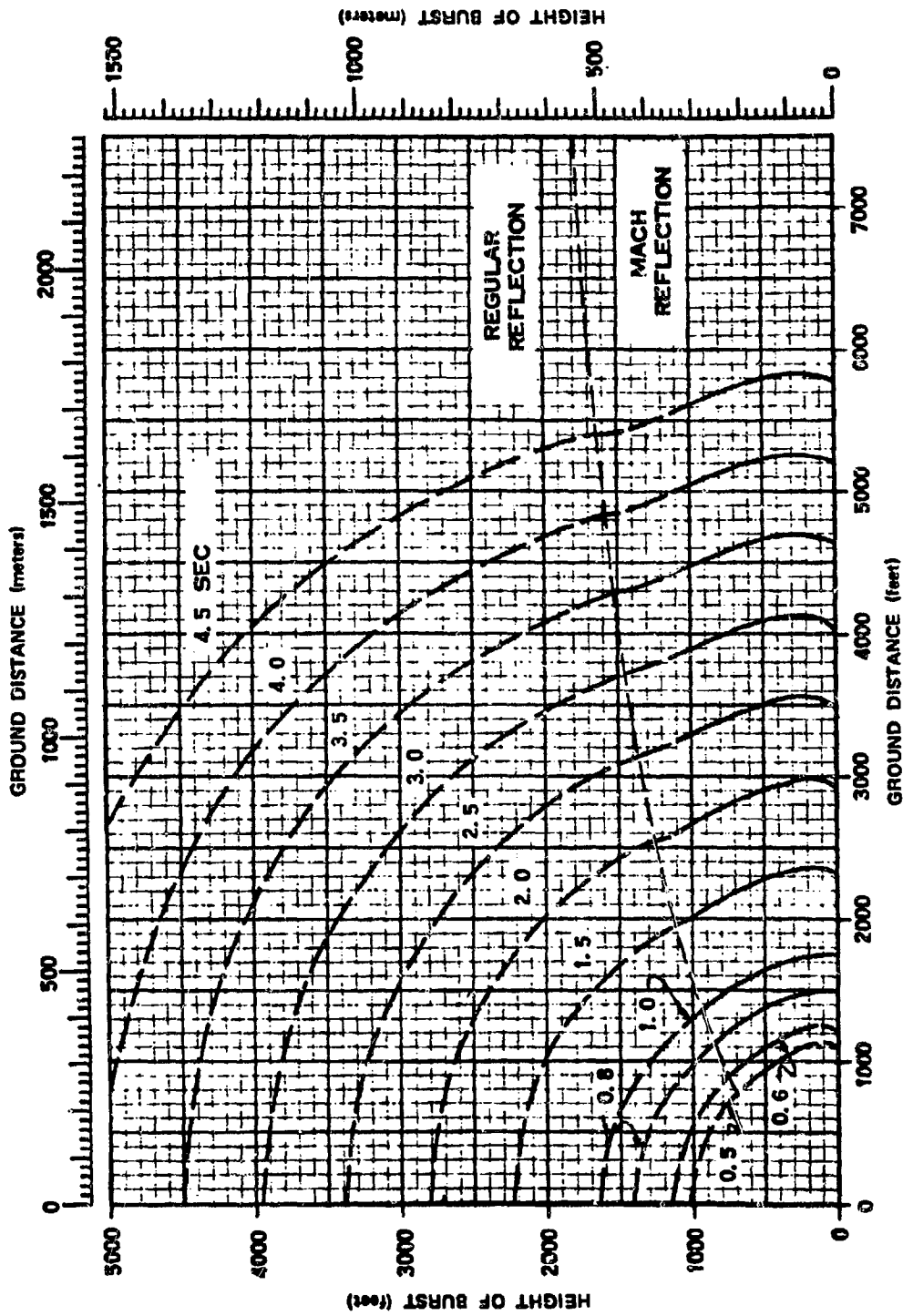
Figure 2-32. Time of Arrival of the Blast Wave Along the Surface from a 1 kt Explosion Over a Thermally Nonideal Surface, Low Overpressure Region

## Problem 2-12. Calculation of Positive Phase Duration of the Blast Wave at the Surface

Figures 2-33 and 2-34 show the duration of the positive phase of the overpressure pulse at the surface as a function of height of burst and horizontal distance from ground zero for a 1 kt explosion in a sea level atmosphere. The two figures are for near-ideal and thermally nonideal surface conditions, respectively. Positive phase duration of the dynamic pressure pulse may be estimated from data obtained from Figures 2-33 and 2-34, and Table 2-4.

Scaling. For yields other than 1 kt, the duration of the positive overpressure, height of burst, and distance from ground zero scale as follows:

$$\frac{t_p^+}{t_{p1}^+} = \frac{h}{h_1} = \frac{d}{d_1} = W^{1/3},$$

where $t_{p1}^+$, $h_1$, and $d_1$ are the positive overpressure duration, height of burst, and ground distance for a 1 kt explosion, and $t_p^+$, $h$, and $d$ are the corresponding time and distances for a yield of $W$ kt. If the surface is above 5,000 feet, or if the atmospheric conditions at the surface differ from standard conditions, the altitude scaling procedures given in paragraph 2-14 should be used.

Example

Given: A 160 kt explosion 2,700 feet above a thermally nonideal surface.

Find: The positive overpressure and dynamic pressure durations at the surface 9,000 feet from ground zero.

Solution: The corresponding height of burst and ground distance for a 1 kt explosion are

$$h_1 = \frac{h}{W^{1/3}} = \frac{2,700}{(160)^{1/3}} = 500 \text{ feet},$$

$$d_1 = \frac{d}{W^{1/3}} = \frac{9,000}{(160)^{1/3}} = 1,660 \text{ feet}.$$

From Figure 2-34, the positive overpressure duration corresponding to a height of burst of 500 feet and a ground distance of 1,660 feet is about 0.3 seconds for a 1 kt explosion. From Table 2-4, the corresponding duration of the positive dynamic pressure is 0.39 seconds.

Answer: The corresponding positive overpressure and dynamic pressure durations for a 160 kt explosion are

$$t_p^+ = t_{p1}^+ W^{1/3} = (0.3)(160)^{1/3} = 1.6 \text{ seconds},$$

$$t_q^+ = t_{q1}^+ W^{1/3} = (0.39)(160)^{1/3} = 2.1 \text{ seconds}.$$

These are expected values. The range of possible values for the positive phase durations could be obtained by applying the uncertainties in ground distance given below in "Reliability" by methods similar to those illustrated for time of arrival in Problem 2-11. Since the uncertainties in $t_q^+$ are greater than for $t_p^+$, the smaller value of $t_q^+$ may be less than the smaller value of $t_p^+$. In this case, the smaller value of $t_p^+$ should be used as the lower limit for $t_q^+$ since the dynamic pressure positive phase is expected to last longer than the overpressure positive phase.

Reliability: Figures 2-33 and 2-34 were constructed entirely from experimental data. Since overpressure usually is changing slowly

when it passes through zero, the exact time marking the end of the positive overpressure phase is difficult to determine experimentally, and the uncertainty of the curves, in terms of ground distance, is large. Ground distance for $t_p^+$ obtained from these curves is estimated to be reliable within ±25 percent for durations of 300 msec or less and within ±50 percent for longer durations. Use of Table 2-4 to obtain values for $t_q^+$ gives ground distances estimated to be within ±50 percent for durations of 390 msec or less and within ±100 percent for longer durations. *The positive dynamic pressure phase is expected to last longer than the positive overpressure*

*phase. Therefore, the lower limit for $t_q^+$ should be no smaller than the lower limit calculated for $t_p^+$.* For near-ideal surface conditions, these estimates apply to a yield range between 1 kt and 20 Mt; for nonideal surface conditions, the estimates apply to a yield range between 1 kt and 50 kt. The curves may be used outside this range of yields with somewhat less confidence.

■ *Related Material:* See paragraphs 2-13 through 2-15, 2-17 through 2-23 and 2-27. See also Tables 2-1 and 2-2 when atmospheric conditions at the surface differ from standard sea level conditions.
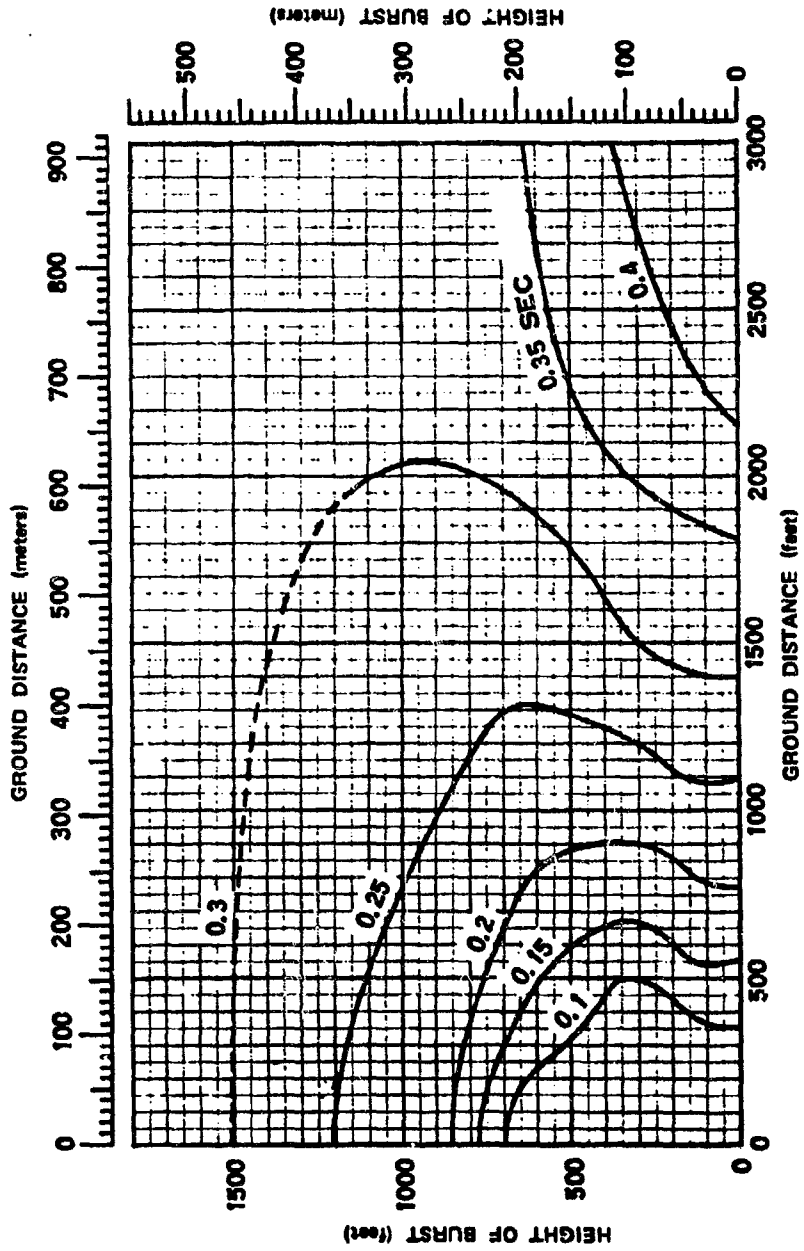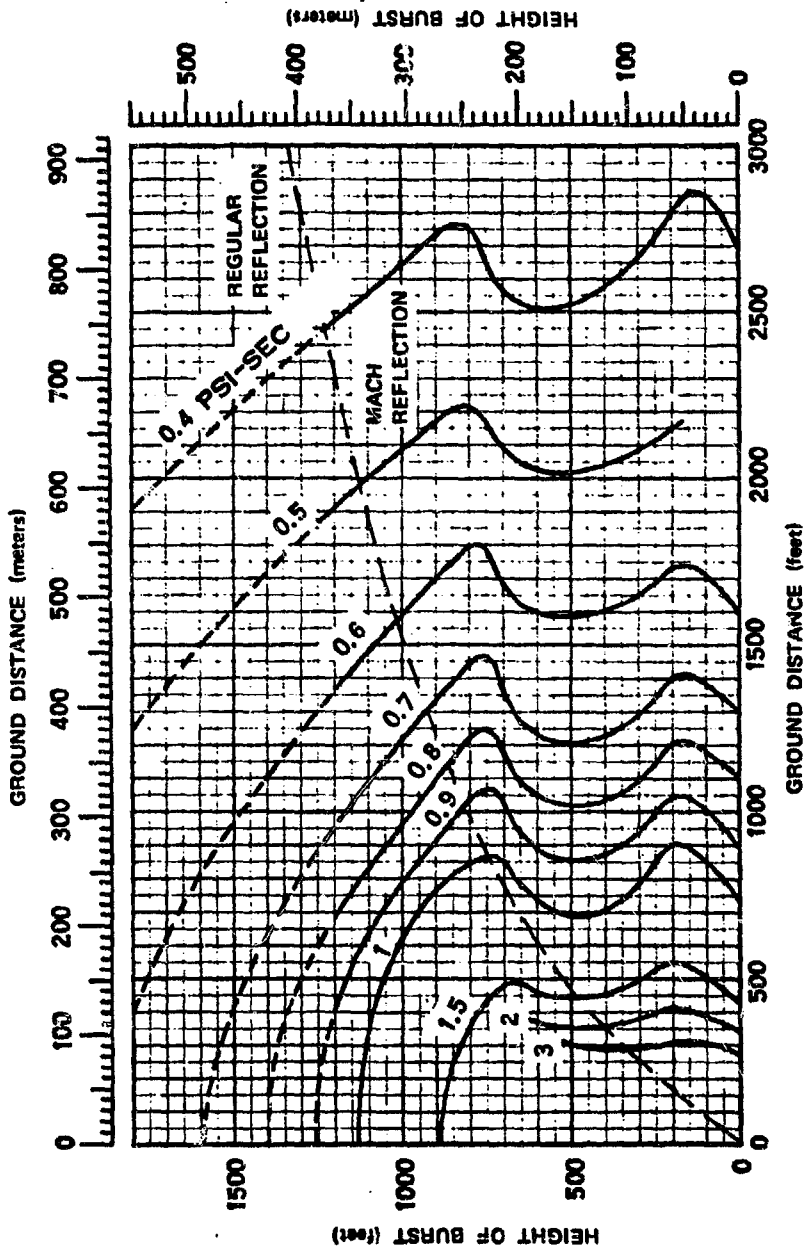
Figure 2-33. ▪▪▪ Duration of Positive Overpressure at the Surface
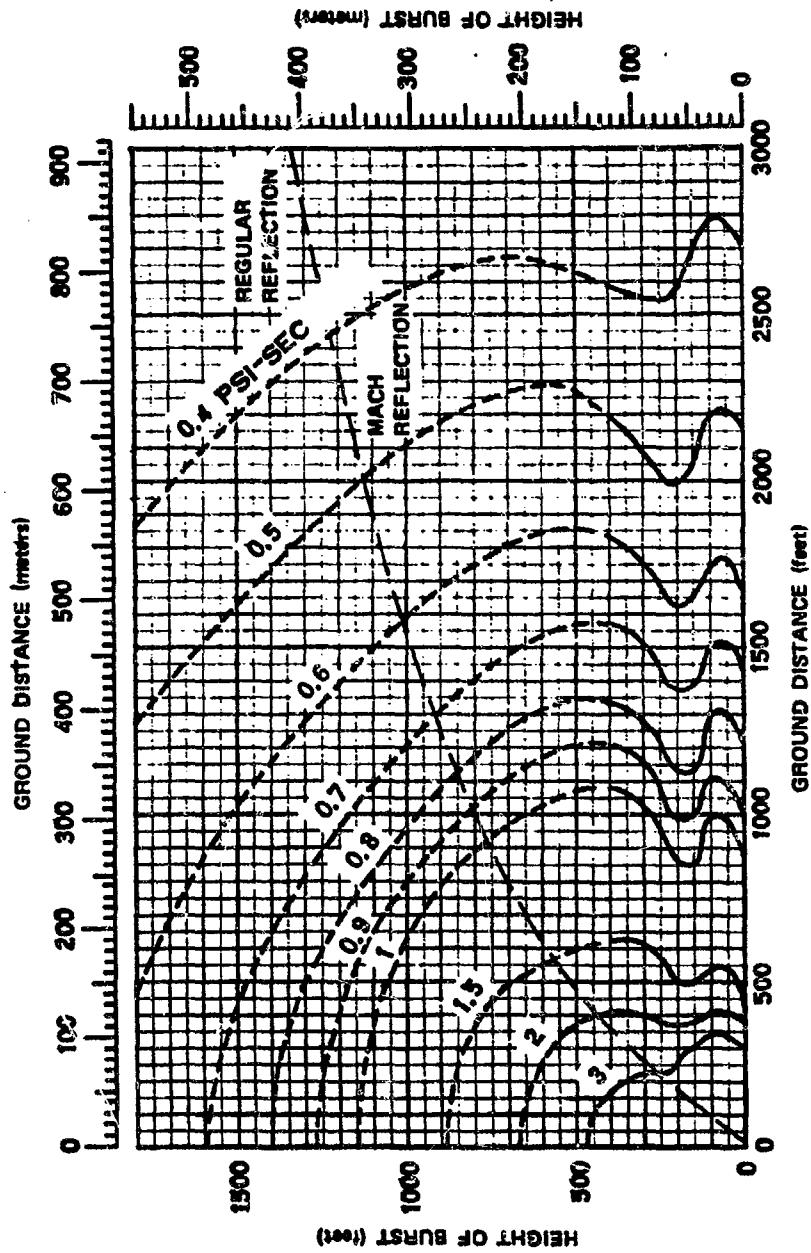from a 1 kt Explosion Over a Near-Ideal Surface ▪▪

2-73
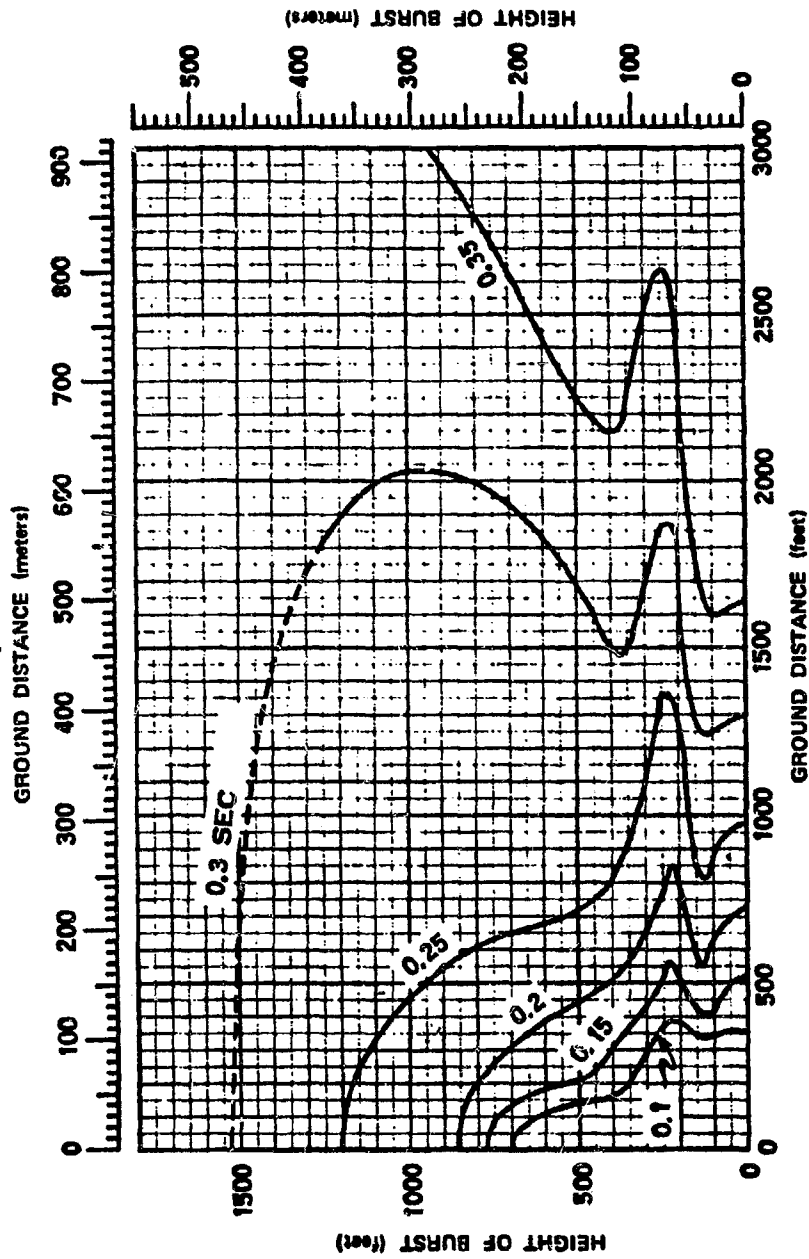
Figure 2-34. ▮ Duration of Positive Overpressure at the Surface from a 1 kt Explosion Over a Thermally Nonideal Surface

## Problem 2-13. Calculation of Positive Overpressure Impulse at the Surface

Figures 2-35 and 2-36 show the positive overpressure impulse at the surface as a function of height of burst and the horizontal distance from ground zero for a 1 kt explosion in a sea level atmosphere. The two figures apply to near-ideal and thermally nonideal surface conditions, respectively.

Scaling. For yields other than 1 kt, the positive overpressure impulse, height of burst, and distance from ground zero scale as follows:

$$\frac{I}{I_1} = \frac{h}{h_1} = \frac{d}{d_1} = W^{1/3},$$

where $I_1$, $h_1$, and $d_1$ are the positive phase impulse at the surface, height of burst, and distance from ground zero, respectively, for a 1 k⁺ explosion, and $I$, $h$, and $d$ are the correspond: impulse and distances from a yield of $W$ k.. 1 the surface is above 5,000 feet, or if the atmospheric conditions at the surface differ from standard conditions, the altitude scaling procedures given in paragraph 2-14 should be used.

Example

Given: A 30 kt explosion 1,000 feet above a thermally nonideal surface.

Find: The overpressure positive phase impulse along the surface 6,000 feet from ground zero.

Solution: The corresponding height of burst and ground distance for a 1 kt explosion are

$$h_1 = \frac{h}{W^{1/3}} = \frac{1,000}{(30)^{1/3}} = 320 \text{ feet},$$

$$d_1 = \frac{d}{W^{1/3}} = \frac{6,000}{(30)^{1/3}} = 1,930 \text{ feet}.$$

From Figure 2-36, the overpressure impulse 1,930 feet from ground zero of 1 kt explosion at 320 feet is 0.55 psi-sec. To account for unpredictable variations in overpressure impulse, the 1 kt ground distance should be taken to be 1,930 ±20 percent (see "Reliability" below), i.e., 1,540 to 2,320 feet. From Figure 2-36, the overpressure impulses at these distances are 0.70 and 0.45 psi-sec, respectively.

Answer: The overpressure positive phase impulse from the 30 kt explosion will be between

$$I = I_1 W^{1/3} = (0.70)(30)^{1/3} = 2.2 \text{ psi-sec},$$

and

$$I_1 W^{1/3} = (0.45)(30)^{1/3} = 1.4 \text{ psi-sec},$$

with an expected value of

$$I = I_1 W^{1/3} = (0.55)(30)^{1/3} = 1.7 \text{ psi-sec}.$$

Reliability: The overpressure impulse contours in Figures 2-35 and 2-36 are estimated to be reliable within ±20 percent of the indicated ground distance. For near-ideal surface conditions, this. reliability estimate applies to yields between 1 kt and 20 Mt and burst heights for 1 kt below 1,000 feet; for nonideal surfaces, the estimates apply to yields between 1 kt and 50 kt and burst heights for 1 kt below 1,000 feet. Outside this range of yields and burst heights, these curves may be used with somewhat less confidence.

Related Material: See paragraphs 2-13 through 2-15, 2-17 through 2-23 and 2-28. See also Tables 2-1 and 2-2 when atmospheric conditions at the surface differ from standard sea level conditions.

Figure 2-35. Positive Overpressure Impulse at the Surface from a 1 kt Explosion Over a Near-Ideal Surface

Figure 2-36. Positive Overpressure Impulse at the Surface from a 1 kt Explosion Over a Thermally Nonideal Surface

Figures 2-37 and 2-38 show the height of the Mach stem as a function of horizontal distance from ground zero for several heights of burst for a 1 kt explosion in a sea level atmosphere. These curves, in effect, show the trajectory of the triple point (paragraph 2-18 and 2-29).

Scaling. For yields other than 1 kt, the Mach stem height, height of burst, and ground distance scale as follows:

$$\frac{H}{H_1} = \frac{h}{h_1} = \frac{d}{d_1} = W^{1/3},$$

where $H_1$, $h_1$, and $d_1$ are the height of the Mach stem, the height of burst, and the distance from ground zero, respectively, for a 1 kt explosion, and $H$, $h$, and $d$ are the corresponding distances for a yield of $W$ kt. If the surface is above 5,000 feet, or if the atmospheric conditions at the surface differ from standard conditions, the altitude scaling procedures given in paragraph 2-14 should be used.

Example:

Given: A 55 kt explosion 1,000 feet above the surface.

Find: The ground distance beyond which an aircraft flying 500 feet above the surface will be in the Mach reflection region.

Solution: The corresponding height of burst and Mach stem height for a 1 kt explosion are

$$h_1 = \frac{h}{W^{1/3}} = \frac{1,000}{(55)^{1/3}} = 260 \text{ feet,}$$

$$H_1 = \frac{H}{W^{1/3}} = \frac{500}{(55)^{1/3}} = 130 \text{ feet.}$$

Interpolation between the curves of Figure 2-37 shows that a 1 kt explosion burst at 260 feet will have a Mach stem height of 130 feet when the triple point is at a ground distance of about 750 feet.

Answer: The corresponding ground distance for a 55 kt explosion is

$$d = d_1 W^{1/3} = (750)(55)^{1/3} = 2,850 \text{ feet.}$$

Since this yield is close to the upper limit at which a ±10 percent tolerance applies (see "Reliability" below), the distance may reasonably be expected to be within about ±15 percent (± about 430 feet). Therefore the Mach stem height may reasonably be expected to exceed 500 feet at a ground range beyond about 3,300 feet.

Reliability: The range at which a given Mach stem height is shown to occur in Figures 2-37 and 2-38 is considered reliable within ±10 percent for yields between 1 kt and 50 kt and within ±25 percent for yields up to 20 Mt. This decrease in confidence with increasing yield results from the lack of knowledge concerning the effect of atmospheric nonhomogeneity on the triple-point trajectory. It is suggested that no correction be made for burst altitude; however, when the data are applied to high-yield air bursts, the results should be treated with somewhat less confidence.

Related Material: See paragraphs 2-13 through 2-15, 2-17 through 2-23, and 2-29. See also Tables 2-1 and 2-2 when atmospheric conditions at the surface differ from standard sea level conditions.
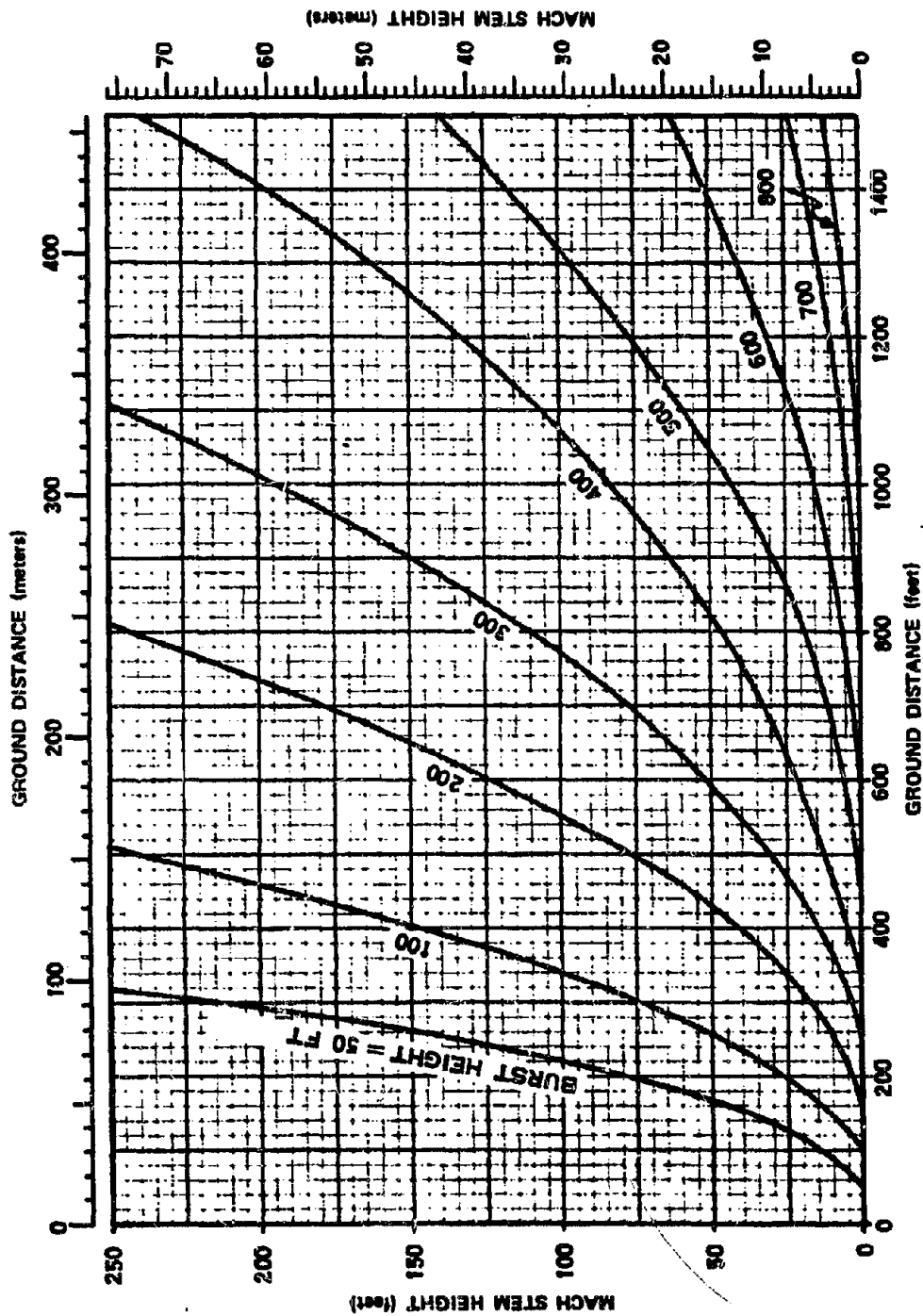
**Figure 2-37.** Mach Stem Height for a 1 kt Explosion, High Overpressure Region
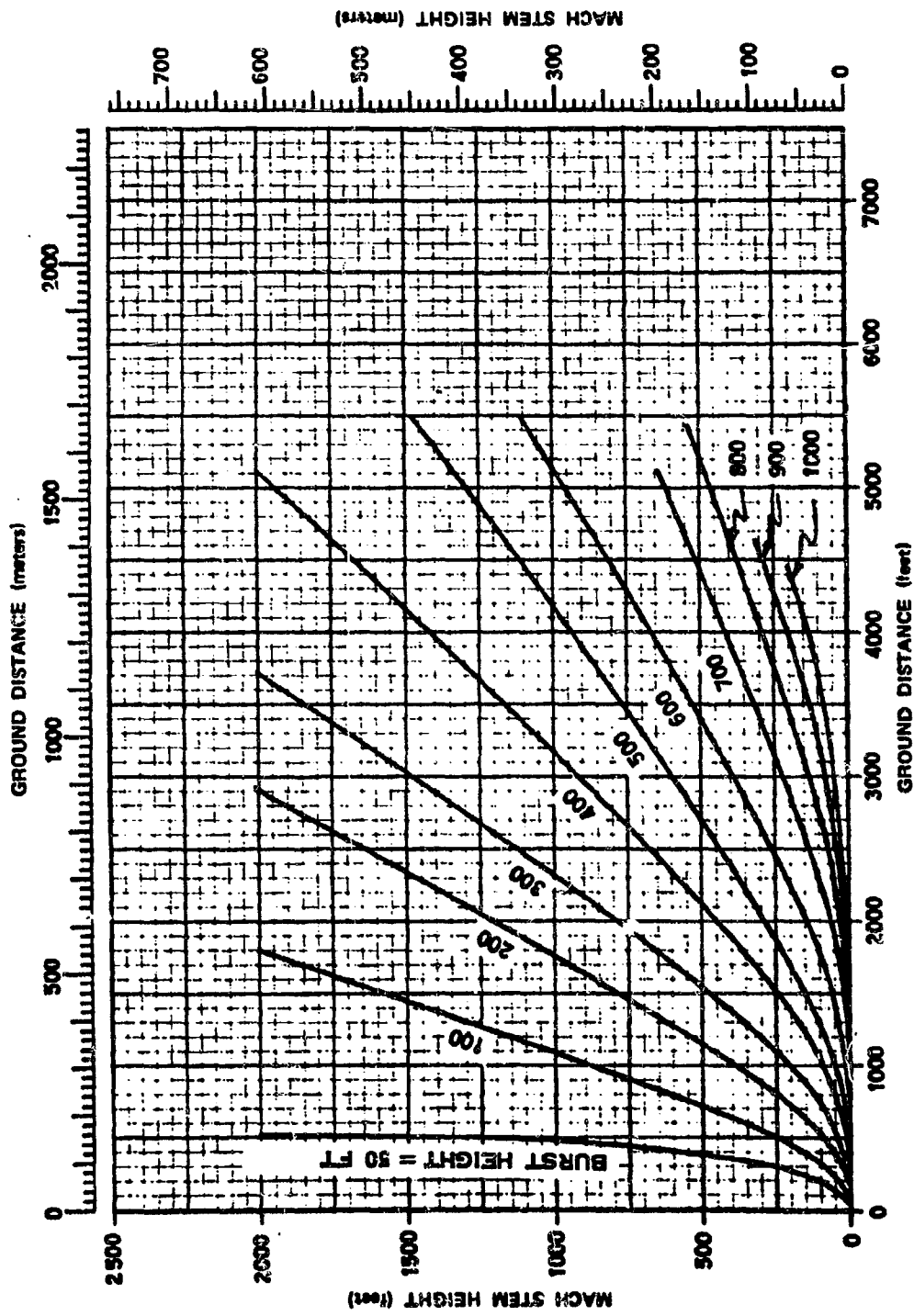
Figure 2-38. Mach Stem Height for a 1 kt Explosion, Low Overpressure Region

## 2-30 Criteria for Precursor Formation

Figure 2-39 shows heights of burst at which an explosion over a thermally nonideal surface is likely to produce a precursor. As indicated in Figure 2-39, bursts higher than 800 $W^{1/3}$ feet are not expected to form a precursor. This is the maximum height that will produce a precursor over asphalt, a surface that produces a precursor more readily than any other that has been tested. A burst below 650 $W^{1/3}$ feet will produce a precursor over desert sand. Since desert sand is considered a more typical nonideal surface than asphalt, it provides the basis for predicting precursors over most thermally nonideal surfaces.

Figure 2-39 also shows that a burst may be too low to produce a precursor as well as too high. At the ranges where a precursor might form, a contact surface burst of less than 30 kt is not expected to heat the surface sufficiently to produce a strong thermal layer; higher yields may create precursors over thermally nonideal surfaces.

Theories suggest that precursor formation depends not only on the amount of thermal energy absorbed by the surface, but also upon the time that is available for the thermal layer to form before the blast wave arrives. When time as well as thermal energy density is considered, theory indicates that the thermal layer and its influence on the blast wave might scale approximately as $W^{1/3}$, as indicated in Figure 2-39; however, no theory has yet been developed that explains the criteria for precursor formation in a completely satisfactory manner. For this reason, these criteria must be based on experimental data. Precursors have been observed from yields as high as 15 Mt; however, the yields that have been detonated between about 650 $W^{1/3}$ and 800 $W^{1/3}$ feet above the surface, and therefore the yields that are of value in confirming these criteria for precursor formation, are limited to the range of about 1 to 50 kt. Over this range of yields, the precursor seems to follow the cube root scaling; however, this may only result from the range of yields for which data are available being inadequate to reveal deviations. No reliability tolerances can be assigned to Figure 2-30, but if the surface is similar to desert sand, precursors may be predicted with reasonable accuracy for yields between 1 and 50 kt.

## 2-31 Overpressure Waveforms

The classical free air overpressure waveform (paragraph 2-12) is seldom found along the surface at overpressure levels above 6 psi. At higher overpressures, such waveforms approach the ideal for special surface conditions such as snow, ice, and water (where thermal effects are normally at a minimum). Even for these surfaces, minor mechanical effects may be present. For example, the rise time over water may not be instantaneous, and there may be a slight rounding of the peak of the overpressure waveform. When these near-ideal conditions exist, overpressure waveforms may be approximated by those for free air, shown in Figure 2-8.

In the simple case of ideal waveforms in free air, all of the properties of the blast wave, and therefore its damage potential, may be determined by specifying the ambient atmospheric conditions plus two blast parameters (for example, peak overpressure and positive overpressure impulse). When the blast wave loses its ideal characteristics, two other properties of the overpressure waveform become important: (1) for most overpressure-sensitive targets, a gradual rise to a given overpressure is less destructive than the abrupt rise of an ideal pulse; (2) as a result of the sustained overpressures often found in nonideal waveforms, a given peak overpressure may be associated with a much larger positive impulse than if overpressure pulse shape were ideal. Additional effects caused by changes in the dynamic pressure waveform are discussed in succeeding paragraphs.
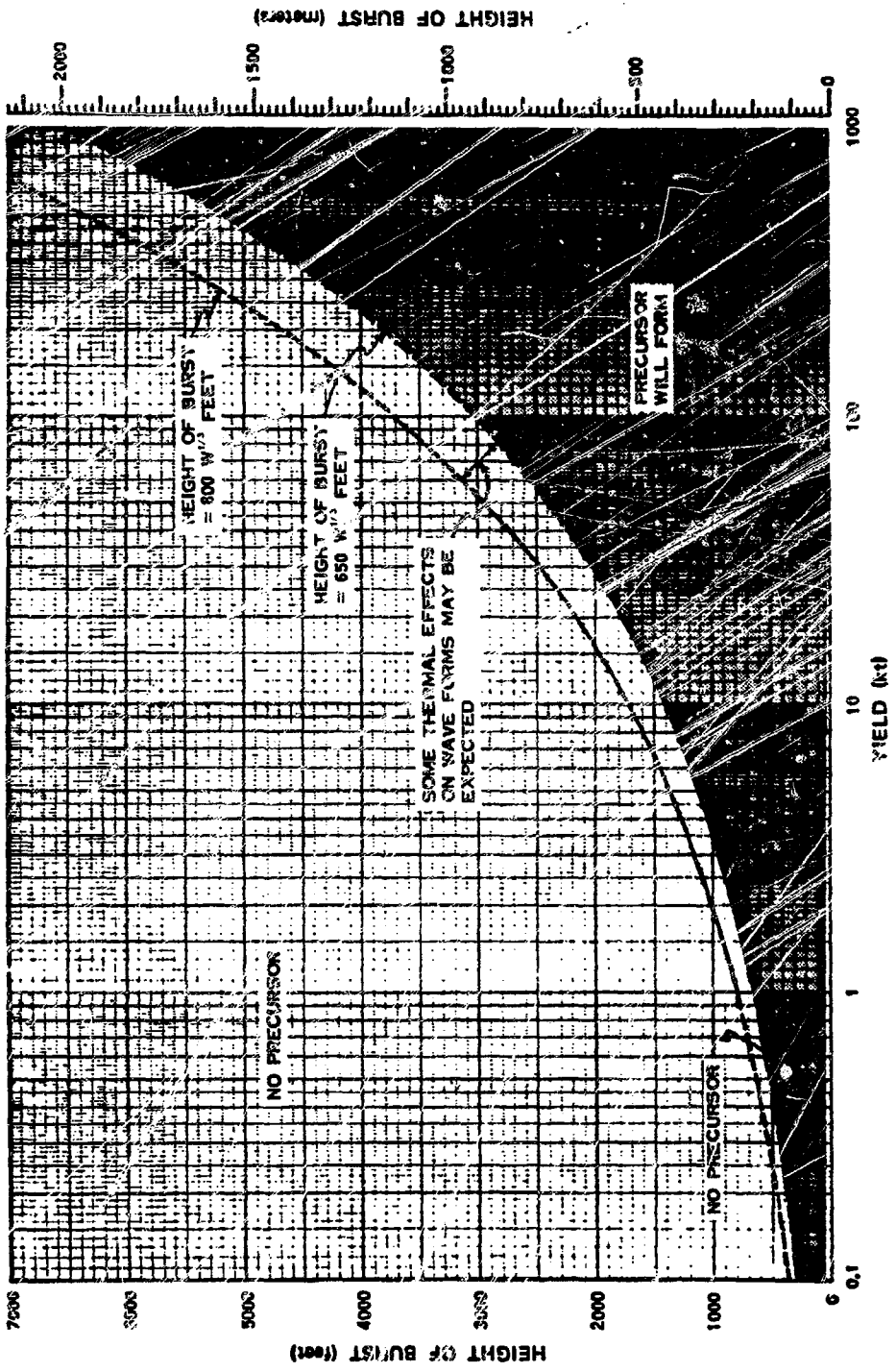
HEIGHT OF BURST
= 800 $W^{1/3}$ FEET

HEIGHT OF BURST
= 650 $W^{1/3}$ FEET

PRECURSOR
WILL FORM

SOME THERMAL EFFECTS
ON WAVE FORMS MAY BE
EXPECTED

NO PRECURSOR

NO PRECURSOR

YIELD (kt)

HEIGHT OF BURST (feet)

Figure 239. Criteria for Precursor Formation

A series of eleven waveforms character-istic of the blast wave over a thermally nonideal surface is shown in time sequence in Figure 2-40. Although the evolution of a precursor is a continuous process, the waveforms may be classified loosely into five types, according to the state of development of the precursor:

Type I: Waveform before precursor forms (a)
Type II: Development of the precursor (b, c, d)
Type III: Evolution of fully developed precursor (e, f, g)
Type IV: Decline of precursor (h, i, j)
Type V: Return to nearly ideal waveform (k)

The overpressure waveforms generated under any particular set of conditions depend strongly on the degree to which nonideal surface effects interact with the blast wave. In general, the more nonideal the surface conditions, the more nonideal will be waveforms near the surface. The waveforms shown in Figure 2-40 are typical for scaled heights of burst between 100 and 400 feet over flat desert surfaces. Characteristics of these waveforms are discussed below.

- Type I — Just before the precursor forms, the waveform a is relatively ideal.

- Type II — As the precursor starts to develop, a separate shock front forms in the thermal layer and moves out ahead of the main shock. In waveform b these two shock fronts are nearly ideal but, as the precursor develops, its diverging flow pattern weakens its own shock front. At the same time, the growing precursor interferes more strongly with the main blast wave, which apparently loses any semblance of a true shock front at the surface. Separation of the two peaks indicates the forward growth of the precursor; however, the second peak in waveforms c and d no longer marks the exact position of the main blast wave. Typical changes in Type

II waveforms at early times are a rapid attenuation of the first peak and a rounding of the second peak. At later times, the second peak is attenuated more rapidly than the first, and the first loses its shock-like rise. The slow decay after the first peak in waveforms c and d is sometimes replaced by a plateau.

- Type III — As the distance from ground zero increases, the peaks and valleys become poorly defined. At close distances, the waveform e has a large rounded maximum followed by a slow decay, and a later and smaller second peak. At longer distances, the first peak is attenuated more rapidly than the second, and the two peaks become comparable in magnitude (f). The rise times also become longer. The second peak disappears at longer distances, leaving a low, rounded, flat-topped waveform g with a long initial rise and slow decay, during which there is considerable turbulence. This waveform is typical of strong precursor action.

- Type IV — Farther from ground zero, the thermal layer becomes less intense, and the precursor begins to weaken and lose forward speed. The second peak reappears, and both peaks become sharper. The rounded plateau in waveform h and the step-like appearance of i are typical. As the main shock overtakes the precursor, the waveform assumes an almost classical form j with a sharp rise to a more or less level plateau, followed by an essentially regular decay. This waveform is typical of the "clean-up" portion of the precursor cycle.

- Type V — After the precursor has disappeared, the pressure pulse again approaches a classical waveform k. This waveform is longer than it would be if a precursor had never formed.

Methods for determining ground dis-

TYPE I (a)

TYPE II (b)   (c)   (d)

TYPE III (e)   (f)

(g)

TYPE IV (h)   (i)   (j)

TYPE V (k)
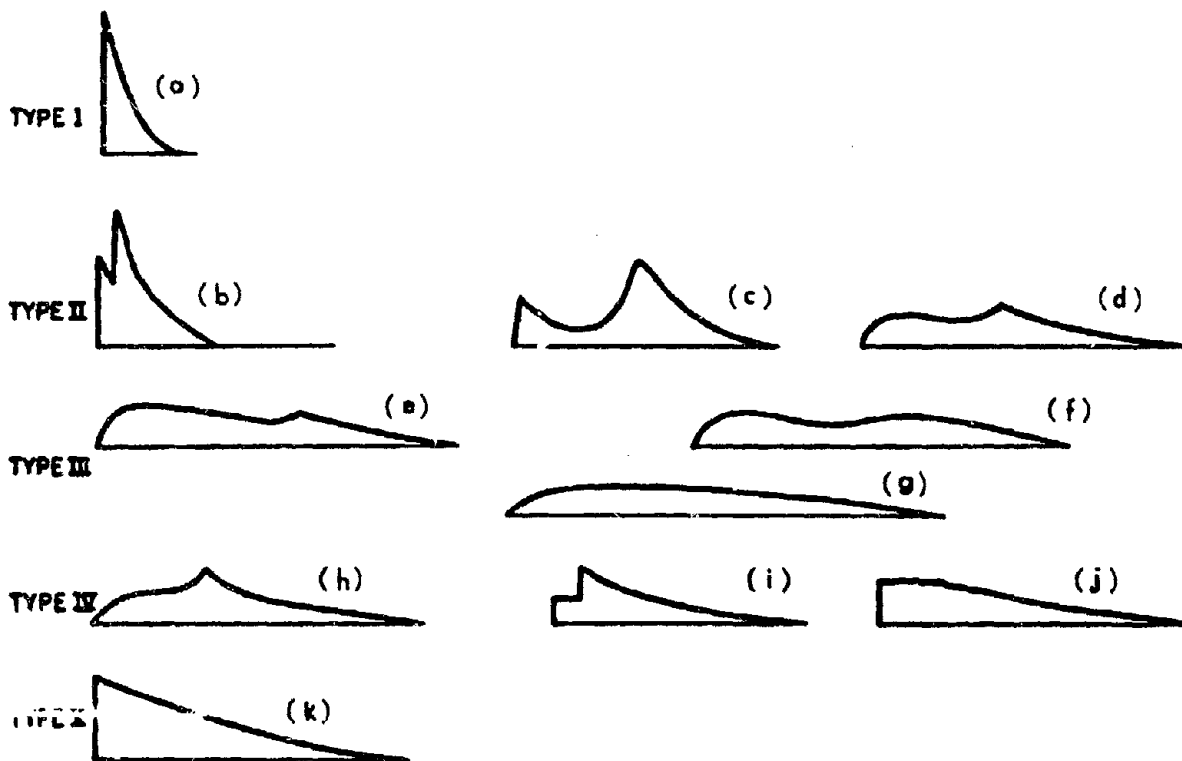
Figure 2-40. ▨ Typical Sequence of Overpressure Waveforms
Over Thermally Nonideal Surfaces ▨

tances at which the waveforms described above will occur are described in Problem 2-15.

## 2-32 Dynamic Pressure Waveforms ▮▮

▮▮ Dynamic pressure waveforms at the surface approach the classical shape shown in Figure 2-9 when the surface conditions are near-ideal. The conditions under which this occurs are more restricted than those for overpressure waveform. Differences result from surface conditions that do not lead to precursor formation but do lead to dust or spray loading of the air. Such surfaces are expected to modify the dynamic pressure waveform without changing the overpressure waveform to any great extent.

▮▮ Dynamic pressure waveforms that appear over thermally nonideal surfaces are more difficult to measure than overpressure waveforms, and the measurements are subject to wider variations. For these reasons it is not possible at this time to provide a figure that shows zones in which various waveforms can be expected. However, representative waveforms have been constructed (Figure 2-41), and tentatively have been classified into five categories: A, B, C, D, and E (letters rather than Roman numerals are used with dynamic pressure waveforms to emphasize that the various types cannot be directly correlated with the waveform types used to classify overpressure waveforms). These waveforms are discussed below.

- Type A — Before the precursor forms, the waveform is relatively ideal (1).
- Type B — As the precursor starts to develop, the waveform shows two distinct peaks. The first, corresponding to the precursor, has a shock type rise in most cases. The second is larger than the first at close distances (waveforms 2 and 3), but at longer distances (waveform 4) it becomes comparable in magnitude to the first.

- Type C — As the precursor becomes fully developed, the waveform retains its double peak but loses its rapid initial rise time. Actual record traces have a very turbulent appearance. The second peak is smaller than the first (5) and tends to become indefinite with increasing distance (6).

- Type D — As the precursor becomes weaker, the waveform assumes an essentially single peaked form, characterized at close distances (waveform 7) by a low-amplitude plateau with a slow rise. Actual traces have a very turbulent appearance. As the distance from ground zero increases (waveform 8), the turbulence lessens, and the plateau develops a shock rise with either a flat top or a slow steady increase to a second shock rise, followed by a smooth decay. The second shock eventually overtakes the first (waveform 9), leaving a smooth, clean trace with a slight rounding after the initial shock type rise.

- Type E — After precursor cleanup, the waveform (10) resumes its approximately classical shape. Positive phase duration is longer than it would be at this distance if a precursor had not formed. This longer duration is more marked for dynamic pressure than for overpressure.

TYPE A (1)

TYPE B (2) (3) (4)

(5) (6)
TYPE C

(7) (8) (9)
TYPE D

(10)
TYPE E
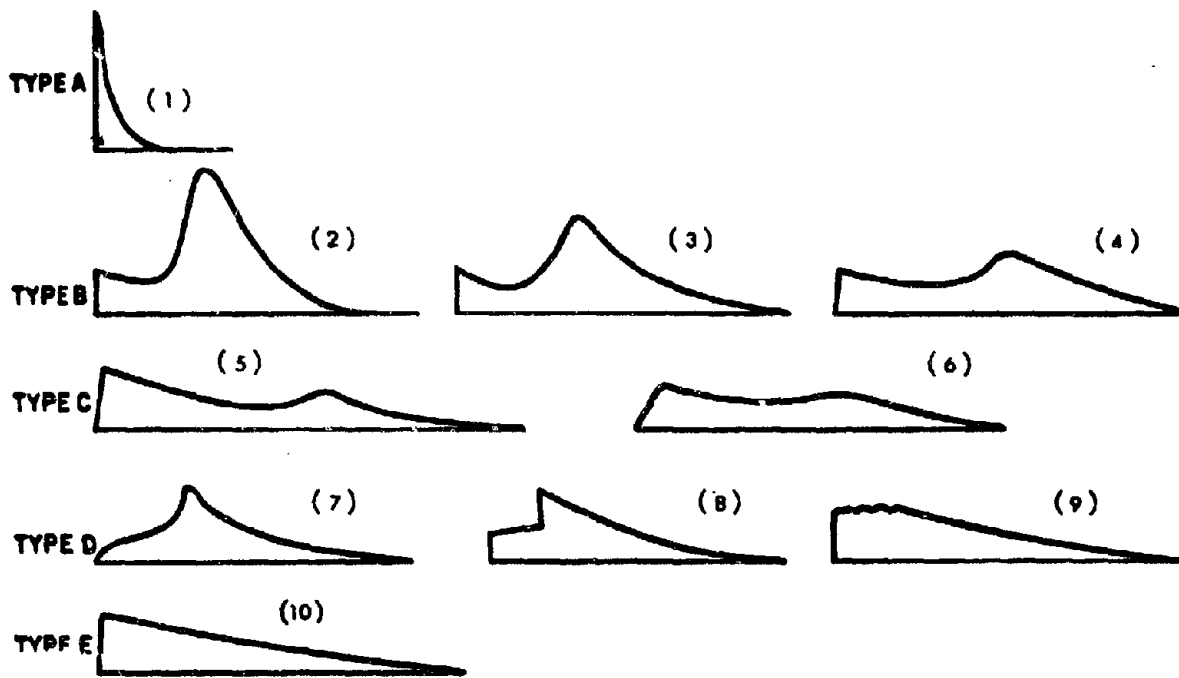
Figure 2-41. ▊ Typical Sequence of Dynamic Pressure Waveforms
Over Thermally Nonideal Surfaces ▊

## Problem 2-15. Calculation of Distances for Overpressure
## Waveforms in the Precursor Region

██ Figure 2-42 shows zones, defined by height of burst and distance from ground zero, wherein overpressure waveforms depicted in Figure 2-40 might be expected to occur from a 1 kt explosion over a thermally nonideal surface. Neither the waveforms nor the ranges at which they occur can be predicted reliably for all conditions. The waveforms will be modified as height of burst changes; if the scaled height of burst is above 400 or below 100 feet, the waveforms may differ significantly from those shown in Figure 2-40. Any other surface effect that modifies the precursor also will modify the waveforms. For example, distortion of the overpressure waveform will be less severe if trees or shrubs decrease the velocity of the surface winds required for precursor formation (other surface interactions are discussed in paragraphs 2-20 through 2-22). Moderate thermal effects may produce disturbed waveforms that are neither ideal nor as extreme as those shown in Figure 2-40. Information from Figures 2-40 and 2-42 should be considered a useful guide, not an infallible prediction.

██ *Scaling.* For yields other than 1 kt, scale as follows:

$$\frac{h}{h_1} = \frac{d}{d_1} = W^{1/3},$$

where $h_1$ and $d_1$ are the height of burst and the ground distance for 1 kt, and $h$ and $d$ are the corresponding distances for a yield of $W$ kt. If the surface is above 5,000 feet, or if atmospheric conditions at the surface differ from standard sea level conditions, the altitude scaling procedures described in paragraph 2-14 should be used.

██ *Example* ██

*Given:* A 100 kt explosion 600 feet above a thermally nonideal surface.

*Find:*

a. The ground distance to which a precursor may be expected to extend.

b. The waveform to be expected at the surface 1,800 feet from ground zero.

*Solution:* The corresponding height of burst for 1 kt is

$$h_1 = \frac{h}{W^{1/3}} = \frac{600}{(100)^{1/3}} = 130 \text{ feet.}$$

a. From Figure 2-42, the precursor zone extends to approximately 1,130 feet for a 1 kt explosion at a height of 130 feet (the zone indicating a Type V waveform shows the region where precursor characteristics disappear and the waveform approaches the classical shape (Figure 2-40)).

b. The ground distance for a 1 kt explosion corresponding to a distance of 1,800 feet for 100 kt is

$$d_1 = \frac{d}{W^{1/3}} = \frac{1,800}{(100)^{1/3}} = 390 \text{ feet.}$$

*Answer:*

a. The distance to which a precursor may be expected to extend from ground zero of a 100 kt explosion at a height of 600 feet is

$$d = d_1 W^{1/3} = (1,130)(100)^{1/3} = 5,240 \text{ feet.}$$

b. From Figure 2-42, a distance of 390 feet from ground zero of a 1 kt explosion at a

height of 130 feet falls within the zone corresponding to waveform II. This same waveform would be expected at a distance of 1,800 feet from a 100 kt burst at a height of 600 feet.

*Reliability:* Specific reliability figures have not been set on the boundary positions in Figure 2-42. The zone boundaries are derived primarily from full scale tests over desert surfaces. Overpressure waveforms over other surfaces are subject to the variations noted above. Yield scaling is uncertain outside the range of 1 kt to 50 kt, but should be used in the absence of confirming experimental data. Altitude scaling is also a questionable procedure, but it should provide reasonable results for surface altitudes below 10,000 feet.

*Related Material:* See paragraphs 2-12, 2-20 through 2-22, and 2-31.
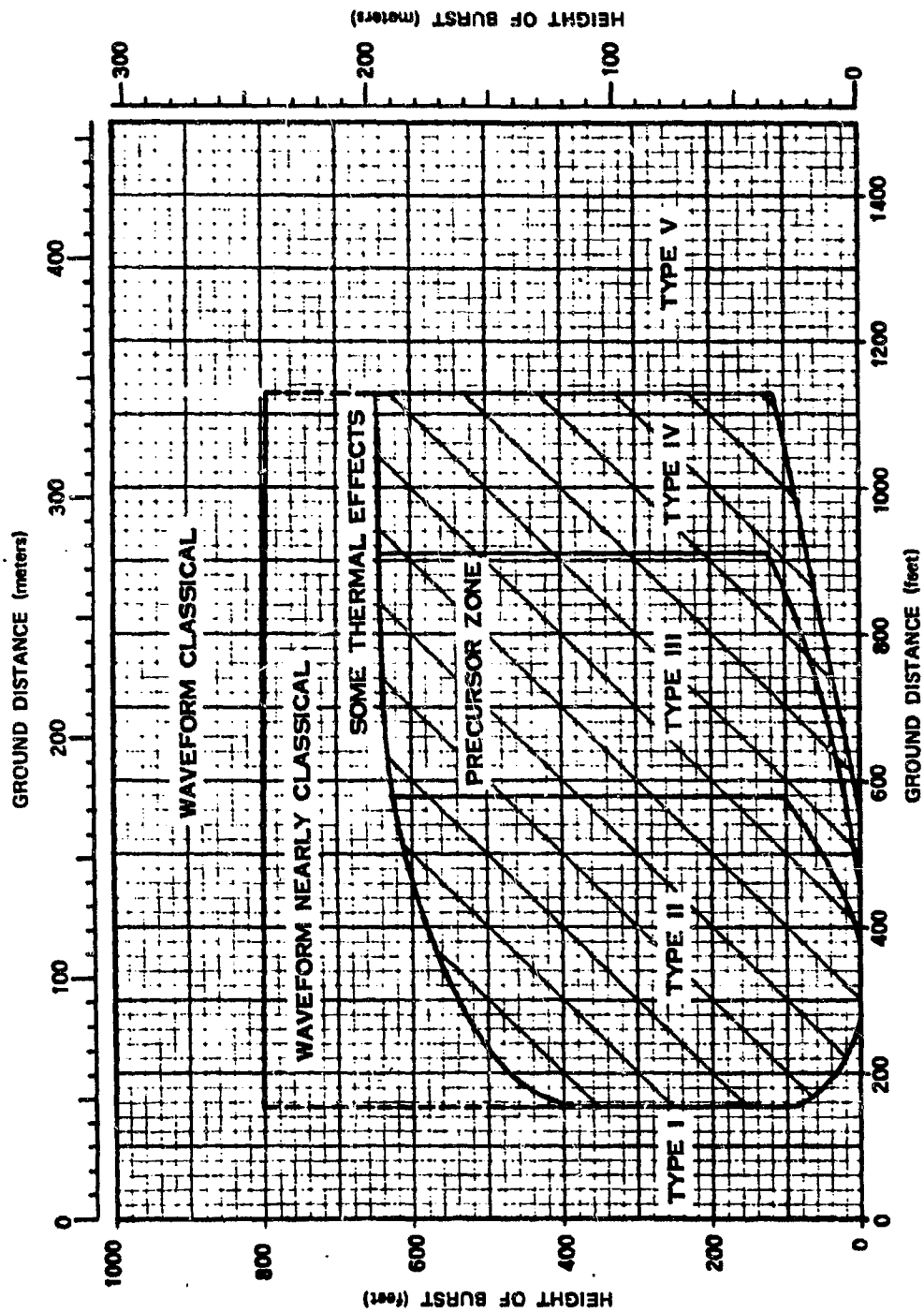
Figure 2-42. ▆ Variation of Overpressure Waveform from a 1 kt Explosion Over a Thermally Nonideal Surface ▆

## 2-33 Effect of Rain and Fog on Overpressure ▮

▮ The effects of atmospheric moisture on blast propagation are not well known; however, theoretical studies agree qualitatively with the small amount of experimental data. As a strong blast wave propagates through air containing water droplets it vaporizes some or all of the water. Vaporization of the water absorbs energy that otherwise would be available for the blast wave to propagate through the air.* As a result, the blast wave is attenuated more rapidly in air that contains water droplets than in air that does not.

▮ The effect of water droplets on peak overpressure may be calculated in terms of effective yield. This procedure is used to obtain lower calculated overpressures at some distance from the burst. Rain or fog has a negligible effect on the amount of available energy close to the nuclear source. The energy density within the fireball is orders of magnitude higher than the energy required to vaporize whatever water may be present, and the amount by which the suspended liquid increases effective air density, even under the extreme conditions within clouds producing severe thunderstorms, is not likely to exceed 2 percent.

▮ Figure 2-43 shows the effective yield for three yields and two conditions of moisture content. Examination of these curves reveals several trends:

● The attenuation produced by heavy rain is greater than the attenuation produced by light rain or fog.

● Effective yield decreases as overpressure decreases, i.e., it decreases as distance (and, therefore, the amount of rain through which the blast wave must propagate) increases.

● At any overpressure level, the blast wave from a 1 kt burst is attenuated less than the blast wave from the two other yields. This difference results from the shorter distances for the 1 kt blast wave. Light rain or fog attenuates the blast wave from a 1 kt explosion to such a small extent that the curve is not included in Figure 2-43.

● At a given overpressure level, the blast wave from a 1 Mt burst is attenuated less than the blast wave from a 125 kt burst. This effect, opposite to that described above, probably results from the relatively large amount of hydrodynamic energy carried by the long-duration blast wave from a 1 Mt source.

▮ The curves shown in Figure 2-43 are based on the assumption of uniform water content between the source and the target. In an actual rainstorm, this assumption is artificial. Typically, water content is several times as high within a rain cloud as it is below the cloud, but without such an assumption the analysis of rain effects would be unduly complex. Actual water distribution patterns are complex, different for different rainstorms, and generally unpredictable. The water densities used in the calculations correspond roughly to precipitation rates of 0.1 and 0.5 inches per hour.

*▮ As a blast wave propagates through air, it continuously expends hydrodynamic energy at the shock front to compress and accelerate the air entering the blast wave. At the same time, the air behind the front expands and decelerates, thereby returning energy to the blast wave. The flow of energy in a weak shock wave resembles that in a sound wave. The expanding air returns nearly all of the energy that it received when it entered the shock front. Consequently, the attenuation of weak blast waves is due principally to spherical divergence. On the other hand, strong shock waves lose appreciable energy, because the sudden compression at the shock front is partially irreversible. Thus, the expanding air beyond the strong shock front returns less energy than was required to compress it, and the corresponding energy loss contributes to the attenuation of the blast wave. If the air contains water droplets, the energy extracted from the blast wave when the water evaporates is returned to the surrounding air when the water condenses; however, condensation occurs too slowly to contribute appreciable energy to the blast wave.

Rain or fog effects should be evaluated only when the optimization of blast against soft targets is important, and then only if the rain or fog extends throughout a volume that includes both the target and the burst. HOB curves for thermally near-ideal surface conditions should be used with Figure 2-43 since thermal energy is attenuated by rain or fog and a wet surface is not expected to form a strong thermal layer.

The effects of atmospheric moisture on other blast parameters, such as time of arrival, positive-phase duration, and dynamic pressure are not well known; however, theoretical considerations indicate that arrival times will remain essentially unchanged, positive-phase durations will be slightly reduced, and dynamic pressures will be slightly increased. Calculations for these other parameters should be made in the normal manner, without applying the yield correction factor obtained from Figure 2-43.

## Problem 2-16. Calculation of Overpressure During a Rainstorm

■■ Figure 2-43 shows the reduced yield in percentage of actual yield, that should be used for overpressure calculations under conditions of rain and fog. This figure should be used together with Figures 2-17 through 2-19 to obtain overpressure values under conditions of rain or fog.

■■ *Scaling.* Interpolation between the curves of Figure 2-43 provides the only yield scaling available. After obtaining an effective yield from Figure 2-43, the scaling procedures described in Problem 2-9 are applicable.

■■ *Example* ■■

*Given:* A 50 kt explosion at a height of burst of 3,000 feet during a heavy rainstorm.

*Find:* The peak overpressure 4,000 feet from ground zero.

*Solution:* The corresponding height of burst and ground distance for a 1 kt explosion yield are

$$h_1 = \frac{h}{W^{1/3}} = \frac{3,000}{(50)^{1/3}} = 815 \text{ feet},$$

$$d_1 = \frac{d}{W^{1/3}} = \frac{4,000}{(50)^{1/3}} = 1,090 \text{ feet.}$$

From Figure 2-18, the peak overpressure expected in clear air is about 13 psi. At this peak overpressure, Figure 2-43 indicates that the effective yield during heavy rain is about 84 percent for 1 kt, 73 percent for a 125 kt burst. A probable effective yield for 50 kt should be between these values and may be about 77 percent. Uncertainty in the degree of attenuation produced by

a rainstorm would cause the effective yield to vary according to the reliability estimates given below. This calculation will determine the most probable value of the peak overpressure rather than the upper and lower limits. The effective yield for further calculations is

$$50 \times 0.77 = 39 \text{ kt.}$$

The corresponding height of burst and ground distance for a 1 kt explosion are

$$h_1 = \frac{h}{W^{1/3}} = \frac{3,000}{(39)^{1/3}} = 885 \text{ feet},$$

$$d_1 = \frac{d}{W^{1/3}} = \frac{4,000}{(39)^{1/3}} = 1,180 \text{ feet.}$$

*Answer:* From Figure 2-18, the most probable peak overpressure is 10 psi.

■■ *Reliability:* Figure 2-43 is based on theoretical calculations and a limited amount of data from small scale field tests and laboratory experiments. Thus, a high reliability cannot be assigned to the curves of Figure 2-43. The upper limit of the effective yield is 100 percent of the actual yield, while the lower limit is estimated to be 60 percent of the value obtained from Figure 2-43. If the burst is below or close to the cloud base in fairly uniform rainfall, somewhat greater reliability might be expected.

■■ *Related Material:* See paragraphs 2-24 and 2-33. See also Problem 2-9.
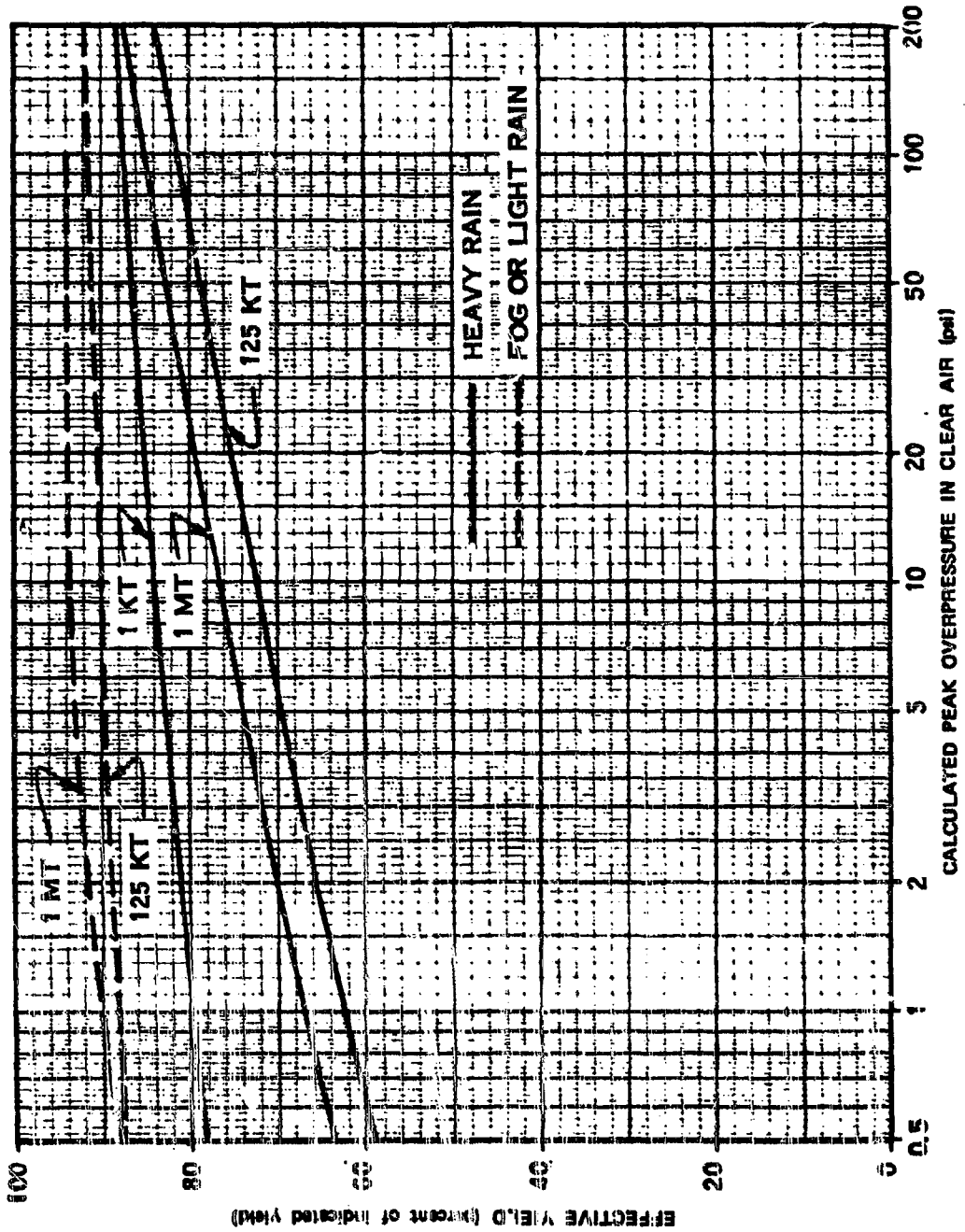
Figure 2-43.  Reduction of Peak Overpressure at the Surface by Rain or Fog—Near-Ideal Surface Conditions

### 2-34 Peak Overpressure at the Surface of Deep Snow █

█ When a shock front enters a layer of snow it is attenuated strongly. Drag forces on the snow crystals dissipate energy contained in the wind behind the shock front. The energy transmitted to the snow crystals is then consumed in compacting the snow layer.

█ Reflection occurs at the top surface of a deep snow layer just as it does at a ground surface. Momentum is conserved in the interaction, and, in the case of a ground surface, the process is analogous to a light, elastic object striking a heavy one. The light object bounces away, retaining most of the energy that it had before the collision. The heavy object receives a small amount of energy. A blast wave striking the earth transmits only a small fraction of its energy as ground shock; consequently, the earth's surface approximates an ideal reflector. A blast wave striking a snow surface is analogous to a ball bouncing from a heavy rug. The reflecting surface has a cushioning effect that makes it a poorer reflector.

█ In the case of a thin layer of snow, the cushioning effect ceases when the pressure wave penetrates the snow layer, reflects from the ground surface, and propagates back to the snow surface. At this time, the snow layer is supported by an internal pressure as high as the pressure produced by the blast wave reflecting from the surface; the reflecting qualities of the snow layer then approach the near-ideal reflecting qualities of the underlying surface.

█ Neither theoretical nor experimental data are available on the effects of thin snow layers on a blast wave, however, a rough calculation is enlightening. If a shock front in snow moves with a speed comparable to that of sound in air, a layer of snow one foot thick, struck by a normally incident blast wave, will absorb energy from the blast wave for about 2 milliseconds and will have the properties of a near-ideal reflecting surface after that time. This 2-millisecond interval is appreciably long only when compared with relatively sharp blast waves. For example, it might alter a 750 psi blast wave from a 1 kt source significantly. The overpressure pulse of this blast wave has an effective triangular duration (see Figure 2-10) of about 20 milliseconds. At lower overpressures, the pulse becomes broader. For a given overpressure, larger yields than 1 kt also produce broader pulses. This comparison indicates the following:

- If a blast wave with a very narrow pressure pulse strikes a thin layer of snow, the snow may alter the leading edge of the pressure pulse enough to reduce peak reflected overpressure.
- In a more typical situation, i.e., one for lower overpressures and yields greater than 1 kt, a thin snow cover affects such a small portion of the overpressure pulse that peak reflected overpressure is essentially the same as at a near-ideal surface.

█ Presently available experimental data on the properties of blast waves over deep snow surfaces are based on high-explosive (HE) experiments. In all of the tests, the snow layers were sufficiently thick to react as though they were infinitely thick. The thinnest snow layers tested (7 inches) correspond to snow layers about 60 $W^{1/3}$ feet thick ($W$ in kt). For an 8 kt burst, this thickness is about 120 feet. Since snow layers thicker than about 120 feet compress to form glacial ice, the 7 inch snow layers have no real scaled counterpart for nuclear bursts larger than about 8 kt.

█ The available data for the effects of snow on the blast wave, when scaled for calculations of the blast wave from bursts larger than 1 kt may be applied with confidence only to regions such as the arctic, where large areas are covered by very thick snow layers.

Scaling HE data over snow to the blast wave from a nuclear burst involves considerable uncertainty. Predictions of peak overpressure over a deep snow surface, are based on the following reasoning: (1) the HE studies show that snow reduces the ground distance to which a given peak overpressure extends by about 10 percent (this figure is never smaller than 0 percent or greater than 20 percent); (2) HE data over snow are not available at points near ground zero, and thus, the experimental data fail to show how much burst height should be changed for a given peak overpressure.

Figures 2-18 and 2-19 may be used to predict peak overpressures over deep snow by reducing all ground distances by 10 percent.

One significant effect of snow cover is that it forms a thermally near-ideal surface. Clean snow reflects most of the thermal radiation that strikes it. Dirty snow absorbs more energy than clean snow but it absorbs it in a way that is unlikely to produce a thermal layer. An experimental study indicates that thermal radiation from a nuclear burst will melt a negligible amount of a clean snow surface and that the water formed will be absorbed quickly by the remaining snow.

An important unknown is the degree to which propagation through snow lengthens the rise time of the overpressure pulse. Even when snow cover is not thick enough to reduce peak reflected overpressure significantly, a layer of snow covering overpressure-sensitive targets may offer protection by reducing the sharpness of the overpressure pulse. This effect may be particularly important in evaluation of ground-shock damage to buried targets.

In the absence of confirming data from nuclear tests over snow, use of the curves in Figures 2-18 and 2-19 must be regarded as tentative. Ground distances obtained from the curves are estimated to be reliable within ±25 percent for yields between 1 kt and 10 kt when used to predict peak overpressures over snow. Outside this range of yields, the curves may be used with somewhat less confidence.

## 2-35 Peak Overpressure at an Infinite Reflecting Surface

Curves showing peak reflected overpressure may apply to finite surfaces, such as the side of a building, or they may apply to the earth's surface, which is effectively infinite in extent. The two types of curves resemble one another except at angles of incidence close to 90°, i.e., at grazing incidence (see footnote to paragraph 2-17 for a summary of the conventions used in specifying the angular orientation of reflecting surfaces). At this grazing angle of incidence, a finite area produces no enhancement of the incident overpressure, the incident overpressure is sometimes called the "side-on" overpressure.

A reflecting surface that is infinite in extent affects the blast wave differently. Figure 2-44 shows that the reflection coefficient $\Delta p_r/\Delta p$ of such a surface at grazing incidence is greater than 1. A blast wave having an angle of incidence of exactly 90° with a flat, infinite surface is, by definition, a contact surface burst. The surface of the earth confines the blast wave from a contact surface burst to half of the volume it would occupy in free air. As a result, peak overpressure is higher than it would be in free air; this fact is indicated by a reflection coefficient greater than 1.

Figure 2-44 has two parts, corresponding to the regions of regular reflection and of Mach reflection. A peak occurs near the boundary between the two regions; at the lower incident overpressures, this peak shows a higher reflected overpressure than that produced by a blast wave striking a surface head-on. The same phenomenon appears in the height-of-burst charts as the knee of an overpressure curve.

At incident overpressures greater than
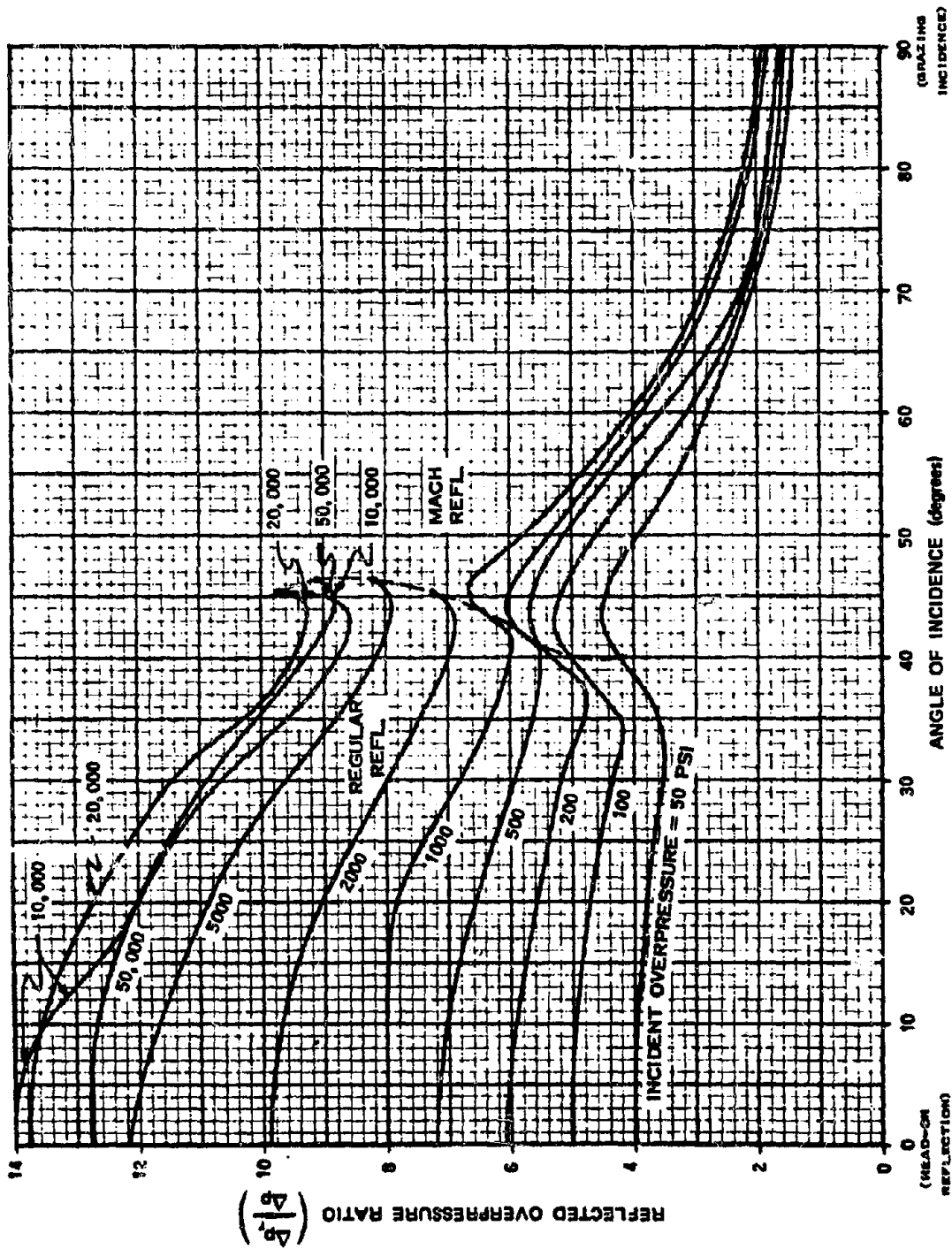
Figure 2-44. Reflection Properties of Strong Shock Waves at an Infinite Surface

5,000 psi, the curves in Figure 2-44 deviate from the regular pattern seen at lower incident overpressures. These deviations result from the high temperatures produced at the shock front, which cause dissociation and ionization of the air atoms to absorb energy that would otherwise increase the pressure of the gas.

The data in Figure 2-44 may be replotted to prepare a height of burst graph. An intermediate plot, consisting of a family of curves, each for a given angle of incidence should be plotted first. Figure 2-45 shows, as an example, the curve for an angle of incidence of 30°. Slant ranges for this intermediate plot are found as a function of incident overpressure from Figure 2-2, the overpressure-distance curve for free air. The data from the intermediate plot may be transferred to the HOB chart by plotting slant range and angle of incidence as shown in the inset of Figure 2-45.

Such a transformation should lead to the HOB chart shown in Figure 2-17; however, certain discrepancies exist between that HOB chart and the data in Figure 2-44. The principal difference is that the peaks shown at angles near 45° in Figure 2-44 have been rounded off in the HOB chart since it is uncertain how well the data in Figure 2-44 describe the actual reflecting properties of the surface of the earth for reasons described below. Although the peaks shown in Figure 2-44 probably occur, the angle at which they occur may be different from that indicated. Therefore, a transformation of every detail of the curves in Figure 2-44 to the HOB chart implies a more detailed knowledge of the shapes of the HOB curves than actually exists.

Uncertainty of the data in Figure 2-44 arises from the way in which these data had to be obtained. The Mach reflection portions of the curves in Figure 2-44 were obtained theoretically, using the shock-wave equations and the air equation of state given in Appendix A. The calculation is complex, involving successive ap-

proximations that are most appropriately handled on a computer.

A large portion of the regular reflection regions of the curves were obtained experimentally. Many data points from nuclear tests document the low pressure curves at angles close to 90°, and theory plus a few data points were used to extrapolate the data to smaller angles and to the highest overpressures shown.

Accuracy of the Mach reflection data is limited because the calculations for these data were based on an ideal reflecting surface. When the burst height is low, errors may result from the resiliency of the earth's surface (or, in the extreme case, cratering), and from thermal energy extracted from the fireball by absorption at the surface. Dirt thrown into the air may alter blast wave properties. Accuracy of the regular reflection data is limited by the difficulty of obtaining a large number of accurate blast wave data points at very high overpressures. These uncertainties are the reasons for smoothing the overpressure contours in Figure 2-17. They are also the reasons for omitting, as unrealistic, curves for peak reflected overpressures higher than 10,000 psi.

### 2-36 Peak Overpressure at a Finite Reflecting Surface

Since a finite surface may cause either regular or Mach reflection, the curves showing reflected overpressure at a finite surface resemble those showing reflected overpressure at an infinite surface.

Figure 2-46 shows curves of reflected overpressure as a function of peak incident overpressure. These curves apply directly to the reflection that occurs at flat surfaces (e.g., sides of buildings) when they are struck by the nearly vertical shock front which characterizes the Mach stem. Although the curves also may be used to determine peak reflected overpressure from the incident free air blast wave when regu-
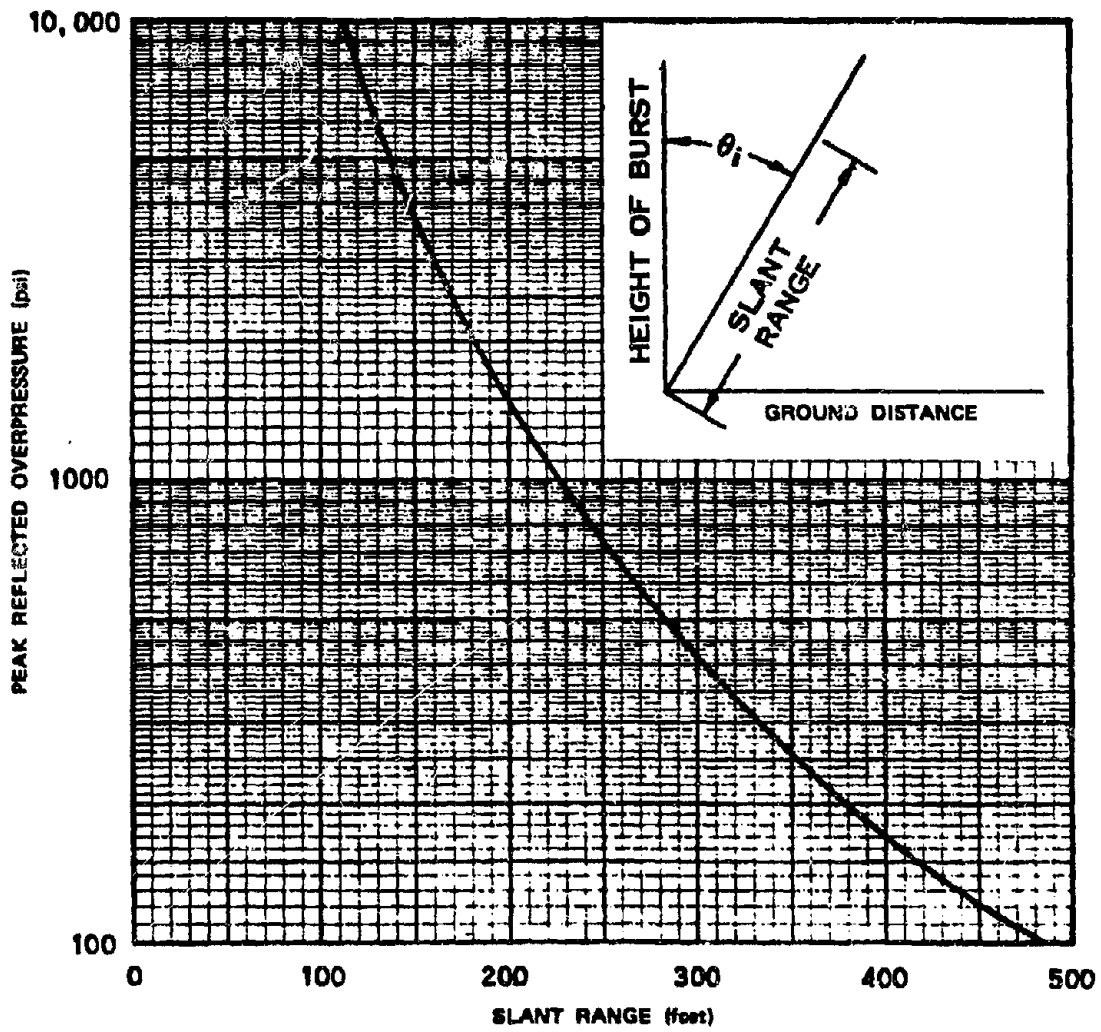
Figure 2-45. ▮ Peak Reflected Overpressure Versus Slant Range for an Angle of Incidence $\theta_i$ of 30° ▮
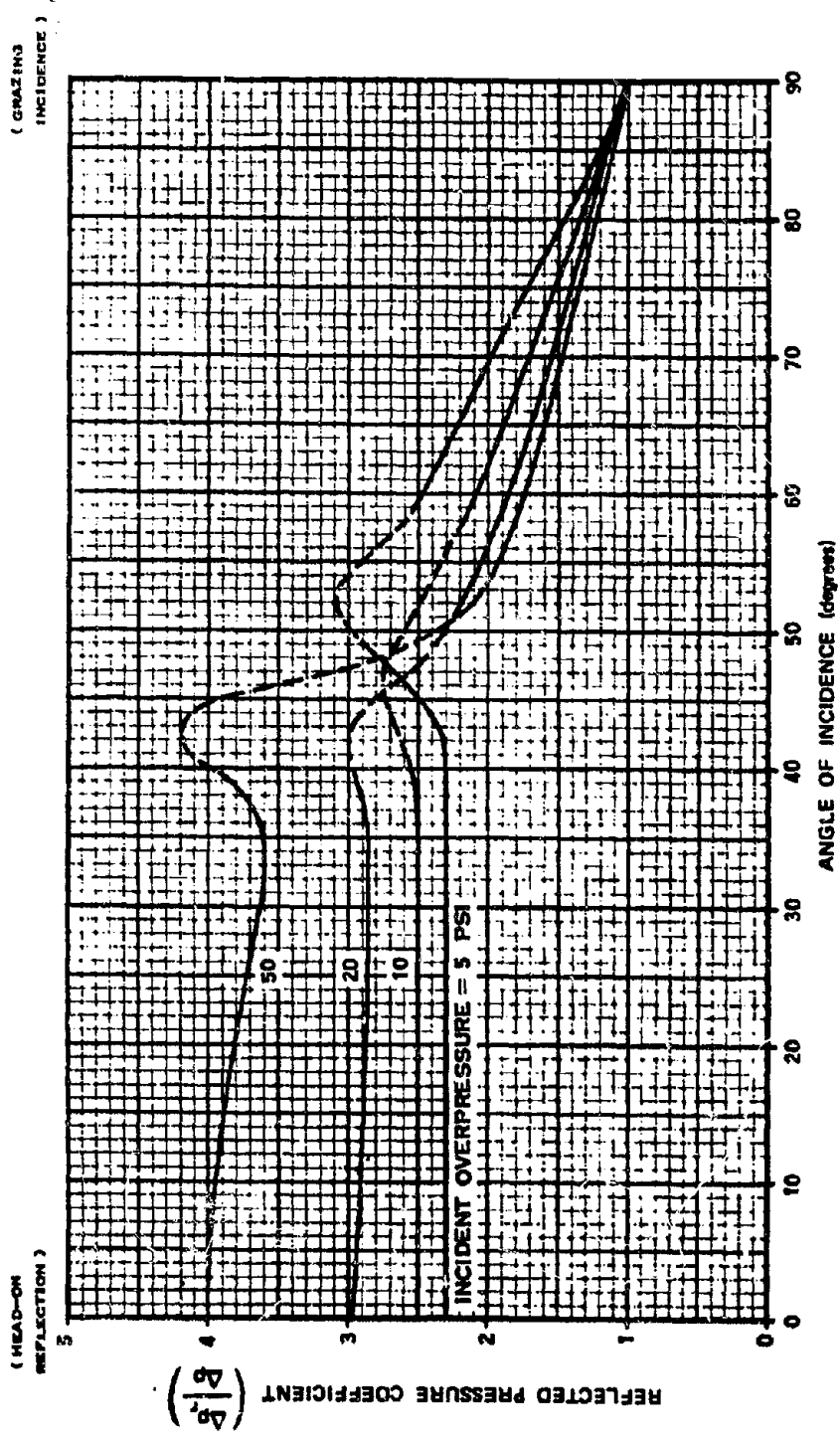
Figure 2-46. Reflection Properties of Shock Waves at a Finite Surface

lar reflection is occurring at the surface of the earth, they do not represent the total effect of multiple reflections that occur when this direct wave strikes the angle formed by the earth and a vertical surface.

These curves only predict the peak overpressure produced when the shock front arrives. In many problems, the total waveform produced by the blast-target interaction also is important; however, the latter is a function of target dimensions as well as blast wave properties as discussed in Section II of Chapter 9 and Section I of Chapter 11.

## 2-37 Peak Overpressure at Rising and Falling Slopes (U)

If a shock wave that is travelling along the ground surface encounters a change in slope, the characteristics of the shock wave will change. If the terrain is characterized by large changes of slope, the changes in the blast wave can be significant. They can result in an overpressure increase by more than a factor of two or a decrease by more than a factor of three.

Interactions with real topography can be exceedingly complex. Therefore both experimental and theoretical studies have, for the most part, dealt with idealized, simplified terrain features. Techniques have been devised for predicting the characteristics of the shock waves that encounter changes in terrain, and methods for applying these techniques to real terrain have been devised.

If the level terrain in front of a slope is in the region of Mach reflection, the blast-wave incident on the slope will have a nearly vertical shock front, the Mach stem. (The nearly hemispherical shock front produced by a contact surface burst is considered a special case of an incident Mach stem.) If the level terrain in front of the slope is in the region of regular reflection, the first shock front striking the slope is the free air blast wave from the nuclear source. This shock front is not vertical, but forms an angle of less than 90° with the level ground in front of the slope.

When the nearly vertical Mach stem strikes a rising slope, the incident wave undergoes either regular (two-shock) or Mach (three-shock) reflection, depending on the angle that the slope makes with the surface over which the shock wave has been moving and on the strength of the incident shock. For a falling slope, diffraction always occurs; the shock wave curves to orient itself normal to the slope. Differences between regular and Mach reflection on a rising slope are illustrated in Figure 2-47. Diffraction on a falling slope is illustrated in Figure 2-48 (in these figures, the shock wave direction of propagation is assumed to be normal to the slope contours).

Similar interactions occur when the direction of shock wave motion makes an angle $\Phi$ with the line of steepest ascent or descent. The geometry of such an interaction is shown in Figures 2-49 and 2-50. In these figures, the angle that is important is $\theta$, the effective slope angle. Its relationship to $\theta_s$, the slope angle is

$$\sin \theta = \sin \theta_s \cos \Phi$$

This relationship is plotted in Figure 2-51. The relationship holds for both rising and falling slopes.

When a Mach stem encounters a rising slope, the incident overpressure and the effective slope angle determine whether regular or Mach reflection will occur. The conditions under which regular or Mach reflection occurs are shown in Figure 2-52.

Figure 2-53 shows how effective slope angle affects the peak overpressure produced by a 10-psi incident Mach stem. Similar data may be obtained from Figure 2-46 for other overpressures by noting that the angle of incidence to use with Figure 2-46 is equal to 90° minus the effective slope angle. The left-hand side of Fig-

2-100

INCIDENT WAVE

REFLECTED WAVE

RAREFACTION

$\epsilon$

$\theta$

D

BOW SHOCK

INCIDENT SHOCK

MACH STEM

SLIPSTREAM

$\theta$
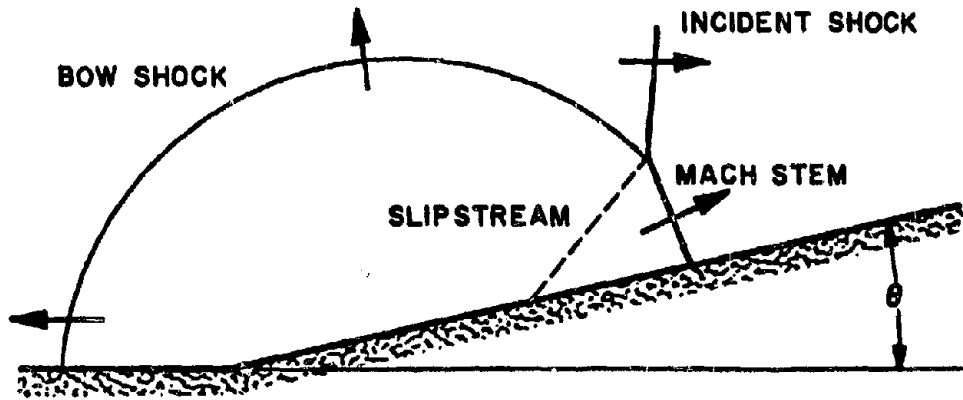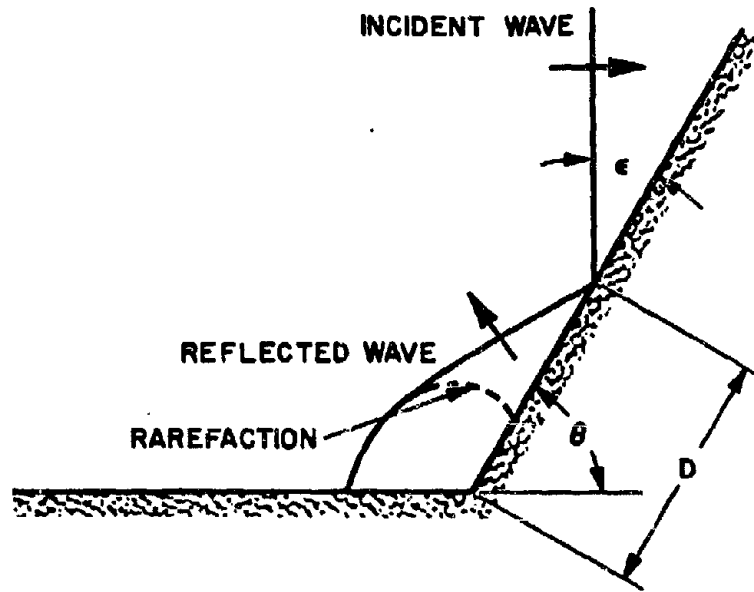
Figure 2-47. ▆ Regular and Mach Reflection Patterns Formed by a Mach
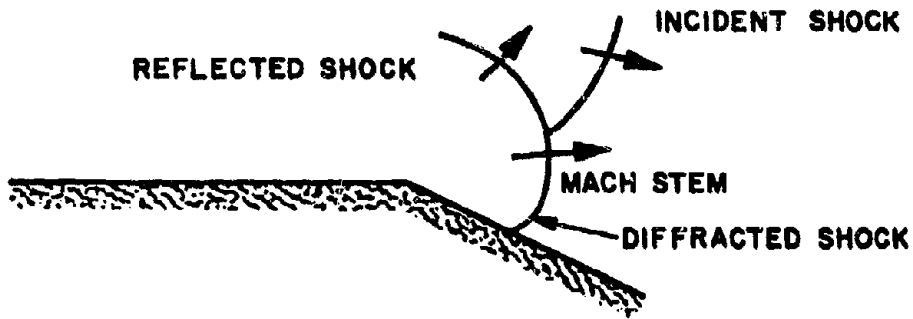Stem Striking a Rising Slope ▆

2-101

Figure 2-48. Diffraction Shock Front Pattern Formed
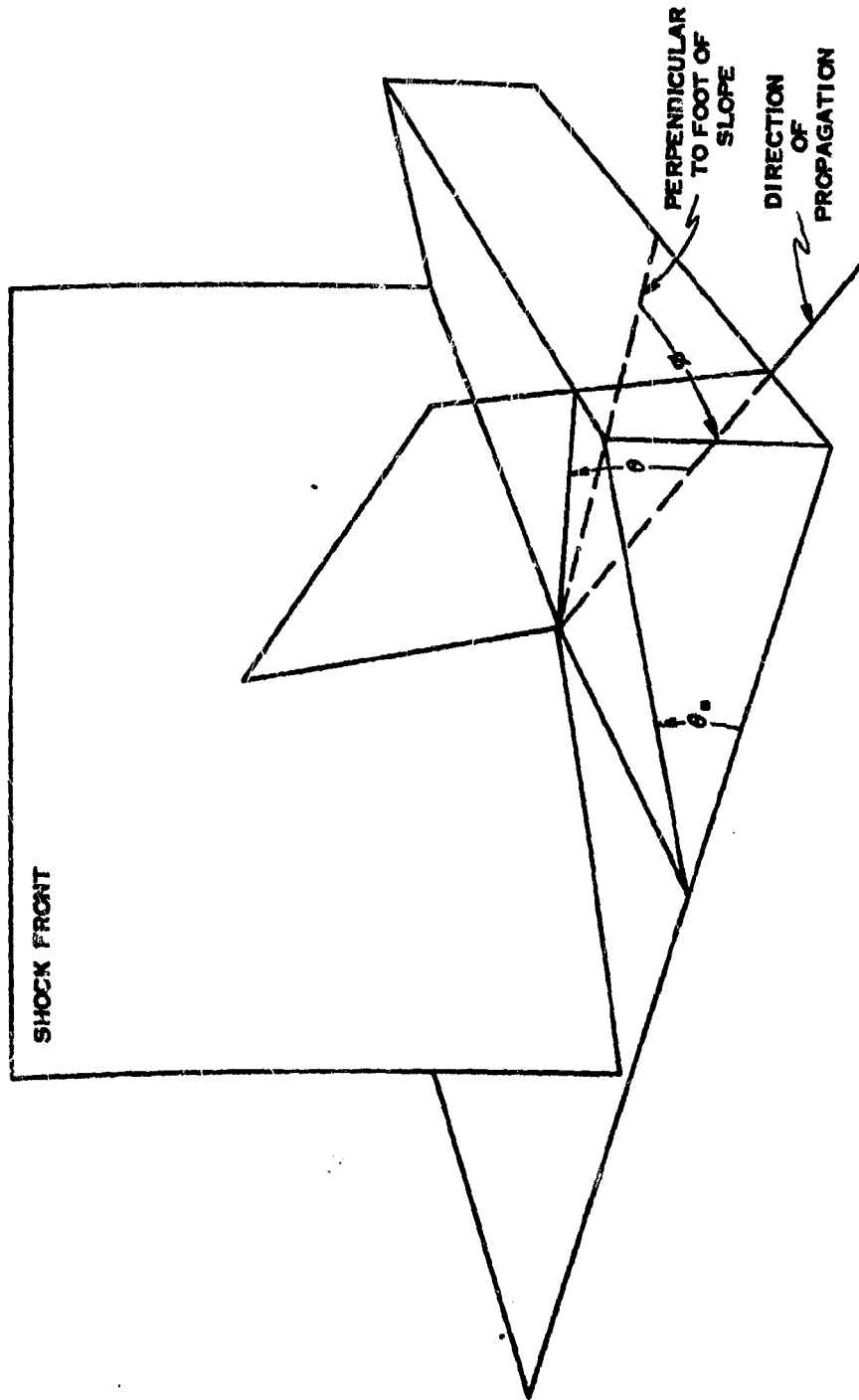by a Mach Stem at a Falling Slope
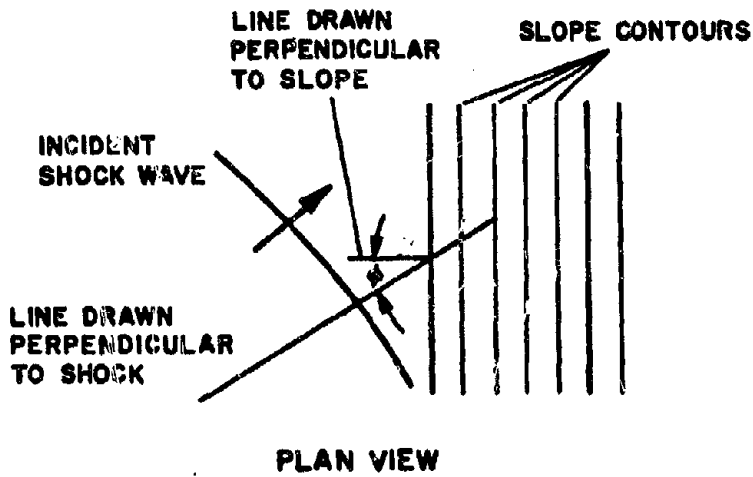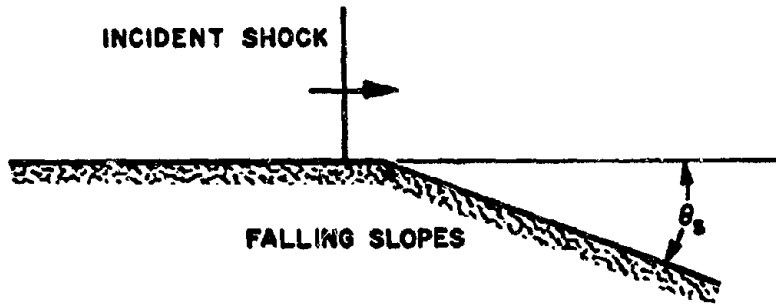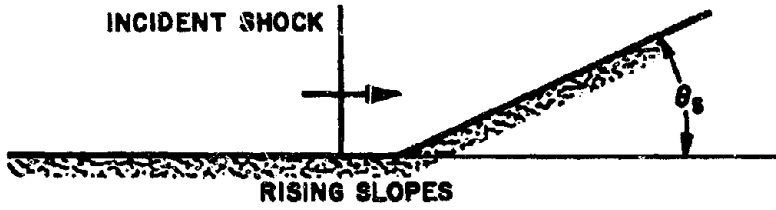
Figure 2-49. Mach Stem at a Rising Slope

SHOCK FRONT

PERPENDICULAR TO FOOT OF SLOPE

DIRECTION OF PROPAGATION

## SECTIONAL VIEWS

INCIDENT SHOCK

$\theta_s$

RISING SLOPES

INCIDENT SHOCK

$\theta_s$

FALLING SLOPES

LINE DRAWN
PERPENDICULAR
TO SLOPE

SLOPE CONTOURS

INCIDENT
SHOCK WAVE

LINE DRAWN
PERPENDICULAR
TO SHOCK

## PLAN VIEW

Figure 2-50. ███ Sectional and Plan Views of a Shock
Front Approaching a Slope ███
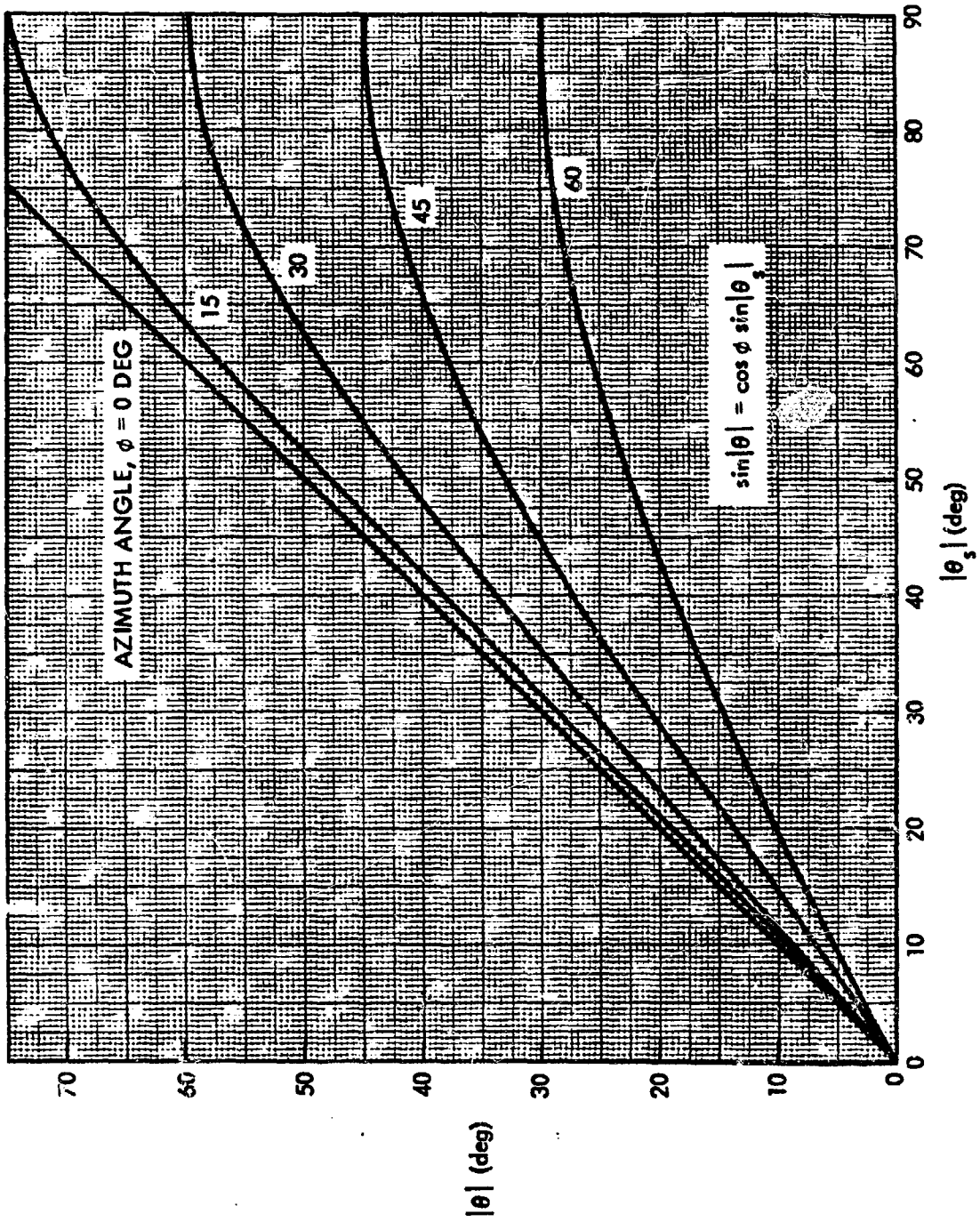
Figure 2-51. Effective Slope Angle θ as a Function of Slope Angle θ_s for Various Angles of Azimuth

$$\sin|\theta| = \cos\phi\,\sin|\theta_s|$$

AZIMUTH ANGLE, φ = 0 DEG
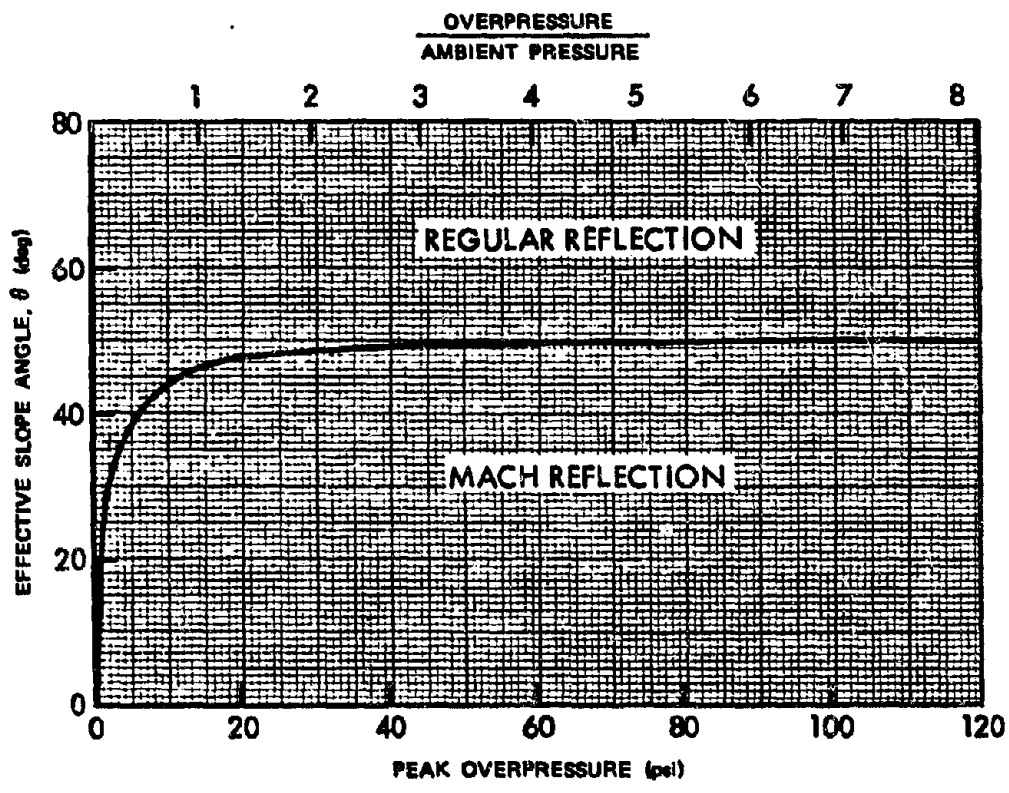
Figure 2-52. ▨ Conditions for Regular or Mach Reflection of Incident Mach Stem ▨
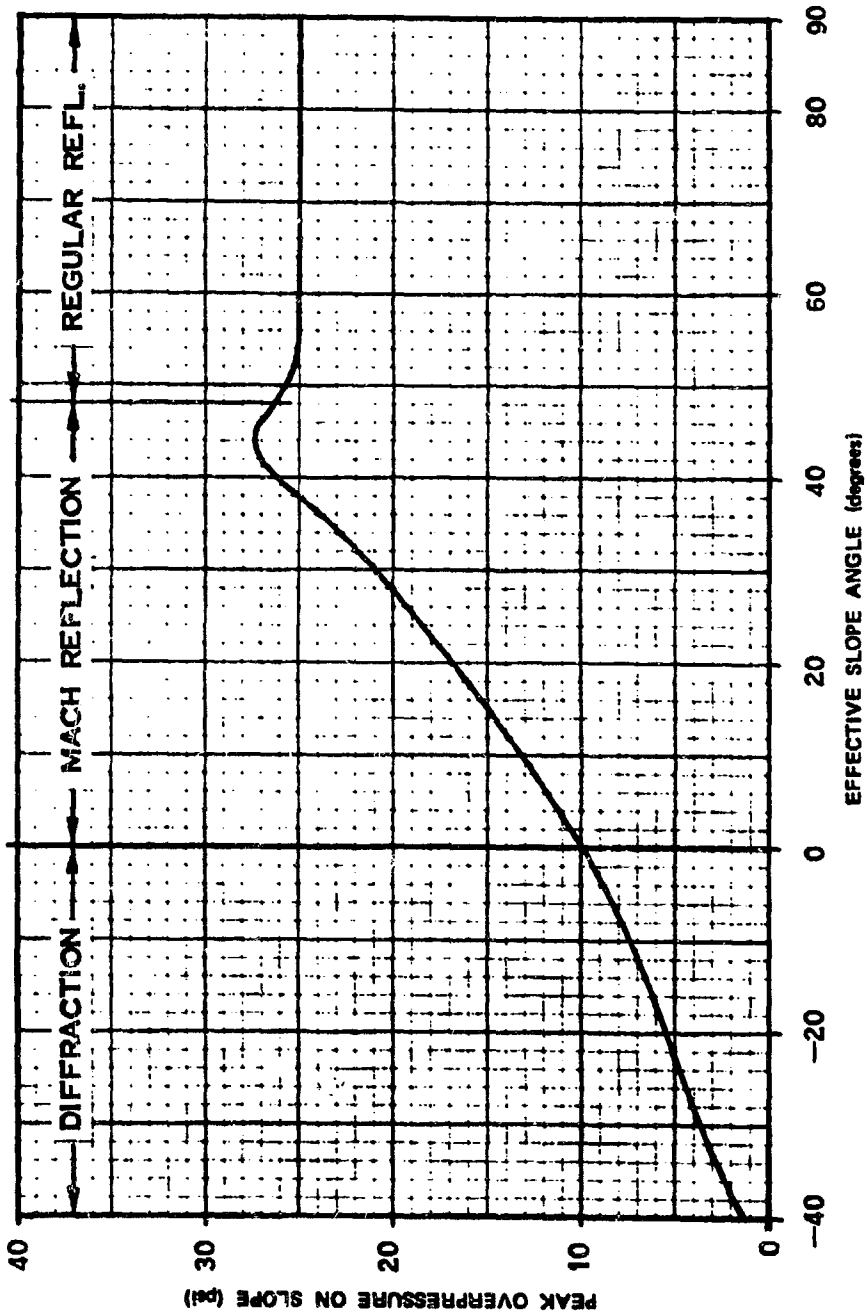
Figure 2-53. ▇ Peak Overpressure Produced on a Slope by a 10-psi Incident Mach Stem as a Function of a Slope Angle

ure 2-53 shows the effect of diffraction at a falling slope.

Figures 2-54, 2-55, and 2-56 show similar data in a more convenient form. The overpressure scales only apply to reflection of shock waves in a sea level atmosphere. At other ambient pressures, the scales marked "overpressure/ambient pressure" should be used. Note that Figure 2-54 is plotted for various values of the angle of incidence while Figures 2-55 and 2-56 are plotted for various values of the effective slope angle.

If the incident blast wave has been undergoing regular reflection before it encounters the rising or falling slope, approximate blast wave characteristics at the target can be determined by (1) constructing a sectional plot showing both the target area and the burst point, (2) drawing a "reference-plane line" through the target area showing the general plane in the vicinity of the target, and (3) drawing a line from the burst point perpendicular to the reference-plane line.

As Figure 2-57 shows, the length of the perpendicular is the effective height of burst; the length along the reference plane line between this perpendicular and the target area is the effective ground range or distance from ground zero, and shock-wave characteristics may be determined from height of burst charts. Although this technique does not take into account the effect of azimuth angle $\Phi$ (where the shock wave moves at an angle to the line of steepest ascent or descent), further refinement is rarely justified.
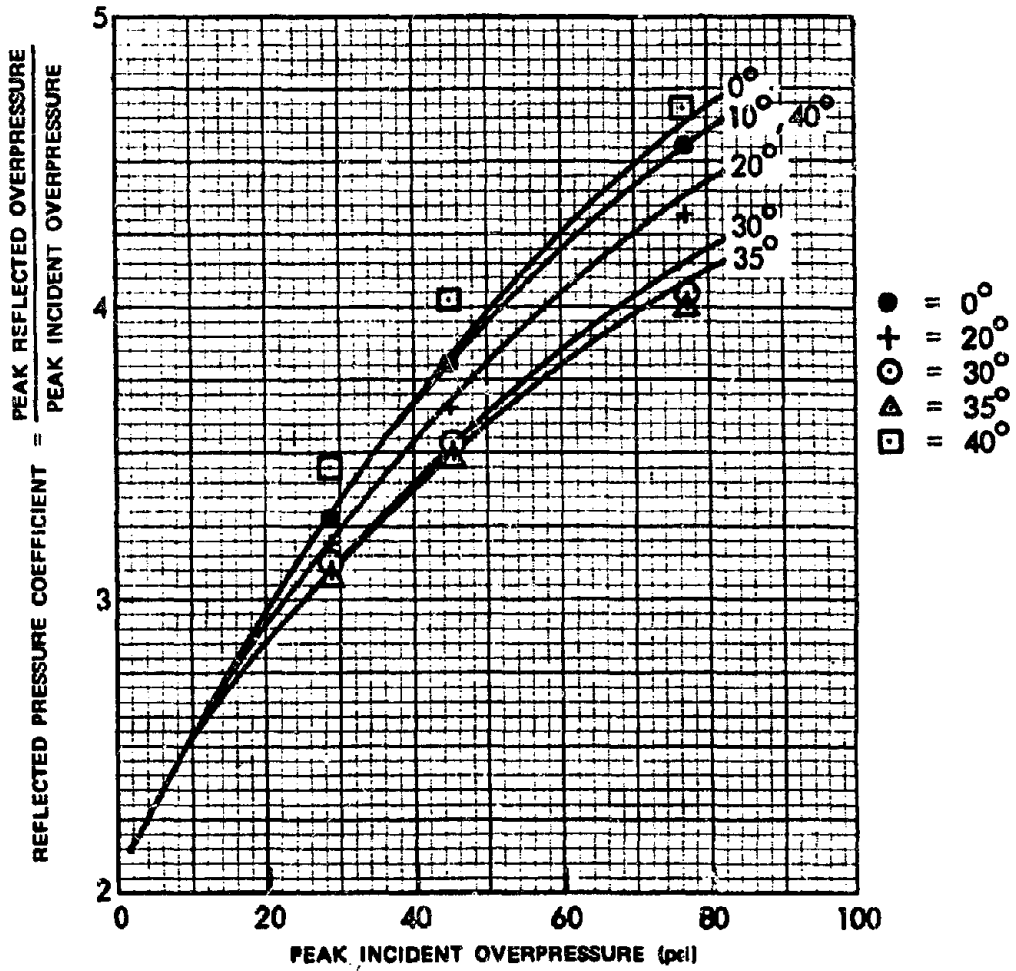
Figure 2-54. ▮ Reflected Overpressure Coefficients for Regular Reflection as a Function Incident Overpressure for Various Angles of Incidence ▮
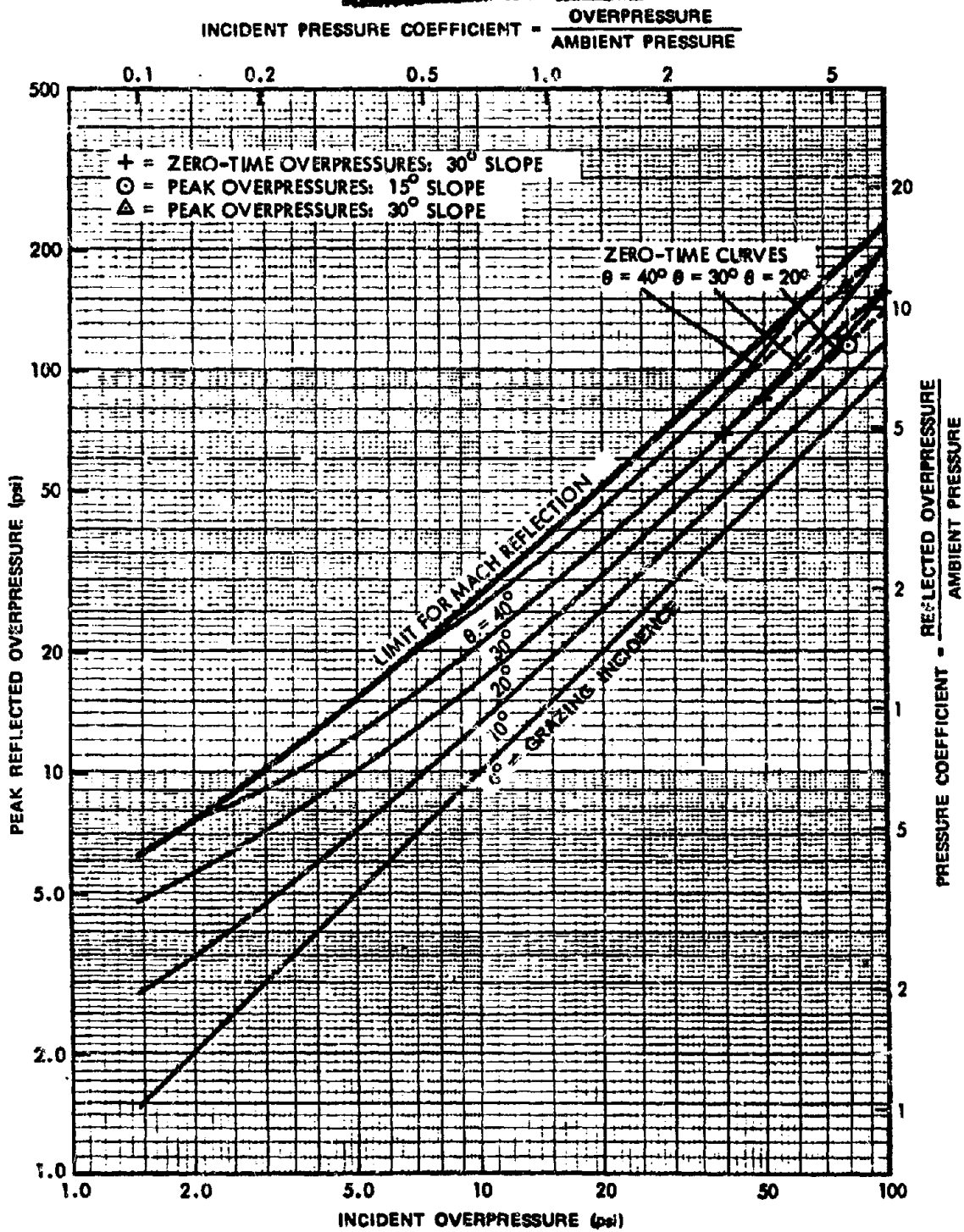
Figure 2-55. ▮ Reflected Overpressure as a Function of Incident Mach-Stem Overpressure for Mach Reflection for Various Slope Angles ▮

DIFFRACTED PRESSURE COEFFICIENT = $\dfrac{\text{OVERPRESSURE}}{\text{AMBIENT PRESSURE}}$

INCIDENT PRESSURE COEFFICIENT = $\dfrac{\text{OVERPRESSURE}}{\text{AMBIENT PRESSURE}}$

INCIDENT OVERPRESSURE (psi)

DIFFRACTED OVERPRESSURE (psi)

⊙ = 15° SLOPE
△ = 30° SLOPE

θ = 0 DEG

90 80 70 60 50 40 30 20 10
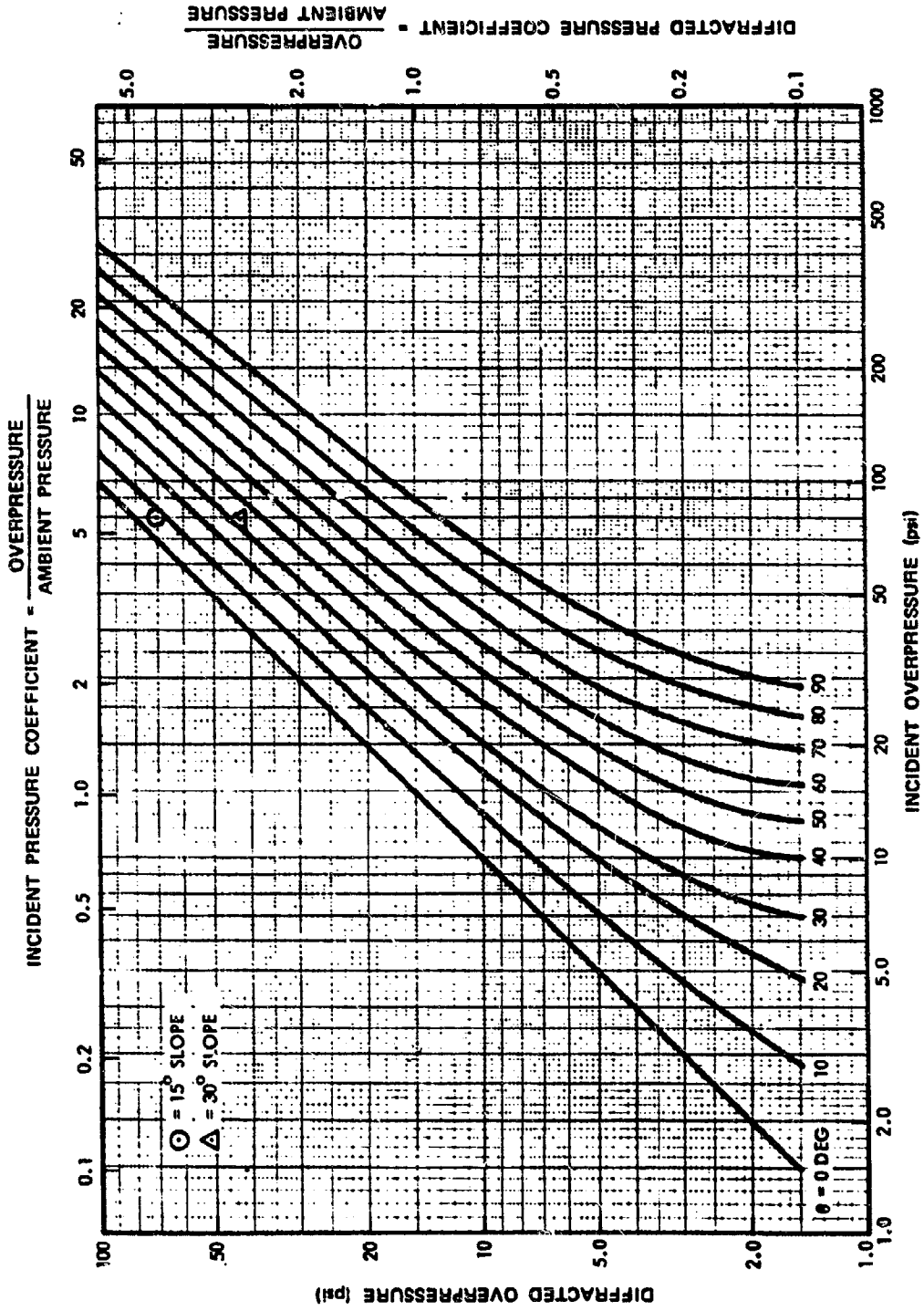
Figure 2-56.    Diffracted Overpressure as a Function of Incident Mach-Stem Overpressure for Various Slope Angles

2-111
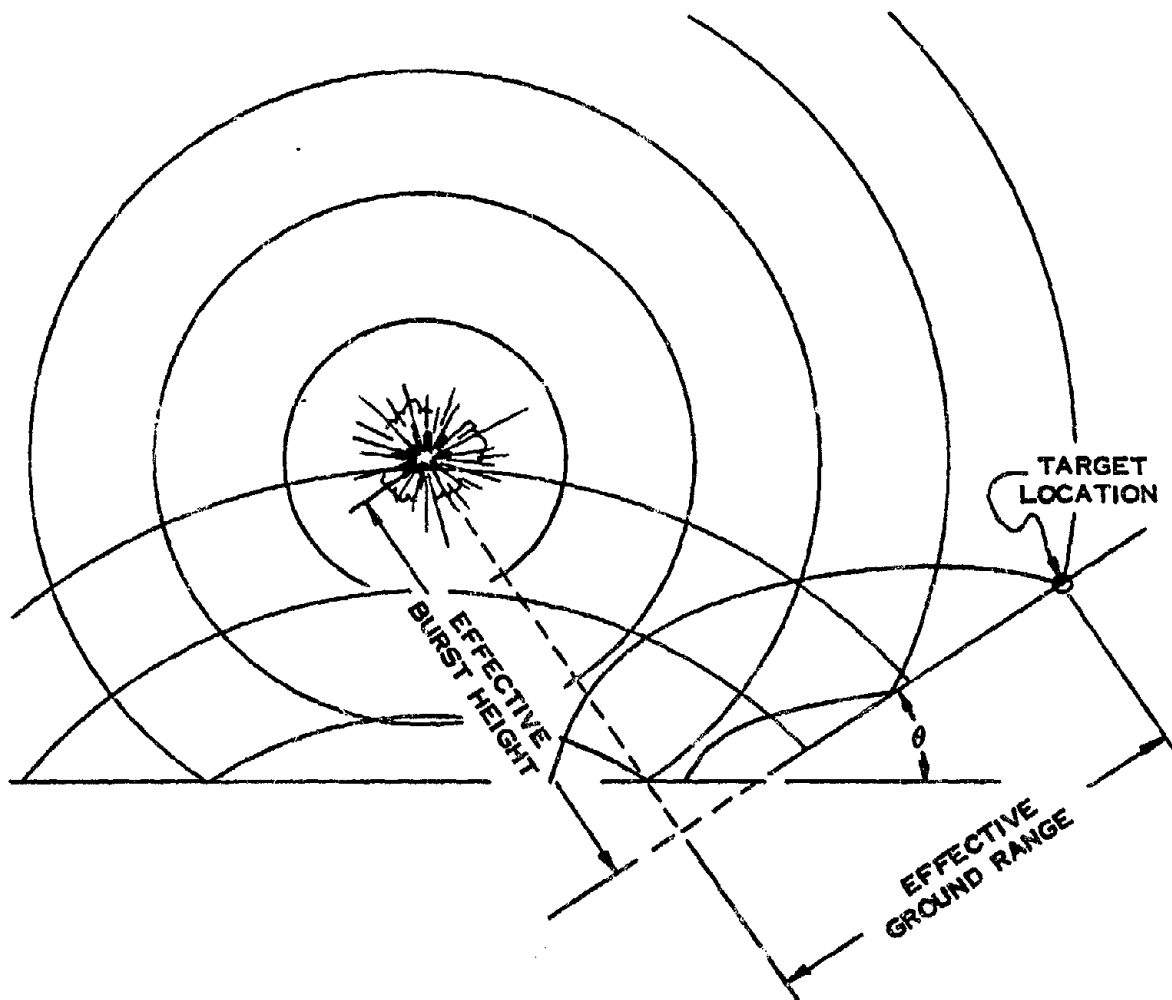
Figure 2-57. █ Construction Procedure Recommended When the Blast Wave
Incident on a Slope Has Been Undergoing
Regular Reflection on Level Ground █

## Problem 2-17. Calculation of Overpressure on a Slope

The information provided in paragraph 2-37 and in Figures 2-47 through 2-57 provides the data to calculate peak reflected overpressures when a blast wave encounters a rising or falling slope. The data are given relative to the incident overpressures that would be expected over flat terrain in a standard sea level atmosphere. These latter values may be obtained from Figures 2-17 through 2-22.

*Scaling.* For target altitudes above 5,000 feet, both the incident and the reflected overpressures scale according to the altitude scaling procedures described in paragraph 2-14, i.e.,

$$\frac{\Delta p_r}{\Delta p_{ro}} = \frac{\Delta p}{\Delta p_o} = S_p,$$

where $\Delta p_{ro}$ and $\Delta p_o$ are the reflected and incident peak overpressures, respectively, in a standard sea level atmosphere, $\Delta p_r$ and $\Delta p$ are the corresponding pressures at the desired altitude, and $S_p$ is the pressure scaling factor described in paragraph 2-14 and tabulated in Tables 2-1 and 2-2.

*Example*

*Given:* A ridge with a slope angle of 27° on otherwise flat terrain at an altitude of 7,500 feet. For a particular set of burst conditions, the predicted blast wave in the absence of the ridge (but including altitude corrections) is a Mach stem with a peak overpressure between 10 and 15 psi. The direction of propagation of the blast wave makes an angle of 20° with the line of steepest ascent.

*Find:* The range of peak overpressures that may be expected on the side of the ridge facing the explosion.

*Solution:* From the equation given in paragraph 2-37 (or by interpolation in Figure 2-51),

the effective slope angle is found as follows:

$$\sin \theta = \sin \theta_s \cos \Phi$$

$$= (\sin 27°)(\cos 20°)$$

$$= 0.427,$$

$$\theta = 25°.$$

From Table 2-1, the altitude scaling factor for pressure at 7,500 feet is

$$S_p = 0.76.$$

Under sea level conditions, the predicted value of the incident Mach stem overpressure would lie between

$$\Delta p_o = \frac{\Delta p}{S_p} = \frac{10}{0.76} = 13.2 \text{ psi, and}$$

$$\Delta p_o = \frac{15}{0.76} = 19.7 \text{ psi.}$$

Figure 2-55 shows that a rising slope will increase these sea level values to

$$\Delta p_{ro} = 19 \text{ psi, and}$$

$$\Delta p_{ro} = 28 \text{ psi, respectively.}$$

An uncertainty of about 20 percent exists in these values (see "Reliability" below). In order to bracket the range of expected values, the lower will be decreased by 20 percent, and the upper will be increased by 20 percent. The resulting sea level reflected overpressures are

$\Delta p_{ro}$ = 15.2 psi, and

$\Delta p_{ro}$ = 33.6 psi, respectively.

*Answer:* The corresponding values of reflected overpressure at an altitude of 7,500 feet are

$\Delta p_r = \Delta p_{ro} S_p$ = (15.2)(0.76) = 11.5 psi, and

$\Delta p_r$ = (33.6)(0.76) = 25.5 psi, respectively.

■ *Reliability:* Full scale nuclear tests indicate that the increase or decrease in peak overpressure at a rising or falling slope is generally within 10 or 20 percent of the predicted value. In the presence of a precursor, less accuracy may be expected. Accuracy also decreases if the slope angle is close to the critical angle that separates the regions of regular and Mach reflection.

■ *Related Material:* See paragraphs 2-14, 2-17 through 2-20, 2-22 through 2-24, and 2-37. See also Tables 2-1 and 2-2.

## 2-38 Effects of Slopes on Other Blast- Wave Parameters ■

■ Methods for determining peak overpressures at rising and falling slopes are described in paragraph 2-37. This paragraph relates the peak dynamic pressure and the duration of the positive phases of the overpressure and the dynamic pressure to the expected overpressures that are determined by the methods described in paragraph 2-37. The relations of the dynamic pressure and positive phase durations to the overpressure will be discussed for three types of interactions of the blast wave with slopes: regular reflection of an incident Mach stem; Mach reflection of an incident Mach stem; and diffraction of an incident Mach stem.

■ Figure 2-58 shows the reflected dynamic pressure as a function of incident Mach stem overpressure in the regular reflection region for various effective slope angles. The duration of the positive phase overpressure after regular reflection can be considered to be the same as that of the incident pulse. The dynamic pressure pulse, on the other hand, changes as the shock wave proceeds up the slope as a result of the presence and growth of a rarefaction wave from the slope corner (see Figure 2-47). The dynamic pressure pulse effectively terminates where the rarefaction wave intersects the reflected wave. The effect depends on the distance up the slope that the shock wave has moved, the slope angle, and the overpressure coefficient in the manner shown in Figure 2-59. In this figure, the number 1116 is the velocity of sound (in feet/sec) for standard sea level conditions (15°C or 59°F). For different ambient temperatures, the appropriate sound speed should be used (see Tables 2-1 and 2-2).

■ In the case of Mach reflection of the incident Mach stem, the peak dynamic pressure at the shock front may be determined from Figure 2-13 once the reflected overpressure is determined as described in paragraph 2-37. Figure

2-13 is only valid when a single shock front is involved. If the rising slope is sufficiently steep to cause regular reflection (Figure 2-52), the peak dynamic pressure should be determined from Figure 2-58. The duration of the positive phase overpressure pulse in the Mach stem after Mach reflection can be assumed to be the same as that of the incident wave, while the positive phase dynamic pressure pulse is shorter than that of the incident wave. Over a range of overpressure coefficients from 2 to 11, and slope angles from 11.8 to 38 degrees, the reflected pulse after Mach reflection may be assumed to be 0.55 times as long as that of the incident blast wave.

■ Figure 2-13 also may be used to determine the peak dynamic pressure from the peak overpressure in a diffracted wave. Although the positive phase duration of both the overpressure and dynamic pressure pulses are known to decrease as a result of the formation of low pressure vortices at the slope change point, neither experiment nor theory is sufficiently extensive to provide a satisfactory prediction technique. As an approximation, the positive phase duration of the diffracted overpressure pulse may be taken to be the same as that of the incident pulse, and the duration of the diffracted dynamic pressure pulse may be shortened by the ratio of diffracted peak dynamic pressure to incident peak dynamic pressure.

## 2-39 Channeling of an Incident Mach Stem Along the Axis of a Valley ■

■ Figure 2-60 illustrates a third type of idealized topographic feature: an elongated valley. Shock waves reflecting from the walls of such a valley tend to enhance each other in the vicinity of the axis of the valley. The simple relations shown in Figure 2-61 have been shown to hold for a wide range of valley forms and for incident overpressures below about 60 psi. The relation for "flat-bottomed valleys" holds for

INCIDENT PRESSURE COEFFICIENT = $\dfrac{\text{OVERPRESSURE}}{\text{AMBIENT PRESSURE}}$
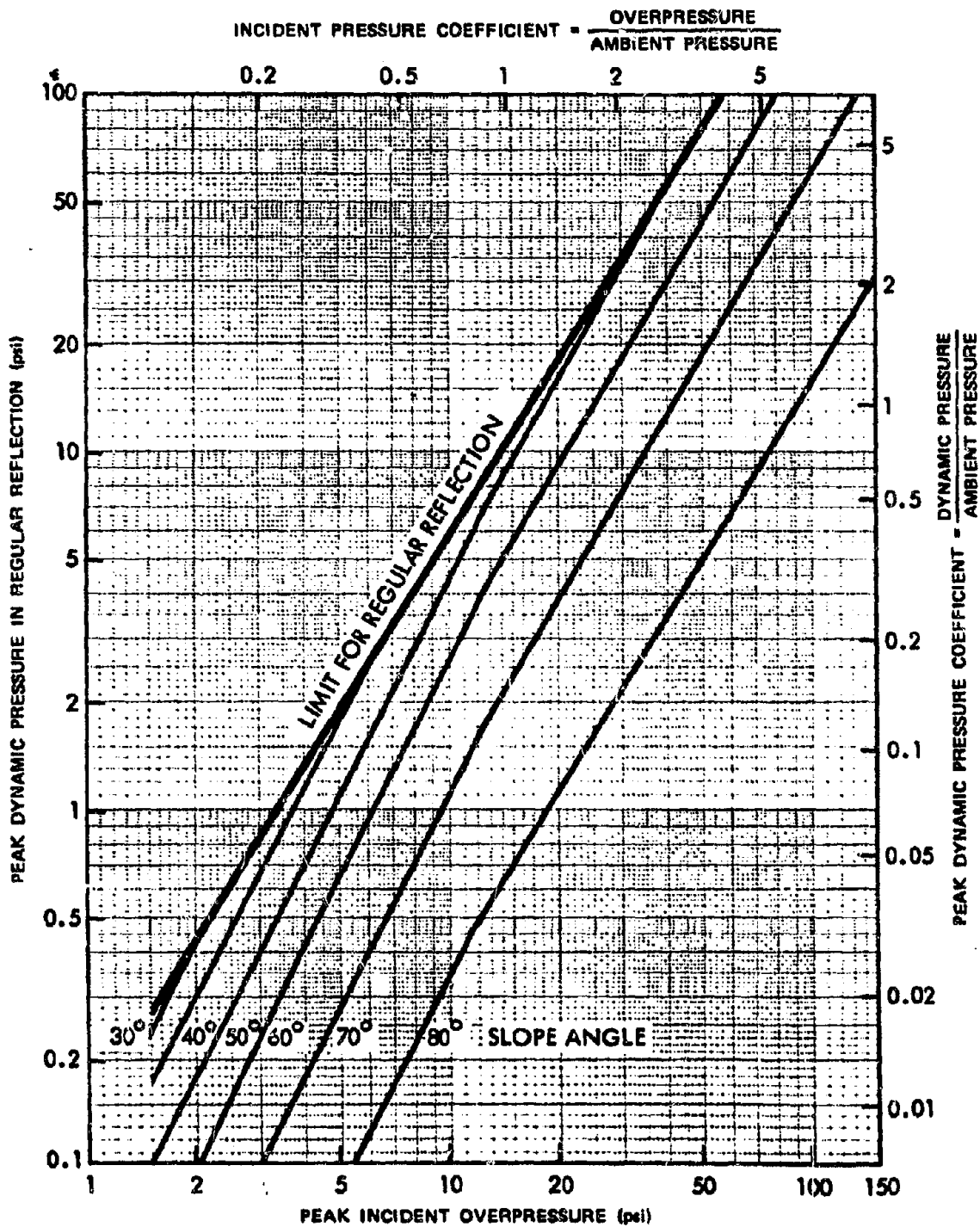


Figure 2-58. Reflected Dynamic Pressure as a Function of Incident
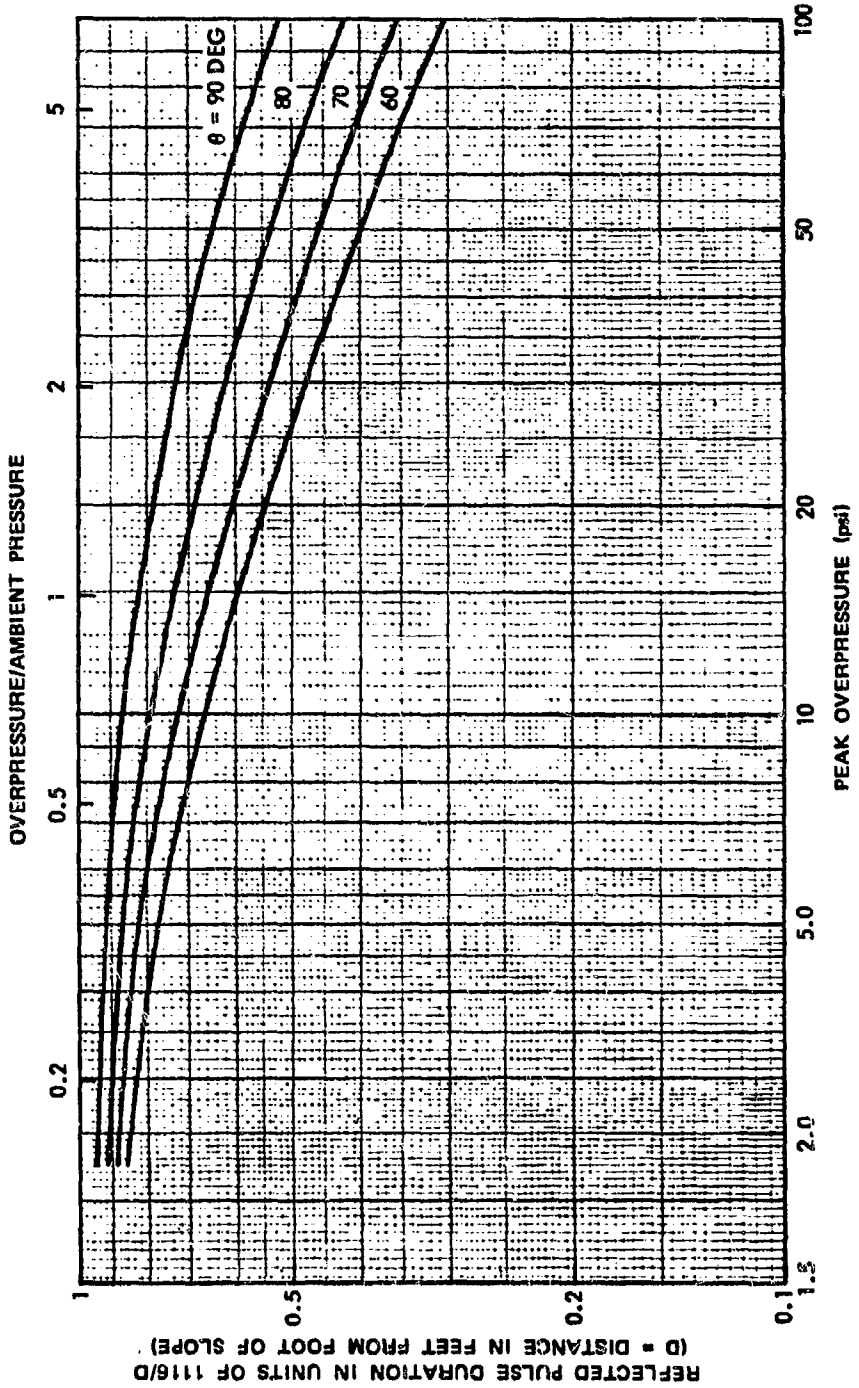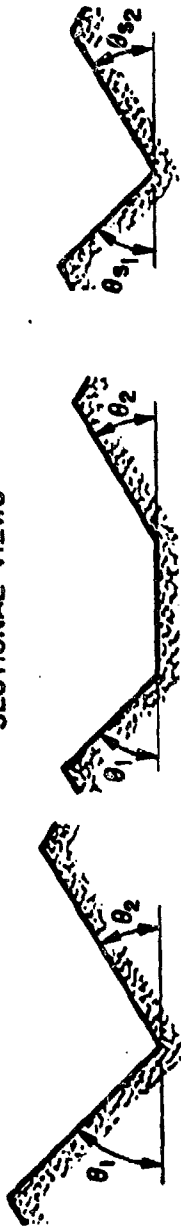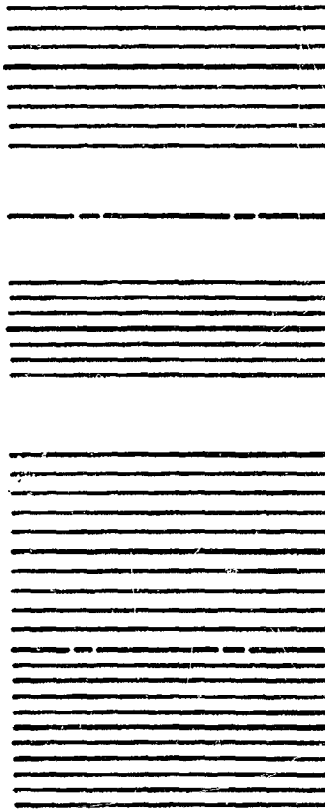Mach Stem Overpressure for Regular Reflections for Various
Effective Slope Angles

Figure 2-59. ▮▮▮ Duration of the Reflected Dynamic Pressure Pulse for Regular Reflection ◤

2-117

SECTIONAL VIEWS

PLAN VIEWS

$\theta_{s_2}$  $\theta_{s_1}$

$\theta_2$  $\theta_1$

$\theta_2$  $\theta_1$

PERPENDICULAR TO CONTOURS

PERPENDICULAR TO VALLEY AXIS

$\phi_2$  $\phi_1$

CONVERGING VALLEY

$\sin \theta_1 = \sin \theta_{s_1} \cos \phi_1$

$\sin \theta_2 = \sin \theta_{s_2} \cos \phi_2$

(SEE FIGURES 2-50 and 2-51)

FLAT-BOTTOM VALLEY

"V" SHAPED VALLEY

Figure 2-60. Sectional and Plan Views of Idealized Valley Shapes
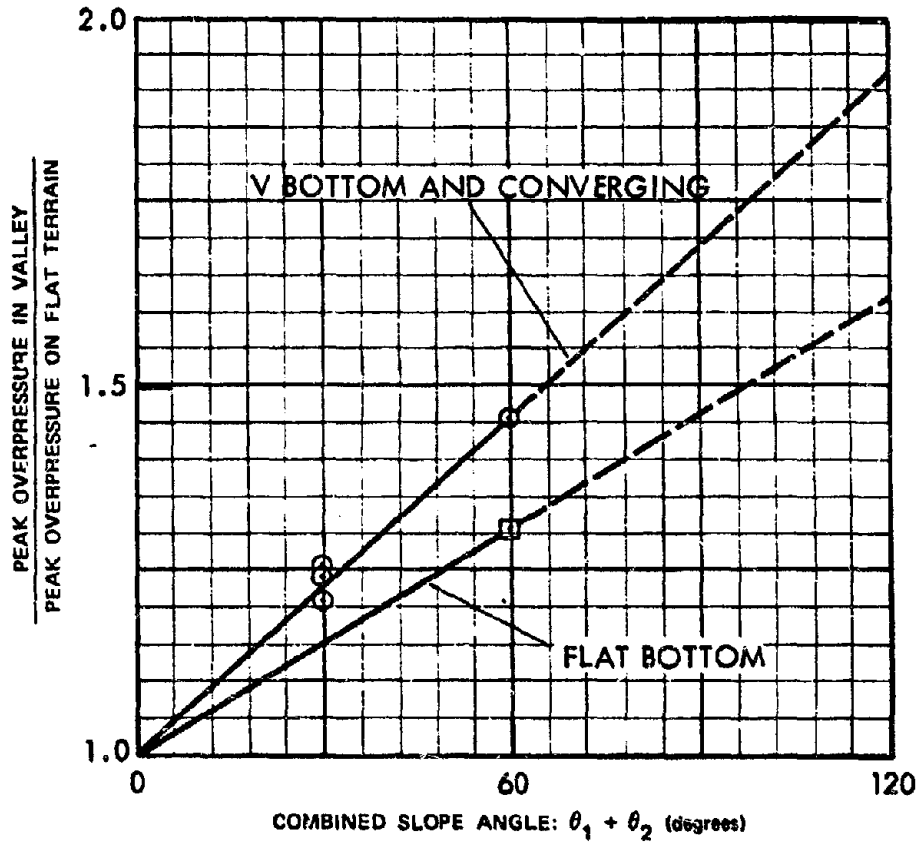
Figure 2-61. ■ Average Peak Overpressure Amplification Factors at the Bottom of Valleys as a Function of Combined Slope Angle ■

valleys whose floor widths (measured perpendicular to the valley axis) are of the same order as, or shorter than, the slope heights of the valley walls (also measured perpendicular to the valley axis). For wider flat-bottomed valleys, each side of the valley and a portion of the adjacent valley floor may be considered independently as a V-shaped valley.

### 2-40 General Application of Prediction Techniques to Actual Topographical Features

Paragraphs 2-37 and 2-38 provide data for only the most significant shock wave characteristics — peak pressures and positive phase durations. More detailed information, e.g., data on pressure waveforms, may be obtained from --DASA 1200, "Nuclear Weapons Blast Phenomena" (see bibliography).

Applicability of the curves that have been presented depends largely on the size of a terrain feature relative to the size of the incident shock wave. If the incident shock is very much longer than a terrain feature of interest, the predicted changes in peak values of overpressure and dynamic pressure will occur on the slope; but the duration will not be affected greatly. The incident pulse length in feet is slightly more than 1116 times the incident pulse duration in seconds, and if this pulse length is more than about three times as long as the slope being considered, no changes in pulse duration can be expected.

Much of the complexity of actual terrain may be eliminated from blast wave calculations by application of the *local-slope* concept. This concept is based on the observation that, in many situations, a shock wave that has passed over a succession of terrain features (hills, valleys, etc.) before encountering a feature of interest interacts with that feature as if the shock wave had previously passed over flat terrain.

This trend was noted during testing programs and has been supported by theoretical inference. The Ranier nuclear test over fairly complex terrain, provided additional checks. Although much of the area around this explosion was subject to precursor type waves, sharp fronted waves traversed many regions that were protected from direct thermal radiation. Predictions of peak overpressures generally were within 10 to 20 percent of observed values.

Determining whether the local slope approximation will give reasonably accurate results requires application of judgment in an examination of the region between the target area and the presumed burst point to determine whether there are significant terrain features between the two, especially in the vicinity of the target. This examination is often based on a sectional plot of the terrain, made along a line between ground zero and the target. Although it is sometimes difficult to draw conclusions from this examination, the following criteria are helpful:

● Features that show slope angles of less than 10 degrees on a sectional plot of the terrain, i.e., about a 20 percent grade, will not create significant effects.

● Symmetrical features at an appreciable distance from the target generally can be ignored. Effects that occur on the front slope of such features compensate for effects that occur on the back slope.

● Terrain features near ground zero have a small effect on the blast wave at large ground distances.

● If the average slope of the terrain tends to follow a straight line, particularly if the deviations from this straight line are small or random, the local slope approximation is justified. However, if the average slope of the sectional plot clearly follows two straight lines, and the angle between these

lines exceeds 10 degrees, and if the break occurs in the region of Mach reflection, the blast wave calculations may have to treat the effects of two slopes in sequence.

Unless the average slope between ground zero and the target is essentially horizontal, use of the local slope concept requires establishment of the primary reference plane (PRP). Over complex terrain, the PRP often follows the average slope of the terrain between ground zero and the foot of the feature upon which the target lies. If the PRP does not seem clearly defined by this criterion, it is better to allow the terrain within the region of Mach reflection suggest the slope of the PRP. If the target is in the region of regular reflection, the average slope of the terrain near the target should be given more weight than the average slope of terrain closer to ground zero.

After the PRP has been established, effective burst height and ground distance *with respect to this plane* may be determined by means of a geometrical construction similar to that suggested by Figure 2-57. Properties of the blast wave incident on the terrain feature of interest may be read directly from height of burst curves in terms of these effective values of distance and height.

Although there are many cases in which the local slope concept will fail in detail if applied to features that are regular and uniform, ordinary terrain is so complex that the uncertainties engendered by terrain irregularities generally will exceed errors resulting from application of the local slope concept. Furthermore, the process of determining *approximate* terrain effects with the local slope concept is generally far simpler than that of obtaining more refined, *but still approximate*, effects with more rigorous techniques.

Once the blast wave properties are determined from height of burst curves, appropriate sectional plots should be made of the target area

slope. Azimuth angle and valley slopes must be determined where appropriate.

## 2-41 Application of Prediction Techniques to Specific Topography

Figure 2-62 is a topographical map with a target area (designated by T) to be investigated. It is desired to determine the locus of ground zeros that would subject the target to an overpressure of 10 psi from a 1 Mt weapon burst at a height of 5,000 feet above the terrain.

Examination of Figure 2-62 shows that the highest point on the terrain around the target area is just over 4,000 feet (note that the grid lines and elevations are given in meters in Figure 2-62, and the highest point in the vicinity of the target is at an elevation of 1,243 meters), so altitude corrections are not required.

In accordance with the instructions in paragraph 2-20, the blast-wave parameters for explosions over mechanically nonideal surfaces are performed by first finding the desired blast parameters over a near-ideal surface. The results then are corrected for the change in the blast wave properties introduced by the mechanically nonideal features. The corresponding height of burst for a 1 kt explosion is

$$ h_1 = \frac{h}{W^{1/3}} = \frac{5,000}{(1,000)^{1/3}} = 500 \text{ feet.} $$

From Figure 2-18, a 1 kt explosion at a height of burst of 500 feet will produce an overpressure of 10 psi at a ground distance of 1,315 feet (about 400 meters). The corresponding ground distance for a 1 Mt explosion is

$$ d = d_1 W^{1/3} = (1,315)(1,000)^{1/3} $$

$$ = 13,150 \text{ feet (or about 4,000 m).} $$

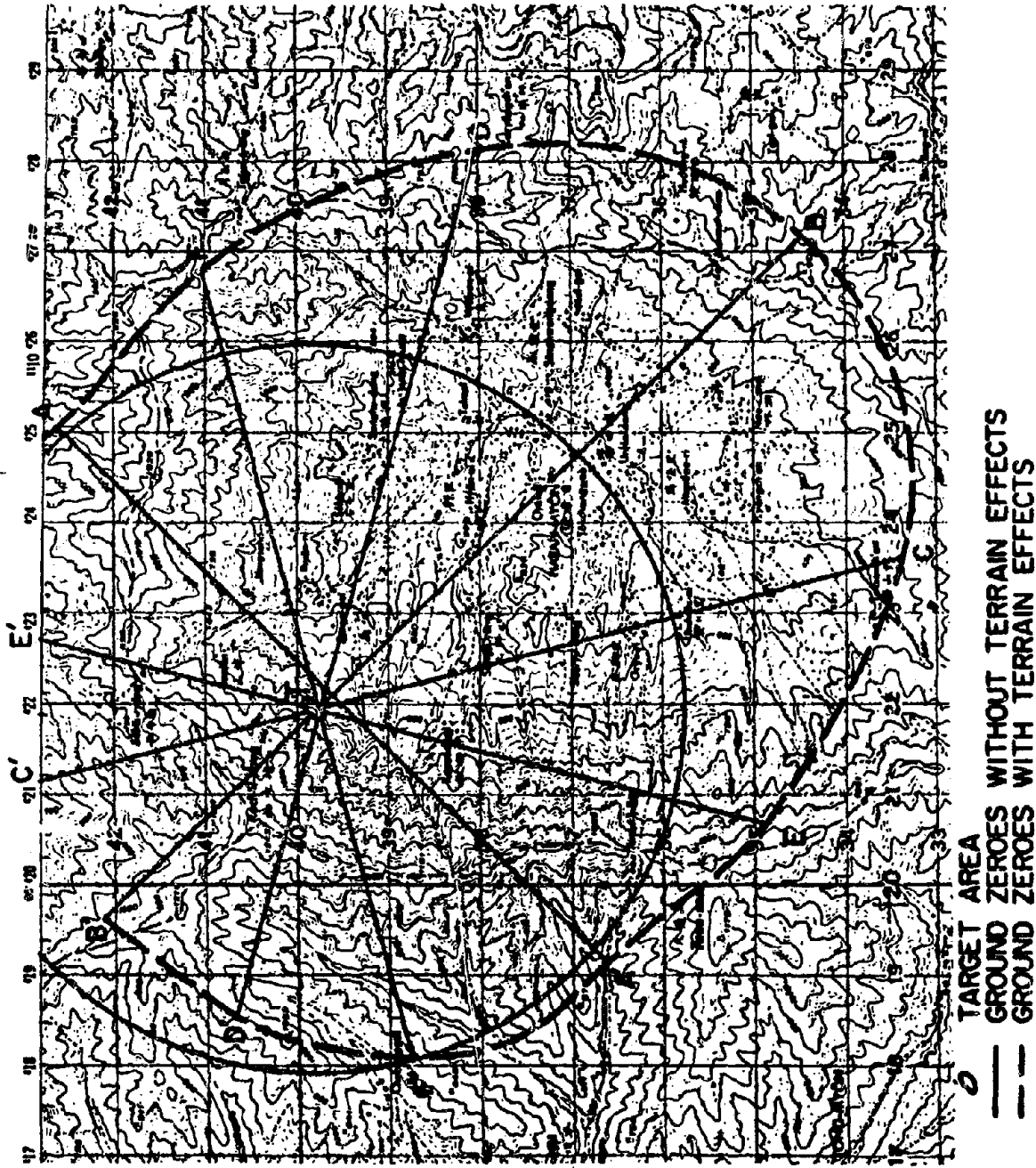A circle, centered on the target, with this radius is shown in Figure 2-62. A 1 Mt explosion at a

Figure 2-62. Terrain Map Used in Example ▨

TARGET AREA
—— GROUND ZEROES WITHOUT TERRAIN EFFECTS
– – GROUND ZEROES WITH TERRAIN EFFECTS

height of burst of 5,000 feet over any point on the circle would produce an overpressure of 10 psi at the target area (burst over points within the circle would produce overpressures in excess of 10 psi at the target).

The target area includes two small converging valleys that are relatively shallow and have relatively flat slopes normal to their axes. Figure 2-61 shows that relatively steep slopes are required to produce large effects in converging valleys, so these minor terrain irregularities may be ignored.

The general direction of the contours in the target area is established as being parallel to line AA'; and a sectional plot along line BB', perpendicular to AA' and through the target area, is constructed (this sectional plot is shown in Figure 2-63 with the distance scales in meters for ease in comparison with the map). The plot in Figure 2-63 is not extended to the ground-zero circle (though it could easily be), since inspection of the area between the target and this circle, and reference to Figure 2-15 shows that Mach reflection would take place long before the shock would arrive at the target area. Furthermore, inspection of the area within the ground zero line indicates that an assumption of a horizontal datum for the slope of the primary reference plane is fairly good.

From Figure 2-63, it can be determined that the tangent of the slope angle (vertical rise/horizontal distances) is 0.57. Thus, the slope angle is

$$\theta_s = 30°.$$

It is therefore necessary to determine the incident overpressure that will produce an overpressure of 10 psi when the shock wave encounters a 30 degree rising slope (along the line BT) or a 30 degree falling slope (along the line B'T). Figure 2-55 (Mach Reflection) gives an incident overpressure of 3.5 psi for the rising-slope condition,

and Figure 2-56 (diffraction) shows an incident overpressure of 20 psi for the falling-slope condition. Figure 2-19 shows that 3.5 psi would occur at a ground distance of about 2,450 feet from a 1 kt burst or 24,500 feet (about 7,500 m) from a 1 Mt burst at heights of burst of 500 feet and 5,000 feet, respectively. Figure 2-18 shows that, for the same heights of burst, 20 psi occurs at a ground distance of 870 feet from a 1 kt burst or 8,700 feet (about 2,650 meters) from a 1 Mt burst.

Lines CC' and DD' are drawn at 30° to line BB'. For these lines, the angle between the direction of shock wave propagation and the angle of steepest ascent or descent is

$$\Phi = 30°,$$

and the effective slope angle is determined by

$$\sin \theta = \sin \Phi_s \cos \Phi$$

$$= \sin 30° \cos 30° = 0.43$$

which yields

$$\theta = 26°.$$

The angle $\Phi$ for lines EE' and FF' is 60°, from which $\theta = 14.5°$. Using these two values of $\theta$ with Figures 2-55, 2-56, 2-18, and 2-19 provides the results shown in Table 2-5.

Along line AA' the hill on which the target lies is, for all intents, a V-shaped valley with combined slope angle (see Figure 2-62) of 30°. Figure 2-60 indicates that an amplification factor of about 1.25 holds for such a valley, so an 8 psi incident overpressure (10/1.25) will yield 10 psi at the target area. Figure 2-19 shows that 8 psi would occur at a distance of approximately 1,375 feet for 1 kt or 13,750 feet for 1 Mt (about 4,200 meters for 1 Mt).
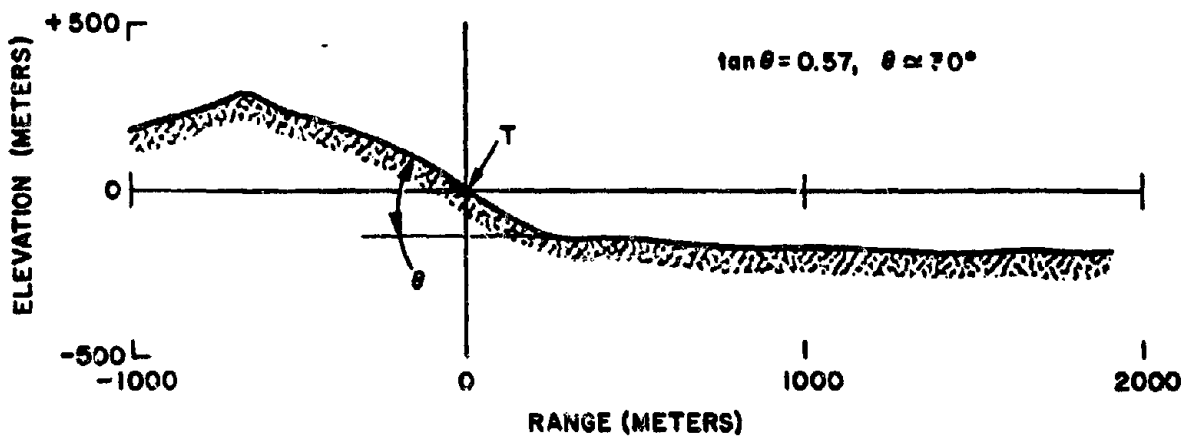
When the various distances given above

Figure 2-63. ▮ Sectional Plot of the Terrain Along BB' in Figure 2-62

Table 2-5. ██ Incident Overpressure and Ranges ██

| Line | $\Phi$ | $\theta$ | Rising Slope Incident Overpressure (psi) | Approximate Distance | |
|------|--------|----------|------------------------------------------|--------------|---------|
| | | | | Feet | Meters |
| BT | 0° | 30° | 3.5 | 24,500 | 7,500 |
| CT, DT | 30° | 26° | 4.1 | 21,500 | 6,600 |
| ET, FT | 60° | 15° | 6.0 | 17,000 | 5,000 |
| **Falling Slope** | | | | | |
| B'T | 0° | 30° | 20.0 | 8,700 | 2,650 |
| C'T, D'T | 30° | 26° | 18.5 | 9,500 | 2,900 |
| E'T, F'T | 60° | 15° | 15.0 | 10,900 | 3,300 |

██ are measured from the target area T along the appropriate lines, the points are connected, the dashed line shown in Figure 2-62 is the result. This line is the approximate locus of ground zeroes that will subject the target area to a peak overpressure of 10 psi.

██ THE BLAST WAVE AT HIGH ALTITUDES ██

██ Nearly all of the energy from a nuclear burst detonated within the atmosphere is absorbed by air molecules. Within a few seconds, most of this energy evolves to three forms: blast energy, radiated thermal energy, and thermal energy retained in a large volume of air. The first two components of energy are useful nuclear effects; the third is harmlessly dissipated over a relatively long period of time. Deviations from Sachs' scaling laws (paragraphs 2-13 and 2-14) above 40,000 feet are caused principally by differences in the partitioning of these three energy components. Between sea level and 130,000 feet, blast energy decreases and radiated thermal energy increases with yield.

██ These changes are, to a large degree, caused by changes in characteristic times. The blast wave develops more slowly at higher altitudes, and the thermal pulse radiates more rapidly. Thus, energy is radiated at high altitudes that would, at lower altitudes, have contributed to the blast wave. At altitudes higher than 130,000 feet, both blast and thermal* efficiencies drop.

**2-42 Effective Blast Yield at High Altitudes** ██

██ To account for the smaller fraction of the yield that appears as blast energy at higher altitudes, the actual yield is multiplied by the blast efficiency factor shown in Figure 2-64 to obtain the effective blast yield. Effective blast yield is that value of yield which, when used in Sachs' scaling laws, predicts the correct value of peak overpressure.

██ Figure 2-64 shows approximate upper and lower limits rather than a single value for

──────

*██ Thermal radiation as used here includes ultraviolet through infrared, but excludes higher frequency radiations, e.g., X-rays. See Chapters 3 and 4.

the blast efficiency factor. At high altitudes, overpressure varies with distance in such a way that effective blast yield is different at different distances. For example, a 100 kt burst at 100,000 feet has an effective blast yield that varies from about 50 kt to 85 kt. It appears impossible to formulate simple rules that state where these numbers apply. It is preferable to consider the upper and lower effective blast yields as defining a range of uncertainty. Methods for making more detailed and complex calculations are suggested in DASA-1200 "Nuclear Weapons Blast Phenomena" (see bibliography).

Although blast efficiency is a correction factor established to determine peak overpressure, it also may be used to calculate other blast-wave parameters. However, because of the non-linear properties of air, blast waves with high shock strengths cannot be scaled exactly, and shock-front parameters other than peak overpressure are defined less accurately by effective blast yield. The waveform behind the shock front is subject to additional variations, and the blast efficiency is least dependable when applied to parameters such as impulse and positive phase duration.

## Problem 2-18. *Calculation of Peak Overpressure at High Altitudes

Figure 2-64 shows the blast efficiency factor as a function of height of burst. This efficiency factor when multiplied by the weapon yield provides the effective blast yield. The effective blast yield may then be used to obtain peak overpressure as a function of distance by the methods described in paragraph 2-7 and Problem 2-1 as modified by the altitude correction procedures described in paragraph 2-14. Other blast parameters may be obtained by using the effective blast yield in the manner described for total yield in paragraphs 2-8 through 2-11, as modified by the altitude scaling described in paragraph 2-14.

**Scaling.** After obtaining the effective blast yield, the various blast parameters are scaled according to the procedures described in Problems 2-1 through 2-5, as modified by the altitude scaling described in paragraph 2-14 and Problem 2-6.

**Example**

*Given:* A 200 kt explosion at an altitude of 100,000 feet.

*Find:* The highest value of peak overpressure that might be expected 5,000 feet below the explosion.

*Solution:* Since Figure 2-64 shows that the highest value of blast efficiency factor for a burst at 100,000 feet is 85 percent, the calculation is based on an effective yield, $W_{eff}$, of

$$W_{eff} = (0.85)(200) = 170 \text{ kt.}$$

While the blast efficiency factor is based on burst altitude, the altitude scaling factors are based on target altitude (paragraph 2-14). From Table 2-1, the distance and pressure scaling factors at 95,000 feet are .

$$S_d \approx 4.2$$

$$S_p \approx 0.014.$$

The distance from a 1 kt explosion that corresponds to a distance of 5,000 feet from a 170 kt explosion is

$$d_1 = \frac{d}{S_d W^{1/3}} = \frac{5,000}{(4.2)(170)^{1/3}} = 215 \text{ feet.}$$

From Figure 2-2, the peak overpressure at this distance at sea level is 210 psi.

*Answer:* The corresponding peak overpressure at 95,000 feet is

$$\Delta p = \Delta p_0 S_p = (210)(0.014) = 2.9 \text{ psi.}$$

The reliability statement of Problem 2-1 indicates that for scaled distances (distances from a 1 kt explosion) less than 1,000 feet the values of peak overpressure obtained from Figure 2-2 are accurate to within ±15 percent. The probable upper limit of the required overpressure is

$$\Delta p = 2.9 + (0.15)(2.9) = 3.3 \text{ psi.}$$

**Reliability:** The data curves in Figure 2-64 are based on computer calculations supported by limited data from full-scale nuclear tests. As a result of the experimental checks, the computed data are believed to be accurate at high overpressures; however, this accuracy is not considered confirmed. At low overpressures (scaled radii under 300 feet, shock strengths less than 7), some of the numerical methods used by the computer introduce errors, and reliable esti-

mates of effective blast yield are not available; however, even at low shock strengths, the blast efficiency factor is believed to be approximately within the limits shown in Figure 2-64. Yield scaling appears to be relatively accurate, introducing errors of only a few percent. Uncertain-

ties in the overpressure values obtained from Figure 2-2 are described in Problem 2-1.

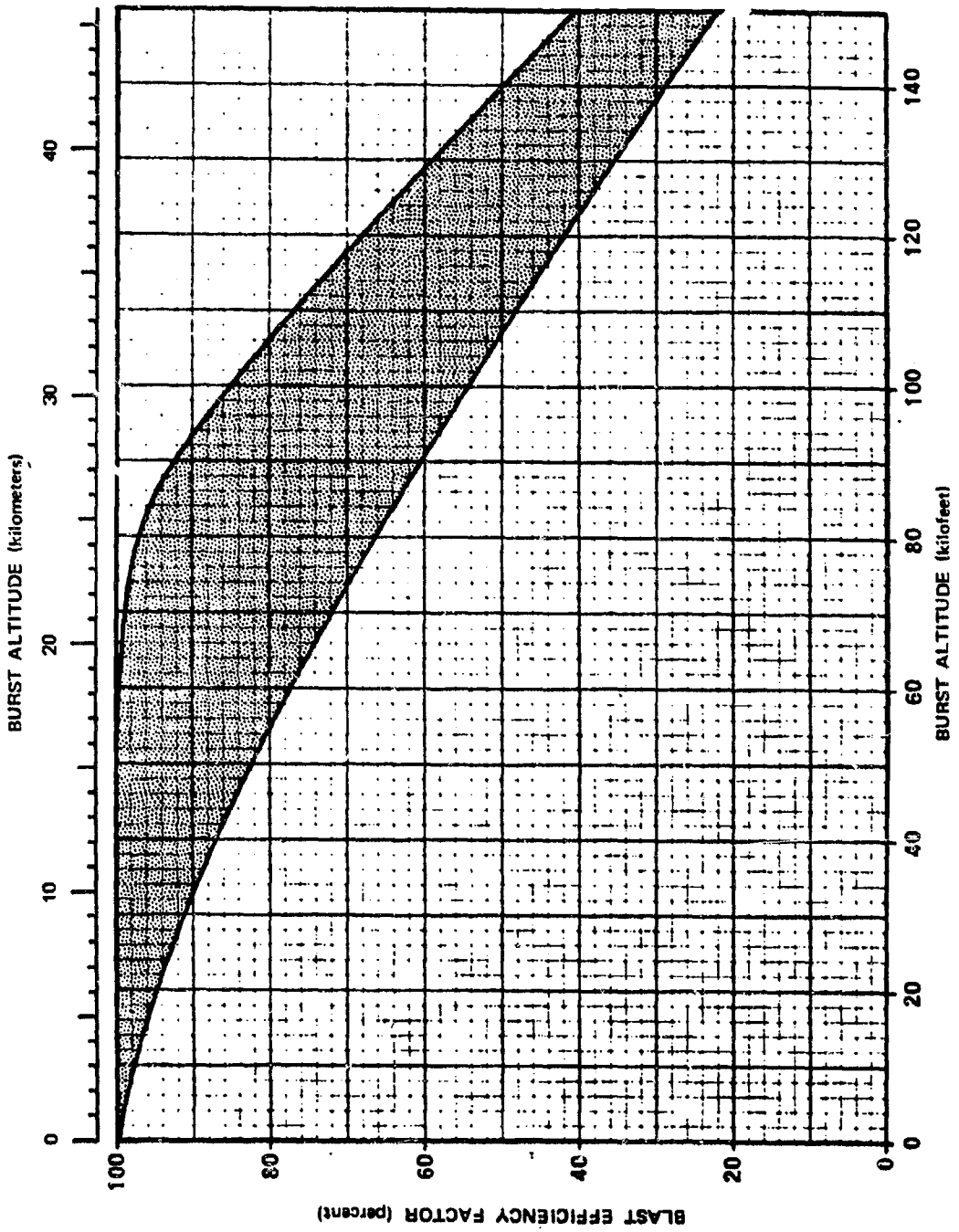*Related Material:* See paragraph 2-41. See also paragraphs 2-7 through 2-11 and 2-14. See also Problems 2-1 through 2-6.

Figure 2-64. Blast Efficiency Factor for High-Altitude Bursts

## 2-43 Peak Overpressure on the Ground from High-Altitude Bursts

The conventional procedure for finding blast-wave parameters at one altitude produced by a burst at another altitude is modified Sachs' scaling (paragraph 2-14). Figure 2-65 uses this principle for the prediction of peak reflected overpressure at ground zero as a function of yield and burst altitude. The curves are based on computer calculations and are compatible with the curves in Figure 2-3, which show peak overpressure in free air.

The curves are drawn as though effective blast yield (paragraph 2-41) were always equal to actual weapon yield. If the burst is above 40,000 feet, a correction for effective blast yield is appropriate, and this reduced yield (rather than actual weapon yield) should be used to enter Figure 2-65.

Since the abscissa is slant range, Figure 2-65 may be used to predict peak reflected overpressure at locations other than at ground zero, provided the locations are within the region of regular reflection and are not too close to the range at which Mach reflection begins. Figure 2-46 may be used to determine the range over which the reflection coefficient has essentially the same value that it has at ground zero.

Since modified Sachs' scaling is an empirical method, there may be doubt as to its application over a wide altitude range. However, comparisons of reflected overpressures at ground zero from Figure 2-65 with calculations performed in a way that is independent of the technique of modified Sachs' scaling show substantial agreement up to burst altitudes of about 150,000 feet, the limit of the latter calculations.

## 2-44 Effects of Early Blast Phenomena

At the overpressures that are ordinarily of interest in blast calculations, the blast wave from a sea level burst has propagated well away from the region in which it originated. At high altitudes, however, the blast wave forms at relatively low overpressures and at long ranges. In making a blast calculation at these altitudes, a possibility exists that the range of interest is closer than that at which a scalable shock front forms.

The first stage of blast-wave formation occurs when the air around the burst, under high pressure because of its suddenly increased temperature, starts to move. In the analysis of computer runs, a convenient criterion for shock front formation is that the ratio of air density behind the shock to ambient air density $(\rho_s/\rho)$ rises at some point to a value exceeding 1.5. This criterion indicates that the pressure waves originating in the air near the burst are starting to merge to form a shock front. Formation of the hydrodynamic shock front then proceeds rapidly, and the actual time and radius of shock formation are close to the values based on the $\rho_s/\rho$ = 1.5 criterion.

## Problem 2-19. Calculation of Peak Reflected Overpressure at Ground Zero from a High Altitude Explosion

███ Figure 2-65 shows the peak reflected overpressure at the ground as a function of slant range for a selected family of weapon yields. The curves in Figure 2-65 are applicable at ground zero and at locations away from ground zero that are in the regular reflection region.

███ *Scaling.* No scaling is required with Figure 2-65; however, for explosions above 40,000 feet, the effective yield obtained by use of Figure 2-64 should be used to enter Figure 2-65.

███ *Example* ███

*Given:* A 100 Mt explosion at an altitude of 120,000 feet.

*Find:* The maximum peak reflected overpressure expected at ground zero.

*Solution:* From Figure 2-64, the maximum blast efficiency factor for bursts at 120,000 feet is 68 percent. The effective yield is

$$W_{eff} = (0.68)(100) = 68 \text{ Mt.}$$

*Answer:* Interpolation in Figure 2-65 indicates that peak reflected overpressure at ground zero is about 2.5 psi.

███ *Reliability* ███

███ The few available experimental data points tend to substantiate the curves in Figure 2-65. A certain amount of uncertainty occurs at low overpressures because the overpressure distance curves in Figure 2-65 are not identical to the results of the calculations independent of Sachs' scaling that were mentioned in paragraph 2-42.

███ No reliability estimate has been made for these curves; however, it should be observed that, for the extreme range of atmospheric conditions found along the path of the blast wave, overpressure values that are within a factor of 2 often represent satisfactory agreement.

███ *Related Material:* See paragraphs 2-7, 2-13, 2-14, and 2-42. See also Tables 2-1 and 2-2.
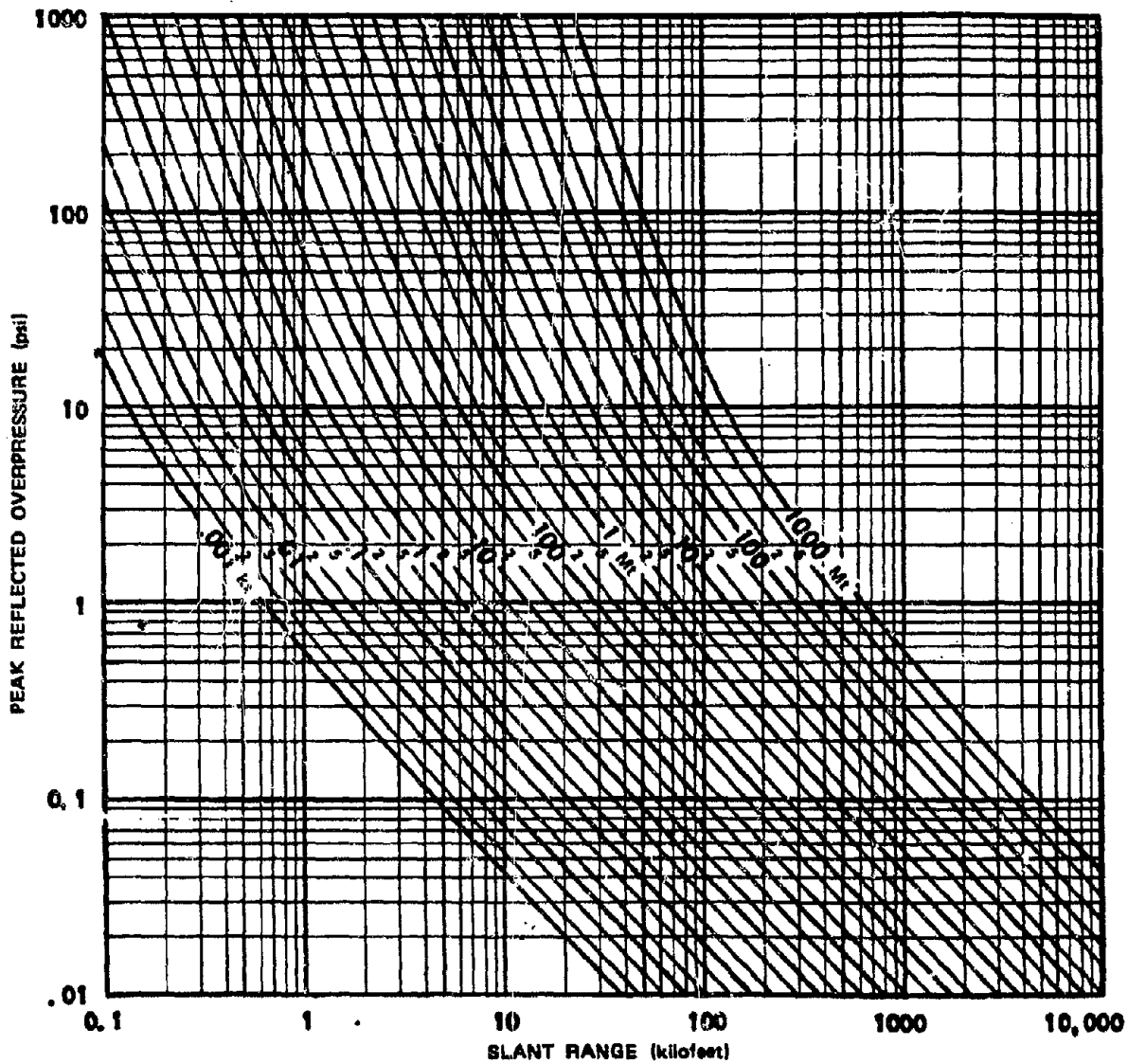
Figure 2-65. ▨ Peak Reflected Overpressure at Ground Zero as a Function of Yield and Slant Range ▨

■ The kinetic energy of the bomb debris, which is typically about 25 percent of the total yield, makes an important contribution to the strength of the blast wave. These high velocity debris atoms, pushing away the air surrounding the burst point, create a shock wave that is known as the nuclear shock or case shock. Until this shock front overtakes and merges with the hydrodynamic shock front, the blast wave will not have acquired its full energy. The fraction of the total energy carried by the debris is a function of weapon design. Therefore the arrival of the case shock at the hydrodynamic shock front, which marks the beginning of a scalable shock wave, also is a function of weapon design.

■ Figure 2-66 shows the approximate ranges of shock-front formation and case-shock arrival as a function of burst altitude for a 1 kt explosion. These ranges were calculated for conventional nuclear devices. Different curves would be required to show these ranges accurately for weapons with enhanced radiation outputs (paragraph 2-45



■ Figure 2-66 also shows curves of blast-wave overpressure levels as a function of range and altitude. Since peak overpressure cannot be scaled accurately until the case-shock front joins the hydrodynamic shock front, the overpressure curves terminate on the curve for case-shock arrival. To emphasize the increasing uncertainty of peak overpressure data with increasing altitude, the overpressure contour lines are dashed above 100 kft.*

■ These overpressure curves were obtained directly from Figure 2-2 and Sachs' scaling laws, including altitude corrections described in paragraph 2-14. However, correction for effective blast yield at high altitudes must be made, as illustrated in Problem 2-20.

■ This procedure will give a reasonably accurate answer only if the range that is used exceeds the range for case-shock arrival. The latter range is obtained by multiplying range obtained from Figure 2-66 for case-shock arrival by $W^{1/3}$ (note that actual yield $W$, not effective yield $W'_{eff}$, is required in this calculation). Similarly, the approximate range for shock front formation is obtained by multiplying the scaled range by $W^{1/3}$.

■ If a blast-wave calculation closer to the burst than the range of case-shock arrival is required, data from Figure 2-2 may be scaled to obtain a rough estimate of peak overpressure. If the calculation is for a range closer than the range for $p_s/p = 1.5$, the discrepancy between the actual overpressure and the calculated overpressure will probably be excessive. Requirement for a calculation of this type generally is a sign that other nuclear effects should be considered. Blast damage at ranges closer than shock-front formation usually is less serious than damage caused by neutrons, X-rays, gamma rays, and thermal energy.

■ The stages of development of a nuclear blast wave are most accurately known in terms of time, because accurate comparisons can be made between experimental data and points in computer calculations. Approximate equations for determining three times of interest are given below.



■ See NOTE in Reliability paragraph of Problem 2-20.

2-133

DNA
(6X1)

DNA
(6X1)

2-134

█ Figure 2-66 shows the approximate ranges of shock-front formation and case-shock arrival as a function of burst altitude and distance from a 1 kt explosion.

█ Scaling. For yields other than 1 kt, the range for case-shock arrival scales as follows:

$$\frac{d}{d_1} = W^{1/3},$$

where $d_1$ is the range for case-shock arrival for 1 kt (obtained from Figure 2-66), and $d$ is the corresponding range for a yield of $W$ kt. For heights of burst above 40,000 feet the range for a given *overpressure* scales as follows:

$$\frac{d}{d_1} = (W_{eff})^{1/3},$$

where $d_1$ is the range for the desired overpressure for a 1 kt explosion and $d$ is the corresponding range for a yield of $W_{eff}$ kt ($W_{eff}$ is the effective yield for a high altitude burst obtained from Figure 2-64 as illustrated in Problem 2-18).

█ *Example* █
Given: A 100 kt explosion at an altitude of 110 kilofeet above sea level.

*Find·* The peak overpressure at a range of 1,000 feet.

*Solution:* From Figure 2-66, the range for case shock arrival from a 1 kt burst at 110 kft is about 180 feet. The corresponding range for 100 kt is

$$d = d_1 W^{1/3} = (180)(100)^{1/3} = 835 \text{ feet}.$$

Since this is less than 1,000 feet, peak overpres-sure is scalable at the range of interest. From Figure 2-64, the blast efficiency for a burst at 110 kft is expected to be between 48 percent and 77 percent. The effective blast yield is therefore between 48 and 77 kt. The corresponding distances for a 1 kt explosion are

$$d_1 = \frac{d}{(W_{eff})^{1/3}} = \frac{1,000}{(48)^{1/3}} = 275 \text{ feet},$$

and

$$d_1 = \frac{d}{(W_{eff})^{1/3}} = \frac{1,000}{(77)^{1/3}} = 235 \text{ feet}.$$

*Answer:* From Figure 2-66, the overpres-sures are 90 and 150 psi at these ranges from a 1 kt explosion at 110 kft. The 15 percent uncer-tainty in overpressure data (see "Reliability") extends the range of 1 kt overpressure values to between 75 and 170 psi.

█ *Reliability* █
█ Ranges for shock formation and case-shock arrival were obtained from computer cal-culations. Case-shock arrival has been observed in nuclear tests, and the experimentally deter-·mined ranges substantiate the computer data. For conventional weapons (unconventional weapons are discussed in the following subsec-tion), the range for case-shock arrival is believed correct within a few percent. Yield scaling ap-pears to be fairly accurate for these phenomena.

█ Below 40,000 feet peak overpressure data are considered reliable within 15 percent for shock strengths greater than 1.5 (7 psi at sea level), within 20 percent for shock strengths be-tween 1.5 and 1.03, and within 30 percent for shock strengths below 1.03 (~1/2 psi at sea

level). Above 40,000 feet, the additional uncertainty implied by Figure 2-64 should be considered.

Note: Although Figure 2-66 was used in this example to calculate peak overpressure, it is not the preferred source of overpressure data. More accurate values may be obtained by scaling data from Figure 2-2 and, at high altitudes, following the method of Problem 2-18. Figure 2-66 is convenient for rough calculations, because it eliminates the requirement for altitude scaling. However, the important information in this figure is given by the curves that show the approximate ranges of shock-front formation ($p_s/p = 1.5$) and the beginning of a scalable shock wave (case-shock arrival).

Related Material: See paragraphs 2-7, 2-41, and 2-43. See also Problem 2-18.
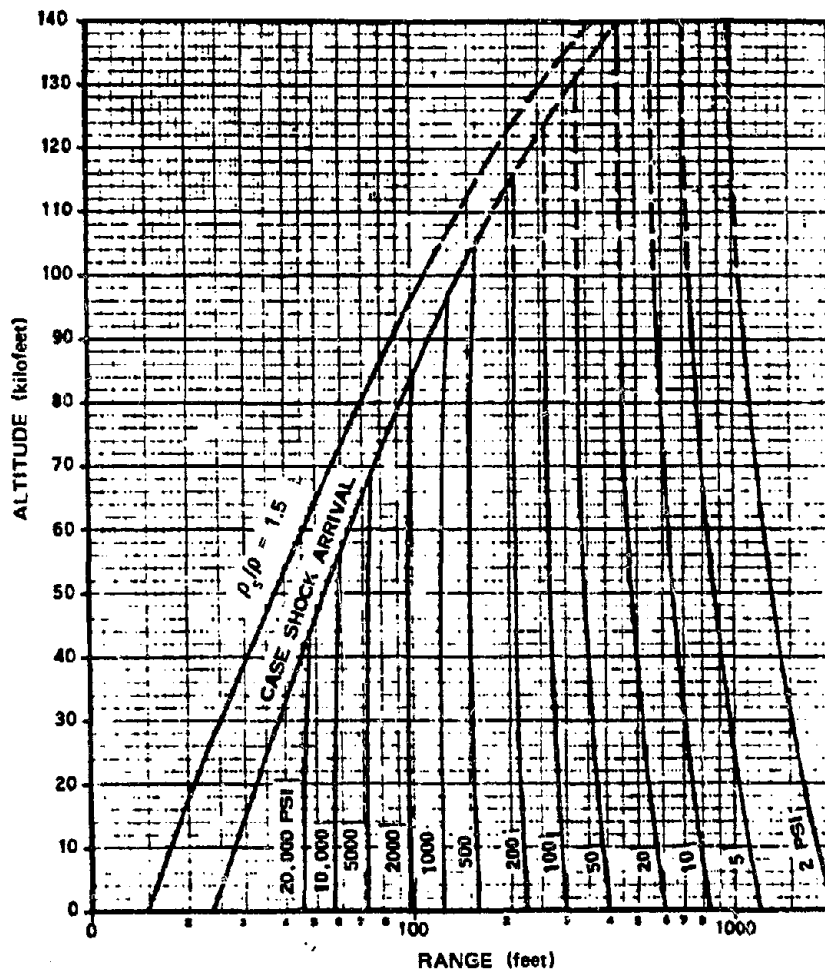
Figure 2-66. ▮▮▮ Limits of Scalable Shock Wave and Calculated Peak Overpressure as a Function of Altitude as a Function of Distance from a 1 kt Explosion ▮▮▮

## WEAPONS WITH ENHANCED OUTPUTS

The initial output energy of a conventional nuclear weapon consists mainly of black body radiation and kinetic energy of bomb debris as shown in Table 2-6. Table 2-7 shows the mean free path of various forms of energy that can be generated by a nuclear device. Most of the output of a conventional nuclear weapon interacts with air atoms near the burst.
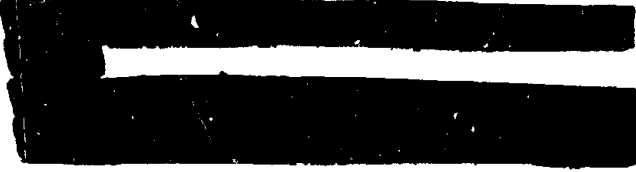
### 2-45 Air Blast from Weapons with Enhanced Radiation Outputs

The strength of the blast wave from enhanced radiation weapons is a complex function of the radiant energy distribution. Accurate blast wave calculations require detailed energy transport calculations, followed by hydrodynamic calculations to account for the motion of the heated air and the bomb debris. Frequently, the variation of ambient air density with altitude is sufficiently important to be included in the calculations. A large digital computer is required to account for all of these factors.

---

*The unit keV is commonly used in two senses. Strictly speaking, it is a unit of energy (1 keV = 1,000 electron volts = $1.602 \times 10^{-9}$ erg) which has a magnitude that is convenient for specifying the energies of X-ray photons. However, by extension of its original meaning, the unit is used to define temperature (1 keV ≈ 11,600,000°K).

The term *1 keV spectrum* means the spectrum of thermal radiation from a black body, i.e., a perfect radiator of thermal energy, that has a temperature of 1 keV. Note, however, that an energy of 1 keV is not representative of the energy of the photons constituting such a spectrum; about 15 percent of the photons have energies of 1 keV or less, and these photons represent less than 3.5 percent of the total spectral energy. Half of the energy is carried by photons with energies greater than 3.5 keV. The spectrum extends roughly to 10 keV; photons with energies higher than this constitute only 1 percent of the spectral energy. See Chapter 4 for further discussion of black body radiators.
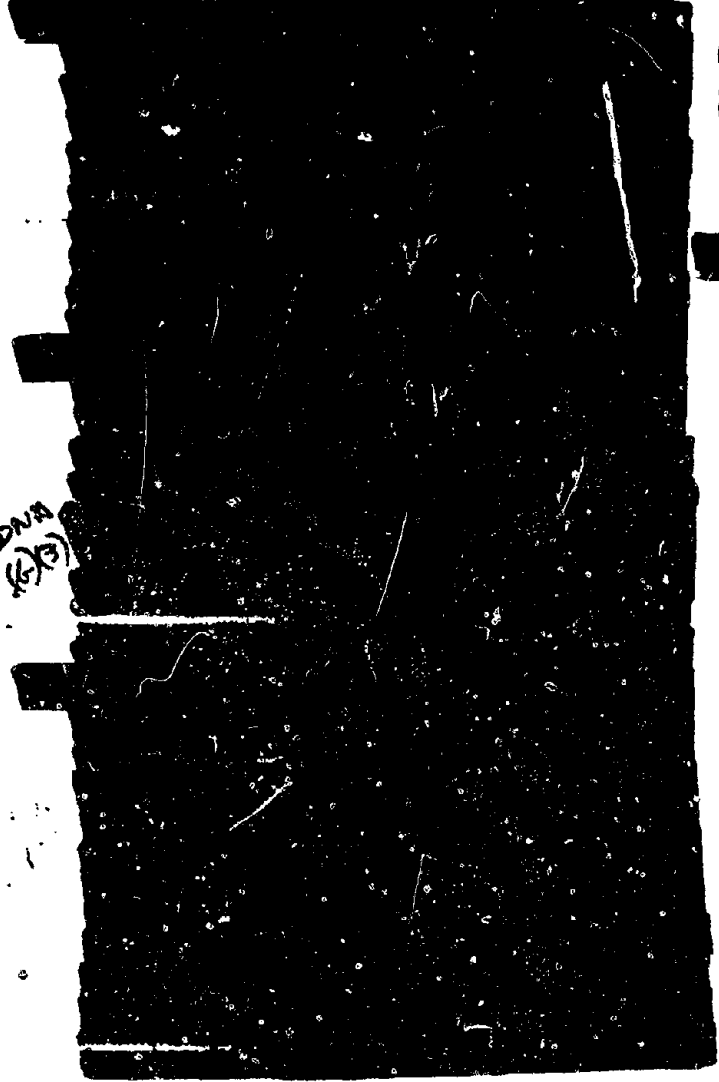
Table 2-7 █ Representative Mean Free Paths of Nuclear Weapon Radiation █

| | | Mean Free Path | |
|---|---|---|---|
| Source | Energy | Sea Level | 80,000 ft |

█

*█ The mean free paths shown in this table are for individual particles in ambient air. Collectively, the particles may travel farther. Debris atoms, for example, assist one another in pushing the air atoms away from the burst point. X-ray photons completely ionize a small region of air near the burst, thus creating a nearly transparent region through which other X-ray photons can travel freely.
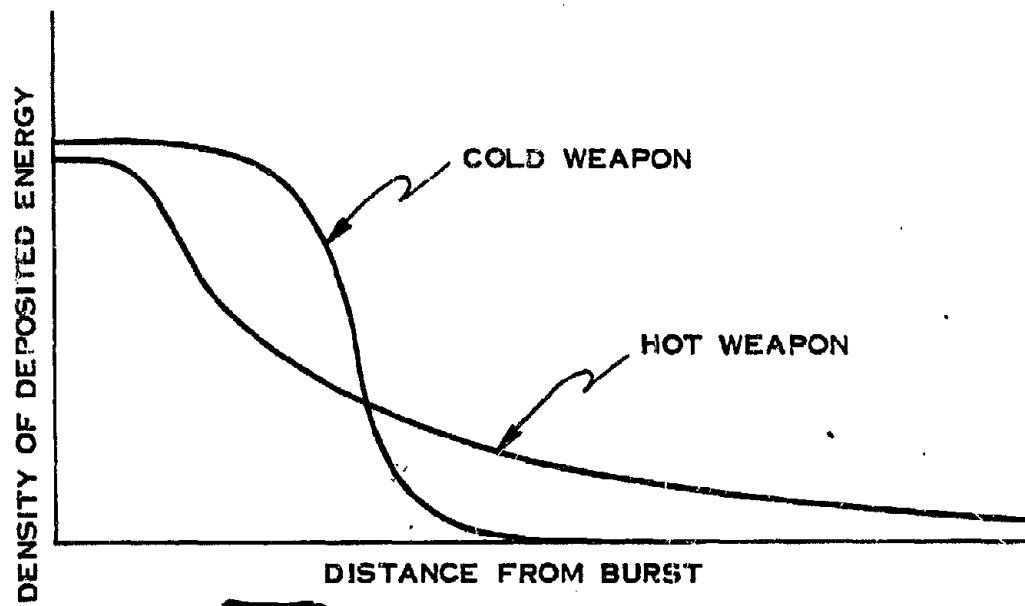


Figure 2-6█ Energy Deposition in Air as a Function of Nuclear Source Characteristics (Not to Scale) █

Rough calculation may be made, however, by applying the following rule of thumb to weapons with enhanced outputs: blast calculations for a given radius may be based on a weapon yield that is equal to the amount of energy contained in the sphere defined by that radius. As this rule implies, the blast wave, as it propagates outward, picks up hydrodynamic energy from the heated air through which it passes.

DNA
(b)(3)

DNA
(b)(3)

DNA
(c)(3)

Deleted

Figure 2-68. ▮ Distribution of Deposited X-ray Energy in a Sea Level Atmosphere as a Function of Source Spectrum

DNA
(4)(3)

.Deleted- ...

Figure 2-69. ▮▮▮▮ Densi♯y of Deposited Energy in Sea Level Air
from Various Energy Sources ▮▮

██████ Many problems that require blast yield correction because of output spectrum will also require a blast yield correction because of altitude (paragraph 2-41). One correction factor does not replace the other, as illustrated in Problem 2-21.

██████ Effective blast yield, in percent, tends to increase with (1) increased range, (2) decreased radiating temperature, (3) increased yield, and (4) decreased altitude. ████████

*DNA*
*(b)(3)*

██████ As yield increases, the range for a given overpressure increases, but the distance that a given form of prompt energy can travel remains essentially the same; therefore, at a given overpressure level the blast wave from a higher yield encloses a greater fraction of the weapon output ████████████████

*DNI*
*(b)(*

██████ As altitude decreases, the denser air confines the radiated energy to a smaller volume. Since the range for a given peak overpressure is relatively insensitive to altitude (Figure 2-66), the sphere defined by this range encloses an increasing fraction of the source energy as altitude decreases.

████████ Paragraph 2-44 describes the differences between the characteristics of blast waves from enhanced radiation weapons and the blast waves from conventional weapons. The following example will illustrate the use of the information discussed in paragraph 2-44.

████████ *Scaling.* Range is scaled in such a way that at a given scaled range the X-ray energy has passed through a given amount of air.

$$\frac{R_0}{R} = \frac{\rho}{\rho_0},$$

where $R$ and $\rho_0$ are range and ambient air density at sea level and $R$ is range in air with an ambient density of $\rho$. The ordinate of Figure 2-68 (percent of radiated energy deposited) does not require scaling. Energy density added to the air is scaled in a way that accounts for spherical divergence and for yield.

$$\frac{\Delta E}{\Delta E_1} = \left(\frac{R_0}{R}\right)^2 W.$$

This equation is equivalent to:

$$\frac{\Delta E}{\Delta E_1} = \left(\frac{\rho}{\rho_0}\right)^2 W,$$

where $\Delta E_1$ is the energy deposited by 1 kt, $\Delta E$ is the corresponding energy deposited by $W$ kt, and the other terms are as previously defined. In addition to the scaling described above, Sachs' altitude scaling (paragraph 2-14) probably will be required.

2-144

Page 2-145 Deleted.

*Reliability:* The procedures described above have been substantiated by analysis of a limited number of computer calculations, and specific reliability estimates have not been made. The amount of error introduced by the procedures is expected to increase as the effective blast yield (in percent) decreases. In typical problems, the change in effective yield that the procedures predict is probably correct within about 25 percent.

*Related Material:* See paragraphs 2-7, 2-14, 2-41, and 2-44. See also Tables 2-1 and 2-2.

## SECTION II
## CRATERING PHENOMENA

A crater is formed when an explosion occurs at or near the ground surface. Figure 2-70a shows an idealized cross section of a crater formed by such an explosion. The diagram illustrates the dimensions that are commonly used to describe the crater, and the zones of subsurface deformation that typically surround a crater. The apparent crater is defined as the crater that is visible on the surface, the dimensions being measured between fallback and the original ground surface elevation. Fallback is material that was lifted or thrown out by the explosion and has fallen back within the true crater. The true crater is delineated by the approximate boundary between the fallback material and the rupture zone. The shape of the true crater is disguised by the fallback.*

The primary variables that affect the size and shape of the crater are the weapon yield and output characteristics, the height or depth of burst (HOB or DOB), the properties of the earth medium, and the geologic structure. As these variables change, the shape, characteristics, and actual dimensions of the crater change. Figure 2-70b illustrates the general cross sectional shapes of craters formed as a result of various burst positions.

---

*It is hypothesized by some that in certain geologies (notably those that are highly porous and water filled) the shock waves from the excavated crater may fracture the geological matrix. This could lead to late-time reconsolidation and liquefaction that could cause the apparent crater and the true crater to coincide and to be larger than the crater in a more competent geology. This theory is one that has been proposed to explain the large shallow craters produced at the Pacific Proving Ground.
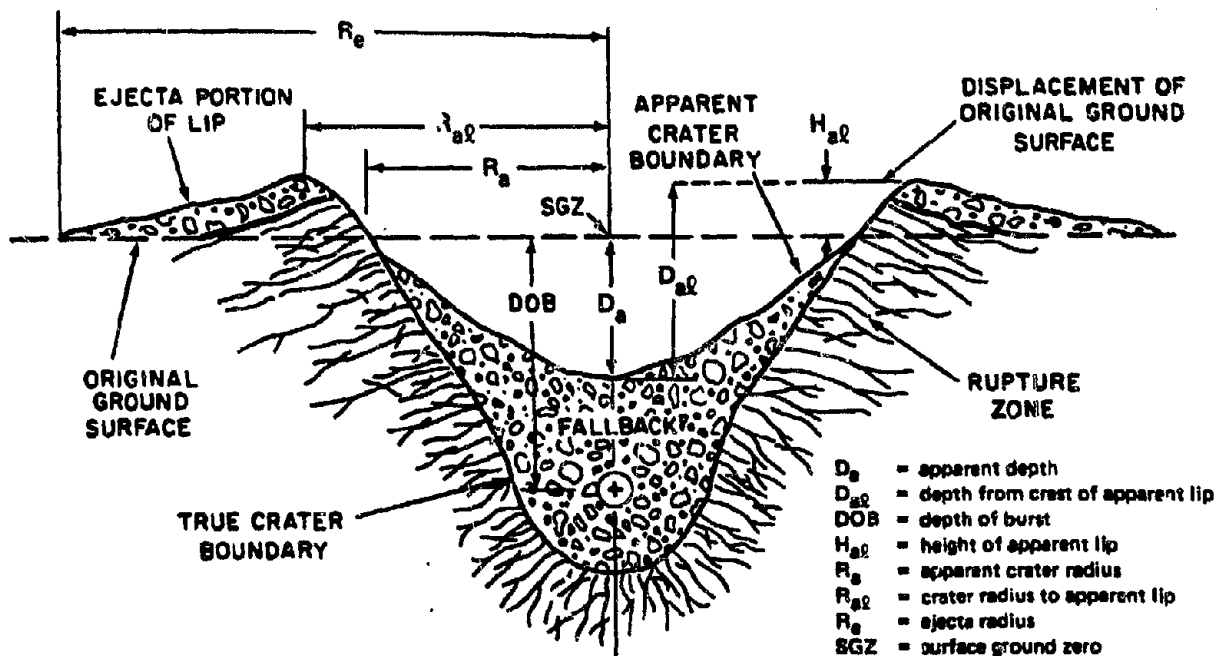


$D_a$ = apparent depth
$D_{a\ell}$ = depth from crest of apparent lip
DOB = depth of burst
$H_{a\ell}$ = height of apparent lip
$R_a$ = apparent crater radius
$R_{a\ell}$ = crater radius to apparent lip
$R_e$ = ejecta radius
SGZ = surface ground zero

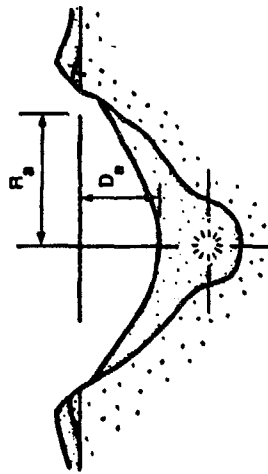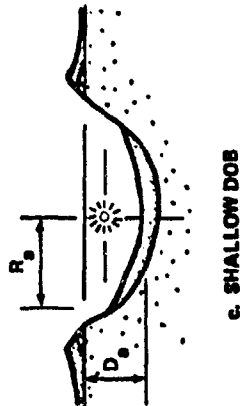Figure 2-70a.   Cross Section of a Crater from a Subsurface Nuclear Detonation
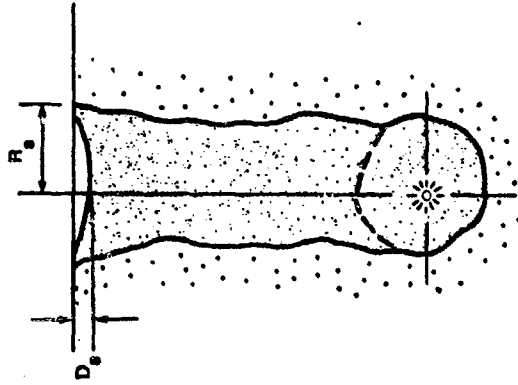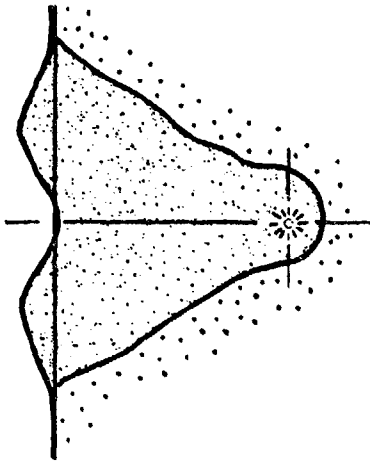
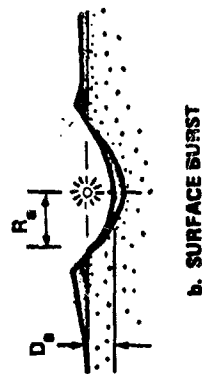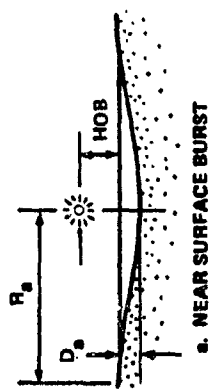Figure 2-70b. Relative Crater Sizes and Shapes Resulting from Various Burst Positions

When a nuclear explosion occurs well above the surface, but low enough that the fireball still intersects the ground surface, a shallow crater is formed by compression of the earth beneath the explosion and no ejecta is produced. As the HOB decreases, the crater volume increases and the proportion of the crater volume that results from excavation and ejection also increases. This holds true in a continuum that includes surface bursts (HOB = 0) and buried bursts from the most shallow to the optimum DOB for the weapon being considered. If the burst takes place at the optimum depth of burial, i.e., at the depth that results in maximum apparent crater dimensions for the weapon being considered, the acceleration of the earth medium upward by the expanding explosion gases is the dominant feature of the cratering process. Figures 2.71a and 2.71b are photographs of apparent craters that occurred from nuclear explosions buried in soil and rock at depths near optimum for crater formation.

Finally, deeply buried explosions may lead to a subsidence crater, to a raised mound above the detonation point, or to no permanent displacement of the surface at all.

## 2-46 Energy coupling

When a nuclear weapon explodes at or above the surface of the earth, there are two phases in the process of energy flow into the ground. The initial phase is referred to as "radiation deposition." Part of the prompt radiation output from the weapon (x-rays; see Chapter 4) reaches the ground and is absorbed in a time that is so short (a fraction of a microsecond) that hydrodynamic motion in the ground will be negligible. The ground is heated rapidly, and most of the absorbed energy is reradiated back into the air above the surface.

In addition to the energy deposited directly in the ground, the atmosphere around the source is heated by radiation diffusion, producing a fireball that radiates energy into the ground. This creates a thin layer of very hot plasma. At this stage, before any significant mass motions have occurred, the plasma, a layer of very hot, high energy-density material, extends along the surface to a radius that depends on weapon yield (about 30 meters for a 1 Mt surface burst).

The radiative coupling is completed in approximately one to three tenths of a microsecond. The net energy permanently absorbed by the ground represents about 6 percent of the total explosive yield.

The second phase of the process of energy flow into the ground is the "debris impact" phase. Vaporized debris from the nuclear device and its associated material impact the ground surface and add more energy to the earth. This debris slap may last for 3 or 4 microseconds, depending on the height of burst, and may inhibit some reradiation out of the ground. The energy from the debris impact represents only about 2 percent of the nuclear warhead yield for a contact surface burst.

The radiation from the air in the fireball continues to add energy to the soil over a period of time that is much longer (up to several hundred microseconds) than the duration of the prompt-radiation deposition and debris impact phases. The amount of energy coupled by this process is very uncertain.

The height of burst has an important effect on the radiative coupling. The air acts as an energy sink for some of the downward directed x-rays, converting them into thermal energy. The radiative coupling of a 1 Mt burst at a height of burst of 5 meters could be a factor of two less than from a contact surface burst (HOB = 0 meters) of the same yield. Because of practical considerations, such as the location of the center of energy release in a reentry vehicle whose nose is just in contact with the ground, it is more likely that the HOB will be greater than zero.
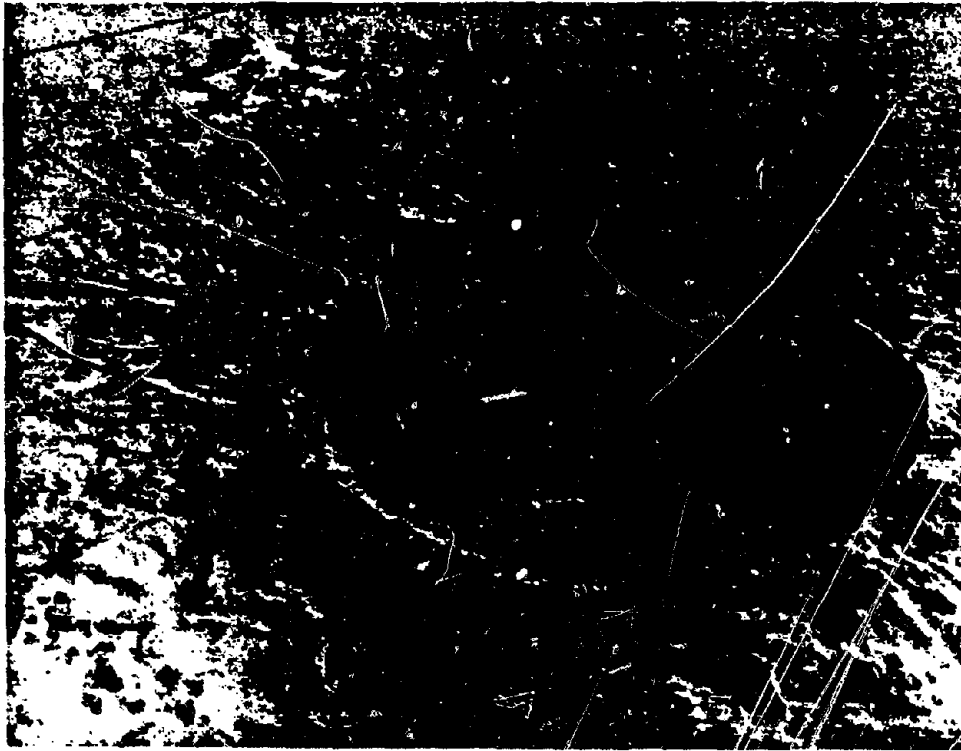
Figure 2-71a. SEDAN Event; Typical Crater Formed by a 100 kt Detonation in a Soil medium at Optimum DOB: $R_a$ = 186 m (611 ft.); $D_a$ = 98.5 m (323 ft.); DOB = 194 m (635 ft.)



Figure 2-71b. DANNY BOY Event; Typical Crater Formed by a 0.43 kt Detonation in a Hard Rock Medium (Basalt) at Optimum DOB: $R_a$ = 33.5 m (110 ft.); $D_a$ = 18.9 m (62 ft.); DOB = 33.5 m (110 ft.)

2-150